(19) Europäisches Patentamt
European Patent Office
Office européen des brevets

(11) EP 1 037 043 A2

(12) EUROPEAN PATENT APPLICATION

(43) Date of publication:
20.09.2000 Bulletin 2000/38

(51) Int. Cl.[7]: **G01N 27/72**

(21) Application number: **00112223.3**

(22) Date of filing: **30.11.1992**

(84) Designated Contracting States:
DE FR GB IT LU NL SE

(30) Priority: **06.12.1991 US 803504**

(62) Document number(s) of the earlier application(s) in accordance with Art. 76 EPC:
93900764.7 / 0 615 619

(71) Applicant:
MASSACHUSETTS INSTITUTE OF TECHNOLOGY
Cambridge, MA 02139 (US)

(72) Inventors:
- **Goldfine, Neil J.**
  Burlington, MA 01803 (US)
- **Melcher, James R.**
  DECEASED (US)

(74) Representative:
Style, Kelda Camilla Karen et al
Page White & Farrer,
54 Doughty Street
London WC1N 2LS (GB)

Remarks:
This application was filed on 07 - 06 - 2000 as a divisional application to the application mentioned under INID code 62.

(54) Magnetometer of increased sensitivity, selectivity and dynamic range

(57) A magnetometer for measuring a geometric property and the conductivity of a material comprising:

an electromagnetic winding structure capable of imposing a magnetic filed in the material when driven by an electric signal and sensing an electromagnetic response;
an analyzer for applying the electric signal to the winding structure to define a spatial wavelength associated with the imposed magnetic field in the material, the electric signal having a preselected temporal excitation frequency; and
a property estimator coupled to the winding structure for receiving sensed responses, the property estimator accessing a property estimation grid for translating sensed responses into substantially independent geometric property and conductivity estimates at the single preselected temporal excitation frequency.

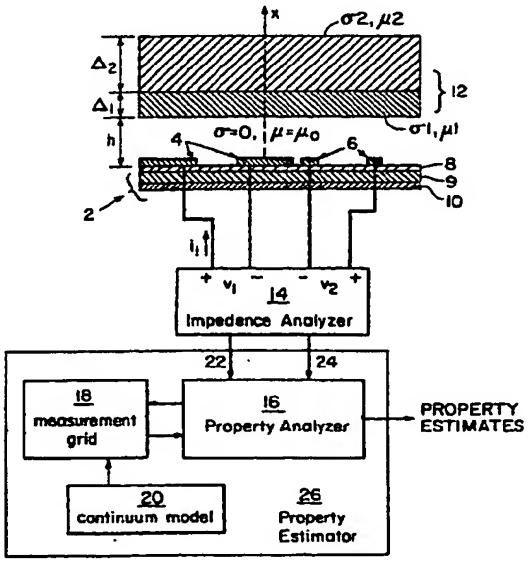

FIG. 1

Printed by Xerox (UK) Business Services
2.16.7 (HRS)/3.6

EP 1 037 043 A2

Description

Background of the Invention

[0001] The technical field of this invention is magnetometry and, in particular, the nondestructive electromagnetic interrogation of materials of interest to deduce their physical properties and to measure kinematic properties such as proximity. The disclosed invention applies to both conducting and magnetic media.

[0002] Conventional application of magnetometers, specifically eddy current sensors, involves the excitation of a conducting winding, the primary, with an electric current source of prescribed temporal frequency. This produces a time-varying magnetic field at the same frequency. The primary winding is located in close proximity to the material under test (MUT), but not in direct contact with the MUT. This type of nondestructive electromagnetic interrogation is sometimes called near field measurement. The excitation fields and the relevant spatial and temporal variations of those fields are quasistatic. The magnitude and phase (or the real and imaginary parts) of the impedance measured at the terminals of the primary winding (i.e., the measured voltage at the primary winding terminals divided by the imposed current) or the transimpedance (i.e., the voltage measured at a secondary winding terminals divided by the imposed current in the primary winding) is used to estimate the MUT properties of interest.

[0003] The tine-varying magnetic field produced by the primary winding induces currents in the MUT that produce their own magnetic fields. These induced fields have a magnetic flux in the opposite direction to the fields produced by the primary. The net result is that conducting MUTs will tend to exclude the magnetic flux produced by the primary windings. The measured impedance and transimpedance at the terminals of the sensor windings is affected by The following: the proximity to the MUT, the physical properties (e.g., permeability and conductivity) of the MUT and the spatial distribution of those properties; The geometric construct of the MUT; other kinematic properties (e.g., velocity) of the MUT; and the existence of defects (e.g., cracks, corrosion, impurities).

[0004] The distribution of the currents induced within conducting MUTs and the associated distribution of the magnetic fields in the MUT, in the vicinity of the MUT, and within the conducting primary and secondary windings are governed by the basic laws of physics. Specifically, Ampere's and Faraday's laws combined with Ohm's law and the relevant boundary and continuity conditions result in a mathematical representation of magnetic diffusion in conducting media and the Laplacian decay of magnetic fields. Magnetic diffusion is a phenomena that relates the distribution of induced currents in conducting materials to the distribution of the imposed and induced magnetic fields. Laplacian decay describes the manner in which a magnetic field decays along a path directed away from the original field source.

[0005] Magnetometers, such as eddy current sensors, exploit the sensitivity of the impedance or transimpedance (measured at the sensor winding terminals) to the physical and geometric properties of the MUT. This is sometimes accomplished by using multiple temporal excitation frequencies. As the primary winding excitation frequency is increased, the currents in a conducting MUT exclude more and more flux until all the induced currents in the MUT are confined to a thin layer near the surface of the MUT. At frequencies for which the induced currents are all at the surface of the MUT, the MUT can be represented theoretically as a perfect conductor. In other words, at high enough frequency variations, the conductivity of the MUT will no longer affect the impedance or transimpedance measured at the sensor windings.

[0006] This affect has been used in proximity measurement relative to a conducting media. Measurement of proximity to a metal surface is possible at a single excitation frequency, if that frequency is high enough that the MUT can be treated as a perfect conductor. For proximity measurement at lower frequencies, it is necessary to account for the effects of the conductivity of the MUT on the measured impedance, either by physical modeling or by calibration.

[0007] In applications requiring the measurement of conductivity, it is necessary to operate at frequencies low enough that the measurements at the terminals of the conducting windings are sensitive to the MUT conductivity. Such applications include The monitoring of aging in conducting media, as well as the direct measurement of conductivity for quality monitoring in metal processing and manufacturing process control. For example, the accurate measurement of the case depth (e.g., the thickness of a heat-affected zone at the surface of a metal after heat treatment) requires a sensor winding geometry and excitation conditions (e.g., frequency, proximity to the MUT) that produce the required sensitivity to the conductivity and thickness of the heat-affected zone.

[0008] Two methods are available for determining the desired conditions: (1) experimentation and calibration, and (2) physical modeling and response prediction from basic principals. In practice, each of these techniques has met with some success. The principal limitations of experimentation and calibration are the need for fabrication of expensive calibration test pieces (standards) for each new application, the relatively small dynamic range (i.e., the small range of permissible MUT property variations over which the measurement specifications can be met), and the inaccuracies produced by variation in uncontrolled conditions such as temperature and lift-off errors.

[0009] The principal limitations of the physical modeling approach are the inaccuracies introduced by modeling approximations and the existence of unmodeled effects. These limitations are most severe for sensor winding constructs that are not specifically designed to minimize unmodeled affects.

[0010] In spite of these limitations, the successful use of conducting windings driven by a current source, as in eddy current sensors, to measure physical and kinematic properties has been widely demonstrated.

[0011] For example, eddy current sensors have been used to measure the thickness of conducting strips of known conductivity, as disclosed in Soviet Patents 578,609 and 502,205. Eddy current sensors have also been used for flaw detection, as disclosed in U.S. Patent 3,939,404. Other eddy current sensor applications include measurement of the conductivity-thickness product for thin conducting layers, measurement of the conductivity of conducting plates using calibration standards, and measurement of proximity to conducting layers. Such sensors are also used in proximity measurement for control of machines and devices.

[0012] The ability to resolve distributions of parameters and properties of different layers in multi-layered materials has been addressed in U.S. Patent 5,015,951. The referenced patent introduced the concept of multiple wavenumber magnetic interrogations of the material of interest, by imposing several different spatial magnetic field excitations, using multiple preselected sensor winding constructs, each with a different wavelength.

[0013] There is a substantial need for enhancements to the measurement performance capabilities of magnetometers. This includes the ability to measure (1) the conductivity and thickness of thin metallic layers independently to improve quality control in deposition and heat treatment processes (in practice, only the product of conductivity and thickness can be measured for thin layers for which the conductivity-thickness product is below a certain threshold); (2) more than one property independently with reliable and predictable performance over a wide dynamic range to provide a more accurate characterization of the MUT; (3) geometric or physical properties over a wide dynamic range without calibration to reduce cost and measurement setup time; (4) material properties such as permeability and conductivity of ferrous metallic layers or conductivity of deposited metallic layers, for quality control and property monitoring after processing (e.g., in situ monitoring of permeabiltiy for sheets of transformer core alloy, or conductivity measurement for thin metallic layers of different conductivity that form on metallic surfaces during heat treatment); (5) the thickness of conducting layers or heat affected zones on conducting substrates that do not have conductivities which are significantly different from that of the surface layer, to control heat treatment and monitor MUT properties; (6) the independent measurement of both the conductivity and height (i.e., the distance between the sensor windings and the MUT) of a conducting layer, to accurately account for lift-off affects in applications such as crack detecting (i.e., air gaps between the sensor windings and the MUT surface); and (7) measurement of kinematic properties such as proximity and relative velocity to conducting and magnetic media for actuator and process control.

[0014] Furthermore, there is a need for measurement methods that provide estimates of the actual physical properties of the MUT. Current techniques often measure "effective" properties that are only indirectly related to the actual physical properties (e.g., permeability and conductivity at a specified excitation frequency). These "effective property measurements often provide insufficient characterization of the MUT. For example, multiple temporal excitation frequencies are often used to obtain estimates of conductivity or permeability. This is not acceptable if these physical properties vary with temporal excitation frequency. In applications such as monitoring of aging and fatigue in ferrous and nonferrous metal alloys, it may be necessary to completely characterize the dispersive properties of the MUT, including the variations of conductivity and permeability with temporal excitation frequency. Thus, a technique is required that provides accurate estimates of actual physical and geometric properties of the MUT from measurements at a single temporal excitation frequency.

Summary of the Invention

[0015] To overcome the aforementioned limitations in current practice, magnetometers must provide increased sensitivity, selectivity and dynamic range as well as the capability to measure actual MUT properties without calibration when required. Note that sensitivity is defined herein as the incremental change in the transimpedance measured at the sensor terminals in response to an incremental change in the geometric or physical MUT property of interest. Selectivity is defined herein as a measure of the ability to independently estimate two distinct properties (e.g. conductivity and thickness of a thin conducting layer). Dynamic range is defined herein as the range of MUT properties over which sufficient sensitivity and selectivity can be achieved.

[0016] In accordance with embodiments of the present invention, apparatus and methods are disclosed which provide increased sensitivity, selectivity and dynamic range for non-contact measurement of actual properties of conducting and magnetic materials. These properties are physical and/or kinetic properties. Embodiments of the present invention are based upon various methods for increasing sensitivity, selectivity and dynamic range through proper construction of the magnetometer sensor and proper selection of operating point parameters for the application under consideration.

[0017] In one embodiment, a measurement apparatus for measuring one or more MUT properties includes an electromagnetic winding structure which, when driven by an electric signal, imposes a magnetic field in the MUT and senses an electromagnetic response. An analyzer is provided for applying the electric signal to the winding structure. A property estimator is coupled to the winding structure and translates sensed electromagnetic responses into esti-

mates of one or more preselected properties of the material. In accordance with the present invention, the temporal excitation frequency of the electric signal applied to the winding structure might be proximal to a transverse diffusion effect (TDE) characteristic frequency of the winding structure.

[0018] The TDE characteristic frequency is defined as the temporal excitation frequency at which the currents within a primary winding of the winding structure transition from a nearly uniform distribution throughout the primary winding cross-section to a distribution in which the currents are confined to a thin layer near the surface of the primary winding. In many applications, the sensitivity of response measurements to specific MUT properties of interest, or the selectivity for two MUT properties of interest, is increased when the frequency of the electric signal is near the TDE characteristic frequency. As such, the TDE-based apparatus is intentionally constructed to amplify the effects of the TDE. To that end, the winding structure comprises an optional permeable substrate and an optional conducting backplane for tuning (i.e., intentionally altering) the TDE characteristic frequency of the winding structure.

[0019] The electromagnetic winding structure in the preferred embodiments comprises a plurality of electromagnetic windings forming a meandering pattern. The meandering winding structure is a significant feature of the invention in that its geometry provides physical behavior which may be accurately modeled. As such, the magnetometer is capable of accurately estimating preselected material properties based on sensed responses obtained by the meandering winding structure.

[0020] A TDE-based apparatus may further comprise a model which is successively implemented by the property estimator for generating a property estimation grid which translates sensed electromagnetic responses into estimates of preselected MUT properties; The model provides for each implementation a prediction of electromagnetic response for the preselected properties based on a set of properties characterizing the winding structure and the MUT. The model is described in more detail below in accordance with a method for generating a property estimation grid.

[0021] A TDE-based magnetometer may be manipulated to obtain multiple responses for various operating conditions. For example, sensed responses may be obtained by the winding structure at multiple proximities to the MUT and converted to material property estimates. In another example, sensed responses may be obtained by the winding structure for a plurality of positions along a surface of the MUT. Further, for each position relative to the MUT the winding structure may be adjusted to obtain sensed responses for various proximities and orientations relative to the MUT. In yet another example, the magnetometer winding structure may be capable of being adapted to conform to a curved surface of the MUT for obtaining sensed responses and providing estimates of MUT properties. In another example, the frequency of the electric signal may be varied for obtaining a plurality of frequency related sensed responses with the winding structure.

[0022] A TDE-based magnetometer may be employed in a plurality of specific applications to provide substantially independent estimates of specified properties of interest. To that end, a TDE-based magnetometer is capable of providing independent estimates of each of a pair of properties at a single temporal excitation frequency from a single sensed response. This enables the TDS-based magnetometer to obtain estimates of dispersive properties of single and multiple layered MUTs. Potential pairs of MUT properties include (1) conductivity and thickness, (2) conductivity and proximity, (3) conductivity and permeability, (4) thickness and permeability, (5) permeability and proximity and (7) the real and imaginary parts of the complex permeability. The MUT property estimates may then be processed to estimate other MUT properties such as aging/fatigue, bulk and surface crack location and heat affected zone properties.

[0023] In other preferred embodiments, it is desirable to shift the TDE characteristic frequency away from the characteristic transition frequency associated with magnetic diffusion in the MUT in order to measure preselected MUT properties with required levels of sensitivity, selectivity and dynamic range. This is accomplished by changing the physical and geometric properties of the magnetometer.

[0024] In one embodiment in which the TDE characteristic frequency may or may not be significant, a magnetometer has a winding structure comprising a primary winding capable of imposing a magnetic field in the MUT when driven by an electric signal. The winding structure also includes one or more secondary windings for sensing electromagnetic responses. In this winding structure, the primary winding has a width which is substantially greater than the width of the gap between the primary and secondary windings. Further, the width of the primary winding may also be substantially larger than the thickness of the primary. The winding structure of this embodiment forms a meandering pattern. An analyzer is provided for applying an electric signal to the primary for imposing the magnetic field in the MUT, and a property estimator translates sensed responses into estimates of preselected MUT properties. Preferably, the magnetometer employs a model which is implemented by the property estimator for generating a response prediction table which translates sensed electromagnetic responses into estimates of the preselected MUT properties.

[0025] As in the other embodiments, the magnetometer may be used to obtain multiple responses for a plurality of operating conditions. To that end, in one example the magnetometer winding structure may be capable of being adapted to conform to a curved surface of the MUT for obtaining sensed responses and providing estimates of MUT properties. In another example, the winding structure may be adjusted to obtain sensed responses at multiple proximities to the MUT. In yet another example, a magnetometer with a winding structure comprising a single primary and single secondary may be employed for estimating dispersive properties of an MUT with responses obtained at a single

temporal excitation frequency and for single or multiple proximities to the MUT. In yet another example, the winding structure may be adjusted to obtain sensed responses for a plurality of positions along a surface of the MUT. Further, for each position the winding structure may be adjusted to obtain sensed responses for multiple proximities and orientations relative to the MUT. In another example, the frequency of the electric signal applied to the winding structure may be varied for each sensed response.

[0026] Devices which are constructed to incorporate both magnetoquasistatic (MQS) inductive coupling terms and electroquasistatic (EQS) capacitive coupling terms are referred to as MQS/EQS devices. These devices have applications for materials having properties of interest which are out of the dynamic range of existing MQS magnetometers and EQS dielectrometers. The introduction of capacitive coupling corrections permits the extension of the dynamic range for MUT properties of interest by allowing responses to be obtained at temporal excitation frequencies at which capacitive coupling is significant in order to increase sensitivity to the MUT properties of interest.

[0027] Accordingly, in another embodiment of the invention, an MQS/EQS device provides estimates of distributed properties of a layered MUT. The MQS/EQS device includes an electromagnetic winding structure capable of imposing a magnetic field and an electric field in the MUT when driven by an electric signal and sensing electromagnetic and electric responses. The winding structure comprises a primary winding, a plurality of coplanar first secondary windings and an optional second secondary winding positioned in a different plane. An analyzer provides electric signals to the winding structure and a property estimator translates sensed responses into estimates of preselected properties of the MUT.

[0028] Depending on the application, the MQS/EQS device may be operated in an MQS mode and/or an MQS/EQS mode and/or an EQS mode. Accordingly, when the input current temporal excitation frequency is within the MQS range for the device, the input current is applied to the primary winding for imposing a magnetic field in the MUT. Sensed electromagnetic responses are obtained at the first secondary windings for each layer of the MUT. When the input current temporal excitation frequency is within the MQS range and an input voltage temporal excitation frequency is within an EQS range, the input current is applied to the primary to impose a magnetic field and the input voltage is applied to the first secondary windings in a push-pull sense to impose an electric field in the MUT. Sensed electromagnetic responses are obtained at the second secondary winding for each layer of the MUT. When the input current temporal excitation frequency is within the EQS range, the input voltage is applied to the first secondary windings to impose an electric field in the material. Sensed electric responses are obtained at the primary winding for each layer of the MUT. The property analyzer is employed for translating the sensed responses into estimates of preselected distributed properties of each layer of the layered MUT.

[0029] The present invention also comprises a method for generating property estimates of one or more preselected properties of an MUT. Accordingly, an electromagnetic structure, an analyzer and a property estimator are provided. The first step in the method requires defining dynamic range and property estimate tolerance requirements for the preselected properties of the material. Next, a winding geometry and configuration is selected for the electromagnetic structure. A continuum model is used for generating property estimation grids for the preselected material properties as well as operating point response curves for preselected operating point parameters.

[0030] The grids and curves are subsequently analyzed to define a measurement strategy. Next, operating point parameters and a winding geometry and configuration are determined to meet the dynamic range and tolerance requirements. To accomplish this, property estimation grids and operating point response curves are generated and analyzed for various operating points. Next, sensed electromagnetic responses are obtained at each operating point and converted by the property estimator into estimates of the preselected material properties. Property estimate tolerances are then estimated as a function of values of the estimated preselected properties over the defined dynamic range using the property estimation grids and operating point response curves. If the property estimate tolerance requirements are not achieved, the process is repeated for different operating point parameters and winding dimensions.

[0031] As stated previously, the property estimator implements a model for generating a property estimation grid which translates sensed responses into preselected material property estimates. Accordingly, embodiments of the present invention may include a method for generating a property estimation grid for use with a magnetometer for estimating preselected properties of a MUT. The first step in generating a grid may be defining physical and geometric properties for a MUT including the preselected properties of the MUT. Next, operating point parameters and a winding geometry and winding configuration for the magnetometer are defined.

[0032] The MUT properties, the operating point parameters and the magnetometer winding geometry and configuration are input into a model to compute an input/output terminal relation value. Preferably, the input/output terminal relation is a value of transimpedance magnitude and phase. The terminal relation value is then recorded and the process is repeated after incrementing the preselected properties of the MUT. After a number of iterations, the terminal relation values are plotted to form a property estimation grid.

[0033] Embodiments of the present invention also include a method of selection of a magnetometer winding structure and operating point for measuring one or more preselected properties of an MUT which achieves specified prop-

erty estimate requirements. The first step includes defining physical and geometric properties for the MUT including preselected properties of the MUT. Next, the magnetometer operating point parameters, winding geometry and winding configuration are defined.

[0034] The MUT properties and the magnometer operating point parameters, winding geometry and configuration are then input into a model for computing an input/ output terminal relation value. The preselected properties of the material are then adjusted to compute another terminal relation value. Using the terminal relation values, Jacobian elements are computed. Note each Jacobian element is a measure of the variation in a terminal relation value due to the variation in a preselected material property.

[0035] Next, a singular value decomposition is applied to the Jacobian to obtain singular values, singular vectors and the condition number of said Jacobian. An evaluation is then made of the sensitivity, selectivity and dynamic range of the magnetometer winding structure and operating point parameters using the singular values, singular vectors and condition number. If the material property estimate requirements are not met, the process is repeated with adjusted magnetometer operating point parameters, and winding geometry and configuration until the material property estimate requirements are achieved.

[0036] According to one aspect, there is provided an apparatus for measuring one or more properties of a material comprising:

an electromagnetic winding structure comprising a meandering primary winding which imposes a magnetic field in the material when driven by an electric signal for exciting multiple spatial surface current density modes, the meandering primary winding providing a prescribed dominant spatial wavelength associated with the imposed magnetic field, the winding structure further comprising a secondary winding which senses fields produced by a dominant spatial wavelength surface current density mode and at least one shorter wavelength mode for obtaining electromagnetic response;

an analyzer for applying the electric signal to the winding structure; and

a property estimator coupled to the winding structure for translating electromagnetic responses into estimates of one or more properties of the material based on a modelled response to the dominant spatial mode and the shorter wavelength modes.

[0037] Preferably, the secondary windings are separated from the primary winding by a gap and the primary winding has a width which is greater than the gap width.

[0038] The measured property may be the conductivity of the material, and/or the complex permeability of the material.

[0039] Preferably a property is measured for a spatial distribution of the property near the surface of the material.

[0040] Preferably the primary winding has a spatial wavelength that is on the same order or smaller than the skin depth at a selected operating frequency.

[0041] Preferably the property estimator provides independent estimates of conductivity and permeability.

[0042] Preferably the estimator provides an estimate of conductivity distribution in a material and/or an estimate of permeability distribution in the material.

[0043] Preferably the primary and secondary windings together form a meandering pattern.

[0044] Preferably the winding structure further comprises a conducting backplane located adjacent to the primary and secondary windings.

[0045] Preferably the winding structure further comprises a permeable substrate located adjacent to the primary and secondary windings.

[0046] Preferably a plurality of secondary windings are provided each independently sensing different spatial modes.

[0047] Preferably the secondary windings are located in a different plane than the primary winding.

[0048] The property estimator may access a property estimation grid for translating the sensed electromagnetic responses into estimates of the preselected properties of the material.

[0049] Preferably the electromagnetic structure is capable of being adapted to conform to a curved surface of the material.

[0050] Preferably the sensed responses are obtained at a plurality of proximities to the material.

[0051] Preferably there is provided a pair of meandering electromagnetic winding structures positioned on opposite sides of the material, each meandering winding structure being capable of imposing a magnetic field in the material when driven by an electric signal and sensing an electromagnetic response.

[0052] Preferably the electric signal applied to the winding structure has its temporal excitation frequency proximal to a transverse diffusion effect characteristic frequency of the winding structure.

[0053] According to another aspect, there is provided a method of measuring one or more properties of a material comprising:

forming an electromagnetic winding structure comprising a meandering primary winding;

applying an electric signal to the winding structure to impose a magnetic field in the material for exciting multiple spatial surface current density modes;

with a secondary winding, sensing fields produced by a dominant spatial wavelength surface current density mode and at least one shorter wavelength mode imposed by the primary winding; and

translating electromagnetic responses of the secondary winding into estimates of one or more properties of the material based on a modelled response to the dominant spatial mode and the shorter wavelength modes.

[0054] Preferably the step of translating comprises accessing a property estimation grid characterizing the winding structure and the material.

[0055] Preferably the electromagnetic responses are translated into substantially independent proximity and conductivity estimates at a single preselected temporal excitation frequency.

[0056] Preferably the step of translating comprises translating into substantially independent estimates of conductivity and permeability at a single preselected temporal excitation frequency.

[0057] Preferably the step of translating comprises translating into distributed estimates of spatially distributed properties of the material.

[0058] Preferably the step of translating comprises translating into an estimate of complex permeability.

[0059] Preferably the step of translating comprises translating into estimates of one or more preselected dispersive properties of each layer of a layered material.

[0060] Preferably the method comprises obtaining sensed responses at a plurality of proximities to the material.

[0061] According to a further aspect there is provided a magnetometer for measuring one or more properties of a material comprising:

an electromagnetic winding structure comprising a primary winding capable of imposing a magnetic field in the material when driven by an electric signal and one or more secondary windings for sensing an electromagnetic response, the secondary windings being separated from the primary winding by a gap wherein the primary winding has a width which is substantially greater than the gap width;

an analyser for applying an electric signal to the primary winding for imposing the magnetic field in the material; and

a property estimator coupled to the winding structure for translating sensed electromagnetic responses into estimates of one or more preselected properties of the material.

[0062] Preferably the primary and secondary windings form a meandering pattern in a single plane.

[0063] Preferably the winding structure further comprises a plurality of layered primary and secondary windings capable of imposing magnetic fields in the material and sensing electromagnetic responses.

[0064] Preferably the secondary windings sense electromagnetic responses for each of a plurality of temporal excitation frequencies of the electric signals.

[0065] According to a further aspect, there is provided an apparatus for measuring one or more properties of a material comprising:

an electromagnetic winding structure capable of imposing a magnetic field in the material when driven by an electric signal and sensing an electromagnetic response;

an analyser for applying the electric signal to the primary winding structure, the electric signal having its temporal excitation frequency being proximal to a transverse diffusion effect characteristic frequency of the winding structure; and

a property estimator coupled to the winding structure for translating sensed electromagnetic responses into estimates of one or more preselected properties of the material.

[0066] Preferably the property estimator accesses a property estimation grid for translating the sensed electromagnetic responses into estimates of the preselected properties of the material, the property characterizing the winding structure and the material.

[0067] Preferably the electromagnetic structure is capable of being adjusted to vary its position and orientation relative to the material, electromagnetic responses being sensed by the electromagnetic structure for each position and orientation of the electromagnetic structure relative to the material.

[0068] According to a further aspect, there is provided a magnetometer for measuring one or more properties of a material comprising:

an electromagnetic structure capable of imposing a magnetic field in the material when driven by an electric signal and sensing an electromagnetic response;

an analyser for applying the electric signal to the structure to define a spatial wavelength associated with the imposed magnetic field in the material; and

a property estimator coupled to the electromagnetic structure for translating sensed electromagnetic responses into estimates of one or more preselected properties of the material, wherein the sensed responses are obtained at a plurality of proximities to the material.

[0069] Preferably the electromagnetic structure comprises a plurality of electromagnetic windings arranged into a meandering pattern.

[0070] Preferably the property estimator accesses a property estimation grid for translating the sensed electromagnetic responses into estimates of the preselected properties of the material.

[0071] Preferably the electromagnetic structure is capable of being adapted to conform to a curved surface of the material.

[0072] According to a further aspect there is provided a magnetometer for measuring a geometric property and the conductivity of a material comprising:

an electromagnetic winding structure capable of imposing a magnetic field in the material when driven by an electric signal and sensing an electromagnetic response;

an analyzer for applying the electric signal to the winding structure to define a spatial wavelength associated with the imposed magnetic field in the material, the electric signal having a preselected temporal excitation frequency; and

a property estimator coupled to the winding structure for receiving sensed responses, the property estimator accessing a property estimation grid for translating sensed responses into substantially independent geometric property and conductivity estimates at the single preselected temporal excitation frequency.

[0073] Preferably the geometric property is the actual or effective thickness of a surface layer of the material.

[0074] Preferably the geometric property is the proximity of the winding structure, to the material.

[0075] Preferably the property estimator generates the property estimation grid by successively implementing a model, which for each implementation provides a prediction of an electromagnetic response for a proximity and conductivity based on a set of properties characterizing the winding structure and the material.

[0076] Preferably the winding structure is formed of a plurality of electromagnetic winding elements arranged into a meandering pattern.

[0077] Preferably the winding structure is capable of being adapted to conform to a curved surface of the material.

[0078] Preferably the analyzer applies multiple electric signals each having a single preselected temporal excitation frequency to the winding structure for measuring the dependence of conductivity on temporal excitation frequency.

[0079] According to a further aspect there is provided a magnetometer for measuring complex permeability of a material comprising:

an electromagnetic winding structure capable of imposing a magnetic field in the material and sensing an electromagnetic response, the winding structure comprising a plurality of meandering electromagnetic windings;

an analyzer for applying an electric signal to the winding structure to define a spatial wavelength associated with an imposed magnetic field in the material, the electric signal having a preselected temporal excitation frequency; and

a property estimator coupled to the winding structure for receiving sensed responses, the property estimator providing a response prediction table for translating sensed responses into complex permeability estimates of the material, the property estimator generating the prediction table by successively implementing a model which provides for each implementation a prediction of a response for a value of complex permeability based on a set of properties characterizing the winding structure and the material.

[0080] Preferably the model provides a response prediction for complex permeability based on a set of properties comprising winding structure dimensions, winding structure geometry, winding structure physical properties, the temporal excitation frequency of the electric signal, winding structure proximity to the material, material dimensions and material physical properties.

[0081] Preferably the winding structure is capable of being adapted to conform to a curved surface of the material.

[0082] According to a further aspect there is provided apparatus for measuring one or more properties of a material comprising:

a pair of meandering electromagnetic winding structures positioned on opposite sides of the material, each meandering winding structure being capable of imposing a magnetic field in the material when driven by an electric sig-

nal and sensing an electromagnetic response;
an analyzer for applying the electric signal to each meandering winding structure to define respective spatial wavelengths associated with the imposed magnetic fields in the material; and
a property estimator coupled to the winding structures for translating electromagnetic responses from each of the pair of meandering winding structures into estimates of one or more properties of the material.

[0083] According to a further aspect there is provided a magnetometer for measuring one or more preselected properties of a material having a curved surface comprising:

an electromagnetic winding structure capable of being adapted to conform to the curved surface of the material, the winding structure comprising a plurality of meandering electromagnetic windings for imposing a magnetic field in a material when driven by an electric signal and sensing an electromagnetic response;
an analyzer for applying an electric signal to the winding structure to define a spatial wavelength associated with the imposed magnetic field in the material, the electric signal having a preselected temporal excitation frequency; and
a property estimator providing a property estimation grid for translating sensed electromagnetic responses into estimates of one or more preselected properties of the material.

[0084] Preferably the winding structure is capable of being adapted to surround the material.
[0085] Preferably the winding structure is capable of being spiralled around the material.
[0086] Preferably the winding structure is spiralled around a magnetic or insulating core to obtain measurements on a separate material.
[0087] According to a further aspect there is provided a magnetometer for measuring one or more dispersive properties of a layered material comprising:

an electromagnetic structure capable of imposing a magnetic field in the layered material when driven by an electric signal and sensing an electromagnetic response;
an analyzer for applying the electric signal to the electromagnetic structure to define a spatial wavelength associated with the imposed magnetic field in the material, the electric signal having a preselected temporal excitation frequency; and
a property estimator coupled to the structure for translating sensed electromagnetic responses into estimates of one or more preselected dispersive properties of each layer of the layered material.

[0088] Preferably the electromagnetic structure comprises a plurality of electromagnetic windings forming a meandering pattern.
[0089] According to a further aspect there is provided apparatus for measuring distributed properties of a material comprising:

an electromagnetic winding structure for imposing an electromagnetic field in the material when driven by electric signals and sensing an electromagnetic response, the winding structure comprising a primary winding and a plurality of secondary windings;
an analyzer for applying the electric signal to the winding structure; and
a property estimator coupled to the winding structure for translating electromagnetic responses into estimates of one or more properties of the material.

[0090] Preferably at least one secondary winding is disposed in a plane other than that of the primary winding.
[0091] Preferably the estimator models each layer as a series of sublayers with each sublayer having homogeneous properties.
[0092] Preferably the sensor is operable in both the magnetoquasistatic and electroquasistatic regimes.
[0093] According to a further aspect there is provided apparatus for measuring one or more properties of the material comprising:

an electromagnetic winding structure comprising a primary winding capable of imposing a magnetic field in the material when driven by an electric signal and one or more secondary windings for sensing an electromagnetic response, the winding having a spatial wavelength that is on the same order or smaller than the skin depth of measurement at a selected operating frequency;
an analyzer for applying an electric signal to the primary winding at the selected operating frequency for imposing the magnetic field in the material; and

a property estimator coupled to the winding structure for translating sensed electromagnetic responses into estimates of one or more preselected properties of the material.

[0094] Preferably the property estimator provides independent estimates of conductivity and permeability.

[0095] Preferably the estimator provides an estimate of conductivity distribution in a material.

[0096] Preferably the estimator provides an estimate of permeability distribution to the material.

[0097] Preferably the primary and secondary windings together form a meandering pattern.

[0098] Preferably the apparatus further comprises a plurality of secondary windings each independently sensing different spatial modes.

Brief Description of the Drawings

[0099]

Figure 1 is an overall schematic diagram of an apparatus for measuring the physical and kinematic properties of a material under test according to the present invention.

Figure 2 is a schematic cross-sectional view of a sensor winding construct showing an embodiment of the invention which has a primary width larger than the gap between the primary and the secondary winding, and showing the distribution of the current density, J, in the span-wise (transverse) direction at two different temporal excitation frequencies.

Figure 3 is a generalized procedure flow diagram for the estimation of MUT properties and measurement tolerances according to the present invention.

Figure 4 is a top view of the winding geometry for an example of a single wavelength sensor construct designed to provide increased transverse diffusion effect sensitivity (TDES)(not an embodiment of the invention).

Figure 5 is a top view of the winding geometry for an example of a single wavelength sensor construct with two secondaries to provide a differential measurement designed to provide increased TDES (not an embodiment of the present invention).

Figure 6 is a top view of the winding geometry for another example of a single wavelength sensor construct designed to provide increased TDES (Not an embodiment of the present invention)

Figure 7 is a top view of an example winding geometry for a single turn winding construct with a primary and a secondary designed to provide increased TDS. (Not embodiments of the present invention)

Figure 8 is a cross-sectional view of an example single wavelength winding geometry and sensor construct with the primary and secondary confined to two planes (levels) and the current in the primary circulating in a direction perpendicular to the winding planes and designed to provide increased TDES (not an embodiment of the present invention).

Figure 9 is a cross-sectional view of an example single wavelength winding geometry and sensor construct with the primary and secondary confined to two planes (levels) and the current in the primary circulating in a direction perpendicular to the winding planes and designed to provide increased TDES (not an embodiment of the present invention).

Figure 10 is a top view of a mask for an embodiment of the invention called the Inter-Meander Magnetometer, an example of a meandering array that applies a magnetic potential to the MUT with several cycles of the same spatial wavelength.

Figure 11 is an (a) cross-sectional view and (b) top view of a sensor winding geometry and construct that has the primary and secondary confined to two planes and applies a magnetic potential to the MUT with several cycles of the same spatial wavelength.

Figure 12 is a cross-sectional view of three winding geometries for measurement of physical and geometric properties of curved parts.

Figure 13 is a cross-sectional view of a III-V compound crystal growth process with a melt-condition-probe, a liquid-solid interface-condition-probe and a crystal-condition-probe.

Figure 14 is a cross-sectional view of a sensor winding construct that has its relative position to the material under test defined by the coordinates (x_s, y_s, α).

Figure 15 is (a) a cross-sectional view and (b) a top view of a sensor winding construct that uses the Inter-Meander Magnetometer winding geometry at the drive plane to induce orthogonal electric and magnetic potentials, and has an optional secondary on a second level.

Figure 16 is a cross-sectional view for a multiple layered material under test with a conductivity which transitions from the conductivity of the metal substrate to the conductivity of air.

Figure 17 is a series of cross-sectional views of the property estimation steps for monitoring and control of the manufacturing of a multi-layer MUT.

Figure 18 is a flow diagram of the generation of a property estimation grid using a continuum model according to the invention.

Figure 19 is a flow diagram of the evaluation and selection of a sensor design and operating point parameter set, using singular value decomposition of a Jacobian relating variations in the design or operating point parameters to variations in the winding terminal measurements according to the invention.

Figure 20 is a schematic top view of another example of a winding construct for a meandering array that applies a magnetic potential to the MUT with several cycles of the same spatial wavelength.

Figure 21 is a table of two example winding dimensions and physical properties for the Inter-Meander Magnetometer which produce significant TDES near the TDECF.

Figure 22 is a flow diagram of the continuum model for the Inter-Meander Magnetometer.

Figure 23 is a side-view of a material under test with P layers above the sensor winding plane.

Figure 24 is a cross-sectional view of one half wavelength of the Inter-Meander Magnetometer (a) and a schematic representation (b) of the collocation surface current density approach used in the continuum model.

Figure 25 is a set of plots of the surface current density distribution, o, and the magnetic vector potential distribution, Δ, over the first quarter wavelength of an Inter-Meander Magnetometer with the original construct, as predicted by the continuum model, at three different temporal excitation frequencies for the collocation on K approach in (d) through (f) and for the collocation on A approach in (a) through (c).

Figure 26 is a plot of the current distribution in the primary winding for an Inter-Meander Magnetometer with the (a) construct as predicted by the continuum model, compared with the $I/(r^{1/2})$ distribution predicted with an analytical model for a perfectly conducting fin.

Figure 27 is a representation of a "Generalized Sensitivity Ellipse" for a singular value decomposition representation of a 2x2 Jacobian that relates variations in the MUT properties, θ_1 and θ_2, to variations in the measurements, Γ, at the sensor terminals.

Figure 28 is a plot of the transinductance magnitude and phase predicted by the continuum model for several different foil thicknesses and conductivities.

Figure 29 is a transinductance magnitude versus phase plot with a two-dimensional property estimation grid constructed from lines of constant foil conductivity and lines of constant foil thickness.

Figure 30 is a plot illustrating the affect of foil thickness on the transinductance magnitude and phase.

Figure 31 is a plot showing experimental data measured with the Inter-Meander Magnetometer prototype sensor for two different foil thicknesses indicated with squares and crosses, and the predicted response simulated with the continuum model indicated with the curved lines.

Figure 32 is an expanded view of the region near the TDECF of Figure 31 to demonstrate the behavior produced by the transverse diffusion effect.

Figure 33 is a plot of the condition number, singular values, and singular vectors of the Jacobian for measurement of conductivity and thickness for a material layer with conductivity of 3.72E7 mhos/m (similar to that of aluminum).

Figure 34 is a plot of the condition number, singular values, and singular vectors of the Jacobian for measurement of conductivity and thickness for a material layer with conductivity of 5.8E7 mhos/m (similar to that of copper).

Figure 35 is an example of a two-dimensional property estimation grid for conductivity and thickness measurement on a metal foil.

Figure 36 is another example of a two-dimensional property estimation grid for conductivity and thickness measurement on a metal foil.

Figure 37 is a plot of the transinductance magnitude and phase measured with the Inter-Meander Magnetometer prototype and predicted by the continuum model for three different copper foil thicknesses.

Figure 38 is a plot of the transinductance magnitude and phase measured with the Inter-Meander Magnetometer prototype and predicted by the continuum model for three different aluminum foil thicknesses.

Figure 39 is a plot of the transinductance magnitude and phase measured with the Inter-Meander Magnetometer prototype and predicted by the continuum model for a brass plate at several different heights above the winding plane.

Figure 40 is a plot of the condition number for the Jacobian for measurement of conductivity and height for a metal plate above the winding plane, as predicted with the continuum model for the Inter-Meander Magnetometer as a function of the height and log(conductivity).

Figure 41 is a plot of the condition number, singular values, and singular vectors of the Jacobian for measurement of conductivity and height of a metal plate above the winding plane as a function of the plate height.

Figure 42 is a plot of the condition number, singular values, and singular vectors of the Jacobian for measurement of conductivity and height of a metal plate above the winding plane as a function of log(conductivity) for the plate.

Figure 43 is a two-dimensional parameter estimation grid for measurement of conductivity and air-gap height for very thick conducting layers.

Figure 44 is a plot of the maximum and minimum singular values and right singular vectors of the Jacobian for

measurement of permeability and height of a high permeability layer.

Figure 45 is a plot of the transinductance magnitude variation with the height of a high permeability layer above the Inter-Meander Magnetometer simulated with the continuum model, (a) with no back-plane, and (b) with a back-plane at 0.5 mm below the winding plane.

Figure 46 is a plot of the transinductance variation with temporal excitation frequency with a high permeability layer at various heights above the winding plane, with a back-plane at 0.5 mm below the winding plane.

Figure 47 is a plot of the surface current density distribution, o, and the magnetic vector potential distribution, Δ, over the first quarter wavelength of an Inter-Meander Magnetometer with the original construct, as predicted by the continuum model, with a high permeability layer immediately above the winding plane

Figure 48 is a plot of the surface current density distribution, o, and the magnetic vector potential distribution. Δ, over the first quarter wavelength of an Inter-Meander Magnetometer with the original construct, as predicted by the continuum model, with a high permeability layer 0.1 mm above the winding plane.

Figure 49 is a plot of the surface current density distribution, o, and the magnetic vector potential distribution, Δ, over the first quarter wavelength of an Inter-Meander Magnetometer with the original construct, as predicted by the continuum model, with a high permeability layer 1mm above the winding plane.

Figure 50 is a universal transinductance plot for a diamagnetic infinite half space used as a two-dimensional property estimation grid for the complex magnetic susceptibility.

Figure 51 (a) is a table of experimental data using the Inter-Meander Magnetometer prototype with the original geometry for measurements on a granular aluminum layer at 0 and 0.8mm above the winding plane, and (b) the first guess and estimated values of the complex magnetic susceptibility estimated using the experimental data for the layer immediately above the winding plane.

Figure 52 is a plot of the experimental (crosses) and predicted (curved line) responses of the transinductance magnitude and phase as a function of the temporal excitation frequency.

Figure 53 is a plot of the predicted and analytically determined complex magnetic susceptibility for the granular aluminum layer.

Figure 54 is a plot of a two-dimensional property estimation grid for conductivity and permeability for the Inter-Meander Magnetometer, with no back-plane, at 1 KHz.

Figure 55 is a plot of a two-dimensional property estimation grid for conductivity and permeability for the Inter-Meander Magnetometer, with no back-plane, at 10 MHz.

Figure 56 is a side view of the magnetic field lines induced by two Inter-Meander Magnetometers located on opposite sides of a material under test layer, operated in the odd and even modes.

Detailed Description of Preferred Embodiments

[0100] Apparatus, devices, methods, and techniques are disclosed for non-contact measurement of physical and kinematic properties of a Material Under Test (MUT). The disclosed measurement apparatus is depicted in Figure 1. The measurement apparatus includes an electromagnetic element 2 comprised of a primary winding 4, secondary winding 6, an insulating substrate 8, an optional highly permeable substrate 9, and an optional conducting backplane 10. The primary winding 4 (also called the driven winding) is driven by an input current or voltage source at a temporal excitation frequency, f, measured in cycles per second where $f=\omega/2\pi$ and ω is the angular frequency of the input electric signal, measured in radians per second. The voltage induced at the terminals of the secondary winding 6 (also called the sensing winding) divided by the current applied to the primary winding 4 is called the transimpedance (or transfer impedance). The transimpedance is measured by an impedance analyzer 14. The magnitude 22 and phase 24 of the transimpedance are inputs to a property estimator 16 which uses a measurement grid 18 to estimate pre-selected properties of a single or multiple layered MUT 12. The measurement grid can be generated either with a continuum model 20 or through experimental measurements on calibration test pieces. The model, measurement grid(s), and property analyzer are part of a property estimator 26 that converts measurements at the sensor terminals for single or multiple operating points (e.g., multiple temporal excitation frequencies) to estimates of pre-selected MUT properties of interest.

[0101] The disclosed invention is founded upon the ability to increase sensitivity, selectivity, and dynamic range through proper design of the electromagnetic element 2 and methods for proper selection of operating point(s) parameters. In many cases, the disclosed invention is the enabling component of measurement systems for MUT properties of interest that are not measurable with alternative winding designs (e.g., independent non-invasive measurement of conductivity and thickness for thin conducting films on conducting or insulating substrates).

The Transverse Diffusion Effect Sensitivity (TDES)

[0102] A principal feature of the disclosed invention is a phenomenon hereinafter referred to as the Transverse Dif-

fusion Effect Sensitivity (TDES). The key factors in the design of TDES-based sensors are (1) the distribution of the currents within the conducting windings of the sensor construct (i.e., the spatial variation of the current density, J, within the conducting windings in the direction transverse, perpendicular, to the direction of the imposed current flow; this distribution is also called the primary winding transverse-current distribution), (2) the sensitivity of this distribution to the properties of the MUT, (3) the selectivity (i.e., the ability to independently measure two or more MUT properties of interest), and (4) the dynamic range for The pre-selected MUT properties of interest, over which high sensitivity and selectivity can be achieved.

[0103] Design methods for conventional eddy current sensors assume the current density within the sensor windings is either uniformly distributed, or confined to a thin layer along the winding surface, and that variations in the transverse-current-distribution has no significant effect on the measurements at the terminals of the sensor windings. A TDES-based sensor is intentionally designed to amplify the effects of the transverse-current-distribution on the measurements at the terminals of the primary and secondary windings.

[0104] This is accomplished by introducing cross-sectional shape to the primary and secondary windings. The dependence of the transverse-current-distribution in the primary on the MUT properties of interest provides increased sensitivity, selectivity, and dynamic range for property estimation in many applications of interest. However, measurements at the terminals of the primary and secondary windings will not be sensitive to the primary winding transverse-current-distribution, unless the windings are properly designed to provide increasing inductive coupling to the secondary as the currents crowd-out closer and closer to the primary winding surface in the direction transverse to the direction of the imposed current flow (i.e., as the current density distribution transitions from a uniform distribution at low temporal excitation frequencies to a distribution with the currents confined to a thin layer at the surface of the conducting windings at high temporal excitation frequencies).

[0105] Increased sensitivity, selectivity, and dynamic range can be achieved for many common applications of conventional eddy current sensors and other magnetometers by amplifying these effects and by increasing the sensitivity of the transverse-current-distribution within the windings to the MUT properties of interest.

[0106] One specific embodiment is shown in Figure 2c. In this winding construct, the winding geometry is designed so that the width c of the primary 4, is larger than the gap g between the primary 4 and the secondary 6. In the embodiment of Figure 2, the thickness, Δ, of the deposited conducting winding material 28 is small compared to the widths, c and d, of the primary and secondary conducting windings respectively. Other winding constructs could exhibit significant TDES without having the major axis of the winding cross-section (c, in this embodiment) much larger than the minor axis (Δ, in this case).

[0107] The transverse diffusion effect characteristic frequency (TDECF) is defined as the temporal excitation frequency of the input electric signal at which the currents within the primary windings transition from a nearly uniform distribution throughout the primary cross-section, as shown in Figure 2a, to a distribution for which the currents are confined to a thin layer near the surface of the conducting windings.

[0108] The TDECF occurs at $f_{TD}=1/\tau m$, where $\tau m=\mu\sigma l^2$. In this relationship, μ and σ are an effective permeability and conductivity, respectively. The effective, conductivity, σ; that is, the effective conductivity which influences the diffusion of magnetic fields within the conducting sensor windings is not only influenced by the conductivity of the winding material 28, but also it is influenced by the conductivity, proximity, and shape of the neighboring media 12. The characteristic length, 1, for diffusion of magnetic fields within the sensing windings derives from the geometry and dimensions of the windings themselves.

[0109] It is important not to mistake the TDECF for the common characteristic frequencies which produce the dominant phase shift in conventional eddy current sensors. In conventional eddy current sensors, The characteristic magnetic diffusion transitions within the MUT dominate the frequency response of the sensor. This characteristic frequency is related to the time constant of magnetic diffusion, τm, within the MUT, where $\tau m=\mu\sigma l^2$; but, now μ, σ and 1 are the effective properties within the MUT.

[0110] The designer has the ability to vary The TDECF by changing the characteristic lengths for the winding construct, altering the electric properties and cross-section shape of the windings themselves, or by adding a conducting back-plane with specified properties or a magnetic substrate of known complex permeability with or without a controlled bias field.

[0111] There are advantages to the winding geometry illustrated in Figure 2 with $c>d>>\Delta$. These advantages are explained in the following few paragraphs.

[0112] At input excitation frequencies well below the TDECF, the current density, J, within the primary winding is essentially uniform throughout the winding cross-section. As the excitation frequency is raised, the currents begin to "crowd out" towards the surface of the conducting windings. This effect is referred to as transverse or span-wise diffusion of currents within the conducting windings. This is often referred to as the skin effect, because at high enough frequencies, the currents within conducting media are confined to a thin layer, "skin", near the surface of the conductor. The approximate thickness of this layer is commonly referred to as the skin depth, and is given by $\delta=SQRT[2/(\omega\mu\sigma)]$. At frequencies well above the TDECF, the surfaces of the conducting windings become equipotentials and the windings

act as perfect conductors.

[0113] One such winding construct which may be accurately modeled is the Inter-Meander Magnetometer construct. The mask for this winding construct is shown in Figure 10. The primary winding 4 meanders through several wavelengths, λ, and has terminal measurements (v_1, i_1). Two secondary windings 6 meander on opposite sides of the primary. As described in the Magnetometer Windings section, these terminals can be connected in several different ways to achieve different measurement objectives. In the principal usage, the secondaries are connected in parallel, and the secondaries links flux over the same area. This winding design is discussed further in the Inter-Meander Magnetometer Design Section. A complete continuum model for this magnetometer is presented in later sections. Examples of parameter estimation grids and measurement optimization techniques are also included for specific applications.

[0114] For the Inter-Meander Magnetometer construct shown in Figure 10, with $\lambda>c>d>g$ and $c>>\Delta$, the ability to accurately predict the response at the terminals of the sensor winding results in the accurate estimation of absolute material properties, without the need for calibration or measurements on calibration test pieces. The measurement of actual, absolute physical properties is possible under many conditions without the use of calibration test pieces. This results in significant cost saving potential for a wide range of applications, as well as a substantial increase in the usefulness of such property measurements for quality monitoring and control, process control.

[0115] Other winding geometries, that do not include multiple wavelengths, such as those in Figures 4 through 9, (not embodying the invention) must be modeled in a different manner. Continuum models for these geometries could use modal analysis with Fourier Transforms, or 2- and 3-dimensional finite element techniques. A variety of different winding geometries are possible, as shown in Figures 4 through 11. These are described in some detail in the Magnetometer Windings and Sensor Construct section.

Generalized Material Under Test Property Estimation Framework

[0116] The methods and techniques of the disclosed invention comprise a general property estimation framework. A typical measurement procedure flow would include the following steps (also shown in the procedure flow diagram in Figure 3):

Step 1 Define MUT property measurement requirements - define the dynamic range and measurement tolerance requirements for the MUT properties of interest.

Step 2 Select sensor winding geometry and configuration - select a sensor winding geometry and configuration (i.e., referring to Figure 1, the structure, shape and design of the primary 4 and secondary 6 windings, and the back-plane 10 and substrate 8 and 9 characteristics, with $c>g$). Selection is based on test and evaluation of property estimation sensitivity, dynamic range, and selectivity, using the predicted responses and measurement grids 18 generated by the continuum model 20 or through experimental measurements on calibration test pieces over the required range of properties for a variety of winding geometries, dimensions and configurations.

Step 3 Analyze the property estimation grids and operating point responses to define the measurement strategy - the measurement strategy includes the number of measurements required at different operating points and with different sensor geometries, dimensions and configurations. A continuum model 20 or set of experiments is used to generate property estimation grids 18 and a set of response curves which are functions of operating point parameter variations. Operating point response curves include (1) the standard temporal frequency response, and responses to (2) variations in the defined spatial wavelength of the sensor winding construct (the defined spatial wavelength λ, is the wavelength of the dominant eigenfunction, or Fourier component, in the magnetic potential, distribution imposed along the surface of the MUT; the defined spatial wavelength can be adjusted in actual measurements by including several similar winding constructs, each with a different defined spatial wavelength, as described in U.S. Patent 5,015,951), (3) the relative position of the winding construct to the MUT (including the height above or below the MUT surface, x_s, the position along the surface, y_s, and the orientation relative to the surface, α, as shown in Figure 14), and (4) adjusting the geometry of the winding construct (including the distance between the primary 4 and secondary 6, g; the relationship between the primary width, c, and the defined spatial wavelength, λ; the relative position of the back-plane 10 to the winding plane; and in the case of magnetic media the magnitude, direction, and spatial or temporal variation of an applied DC or AC bias field.

Step 4 Determine optimal operating point(s) and winding dimensions - a set of operating point parameters, for one operating point, includes the proximity to the MUT, h, the temporal excitation frequency, f, and all other adjustable parameters described in step 3. Singular value decomposition on the Jacobian, relating variations

in the transimpedance magnitude and phase to variations in the MUT properties of interest, is used when an accurate continuum model is available to determine the relative performance potention at different operating points (if such a model is not available, a set of carefully designed calibration experiments can be used, along with models of related winding and MUT geometries to provide additional insight). Relative performance potential includes sensitivity to variations in the MUT properties of interest, selectivity for pairs of properties of interest, and dynamic range for each property of interest. Then parameter estimation grids 18 are generated at optimal/selected operating points along with operating point response curves for use in property estimation, Step 6.

Step 5 Measure transimpedance for MUT at each operating point - measure the transimpedance at each prescribed operating point defined in the measurement strategy, using The impedance analyzer 14.

Step 6 Estimate the preselected MUT properties -estimate the MUT properties of interest, using root-searching techniques, trial and error, table look-up and interpolation; or graphical interpolation from measurement grids 18 generated with the continuum model 20 (or calibration experiments). This is accomplished in the property estimator 26.

Step 7 Estimate the property estimation tolerances -using measurement grids 18 and operating point response curves generated with the continuum model 20 (or calibration experiments) and the measurement tolerance specifications of the impedance analyzer 14, estimate the measurement tolerances and tolerance variations over the dynamic range of interest for each pre-selected MUT property of interest., If the property estimation measurement requirements are not achieved, repeat steps 2 through 7.

[0117] For any application, calibration experiments can be used to tune the model parameters and improve MUT property estimation accuracy. Such calibration, although not always required, should always be used when available.

Magnetometer Windings and Sensor Construct

[0118] As shown in Figures 4 through 11, there are many winding geometries and constructs that can provide the required relationship, c > g, for the sensor winding dimensions. In each of these winding constructs, the deposited windings are confined to one surface as in Figures 4 through 7 or two surface as in Figures 8, 9 and 11. These surfaces can be planes in cartesian coordinates (as in Figures 4 through 11), cylinders or arcs in cylindrical coordinates, as in Figures 12a and 12b, or spiral surfaces (each layer approximately cylindrical, as in Figure 12c) when it is desirable to wrap the winding construct around a circular cylinder for measurements on surfaces with other complex shapes.

[0119] Examples of cylindrical 54, wrapped 56, and curved 48 winding constructs are shown in Figure 12. If the local radius of curvature is much larger than 5 times the defined spatial wavelength of the winding construct for the Inter-Meander Magnetometer, then the cartesian continuum model, presented for the Inter-Meander Magnetometer, can be used to obtain accurate MUT property estimates without calibration. For small cylindrical parts, it is also possible to wrap the winding construct around the part as shown in Figure 12c (this is accomplished by depositing the winding onto a flexible substrate material 56). The windings can also be wrapped around a cylindrical insulating, conducting or magnetic core 58 (i.e., as opposed to wrapping the flexible sensor around a cylindrical MUT 52) to make measurements on curved or flat surfaces 50, which are in close proximity to the cylindrical core 58.

[0120] One application which could use a wrapped Inter-Meander Magnetometer winding construct with multiple turns around a magnetic 58 or insulating cylindrical core is the control of III-V crystal growth processes, such as for gallium arsenide or indium phosphide. An illustration of this application is shown in Figure 13.

[0121] The instantaneous position of the liquid-solid interface, solidification front, may be measured for other MUT geometries as well. For the example in Figure 14, the MUT material in the horizontal layer closest to the sensor might be divided, as shown, into two regions. On the left 72, the material might be solid, and the material on the right 74 of the vertical interface (e.g., solidification front) might be liquid.

[0122] Furthermore, the winding constructs can incorporate multiple defined spatial wavelengths, as shown in Figures 10, 11 and 12, or single spatial wavelengths as shown in Figures 4 through 9. Also, it is possible to design a TDES-based sensor with only a primary winding 4 (i.e., no secondary 6) and measure only the impedance at the terminals of the primary winding. However, with only a primary winding, the effects of variations in the contact resistance must be carefully accounted for.

[0123] The input electrical signal and the measurements at the terminals may vary with application. In the principal embodiment, the primary winding 4 is excited by a controlled current source, i_1, with a prescribed temporal excitation frequency, f, by an impedance analyzer 14. The output is the transinductance, $\Gamma = v_2/(j\omega i_1)$, where v_2 is the voltage measured at the terminals of the secondary winding 6 by the impedance analyzer 14. The transinductance is simply the

derivative with respect to time of the transimpedance (i.e., the transimpedance divided by jω where j=SQRT(-1)).

[0124] It is also possible to conceive TDES-based winding constructs that have the secondary 6 and primary windings 4 confined to different parallel surface levels, as shown in Figure 15, or in perpendicular planes. Figure 8 provides a variation on the latter case, where the currents in the primary circulate in the plane perpendicular to the secondary winding surface, but the primary winding 4 has a cross-section in the plane of the secondary winding 6, with its major axis along that plane. When the primary and secondary windings are not confined to single or multiple parallel planes, then a second defined spatial wavelength, λ', is introduced for completeness, as shown in Figures 8, 9 and 11.

[0125] Figure 14 illustrates the concept described earlier for scanning the relative position and orientation of the sensor to the MUT surface in order to provide additional parameter estimation information. The position (x_s, y_s, α), of the sensor relative to the MUT surface at the instant the measurement is made is considered part of the operating point specifications. The estimation of more than two properties requires sensor terminal measurements at more than one operating point.

[0126] An example of a multiple height, $h=x_s$, measurement to produce an operating point parameter response, with all other operating point parameters constant and with $\alpha=90°$ is described later for measurement of the conductivity of a metal plate (using the Inter-Meander Magnetometer construct). The ability to independently measure the conductivity and air-gap height of the thick metal layer is also demonstrated.

[0127] This independent conductivity and height measurement provides an enabling component of measurement systems designed to monitor aging/ fatigue and detect cracks in metal parts. These systems would be far less costly if the lift-off error did not effect the accuracy of the MUT property measurements. One key capability is the ability to accurately measure dispersive (frequency dependent) conductivity, which would be significantly altered by the presence of macro- and micro-cracks at the surface and in the bulk of the MUT. Further, the variations caused by the presence of different sized cracks would vary with temporal excitation frequency, as well as with variations in other operating point parameters such as the defined spatial wavelength, λ. This supports the potential to estimate the depth below the surface, the size of large cracks, and the density of microcracks, by investigating the variation of the measured dispersive conductivity with the input current temporal excitation frequency. This is not possible with conventional techniques.

[0128] One additional variation on the apparatus illustrated in Figure 1 is the inclusion of a magnetic coupling media which increases the coupling of the magnetic flux to the MUT in a manner similar to the common practice of introducing a coupling media for ultrasonic matching for ultrasonic measurement probes.

[0129] In many measurements, the special design of the Inter-Meander Magnetometer and the accuracy of the continuum model 20 provide the enabling features without requiring operation near the TDECF. For example, The accurate measurement of conductivity-thickness product can be achieved, as demonstrated in Figures 37 and 38, for thin conducting layers by obtaining a single frequency response.

[0130] Another variation on TDES-based sensors, is the use of a driven electroquasistatic electrode, or electrode pair, to alter the distribution of currents within The primary sensor winding 4. As illustrated in Figure 15, a sensing winding 86 could then be located on a parallel plane at a different level. One embodiment, shown in Figure 15, includes the application of an imposed electric potential 82 that is 90° out-of-phase with the imposed magnetic potential 80. The key feature is the capacitive coupling between the wide primary 4, which is driven by a current source, and the two secondaries 6, which are driven by voltage sources, v_2^a and V_2^b, in a "push-pull" manner. Variations on this design permit some active control of the distribution of currents within the conducting windings, and may allow increased sensitivity, selectivity, and dynamic range for specific applications.

[0131] One method for parameter estimation, using the Inter-Meander Magnetometer construct involves the addition of a correction for the capacitive coupling between the primary and secondary windings. The terminal current, i, and voltage, v, are then related by

$$\hat{i} = j\omega C\hat{v} + \frac{\hat{v}}{j\omega L} \tag{1}$$

resulting in a transimpedance with a clear frequency dependent capacitive coupling.

$$\frac{\hat{v}}{\hat{i}} = \frac{j\omega L}{1-\omega^2 LC} \approx j\omega L[1 + \omega^2 + \omega^2 LC] \tag{2}$$

[0132] This is consistent with the behavior observed in experiments with the Inter-Meander Magnetometer at high temporal excitation frequencies, when the capacitive coupling term becomes significant. This could also be modeled in a continuum sense by adding higher order terms in the electric field representation.

[0133] Sensors intentionally designed to incorporate both magnetoquasistatic (MQS), inductive coupling terms and

electroquasistatic (EQS), capacitive coupling terms are referred to here as hybrid MQS/EQS sensors. These sensors may have applications for materials such as biological media, or ceramics which have properties that are out of the dynamic range of existing MQS magnetometers and EQS dielectrometers.

[0134] One application of interest which involves the use of the Inter-Meander Magnetometer in several different modes is illustrated in Figures 16 and 17. For example, consider a multi-layered media designed not to reflect electromagnetic energy in specific wavelengths. Such a multi-layered media might be conceived with the conductivity varying from the conductivity of a conducting substrate (e.g., metal) at the bottom of the first layer, to that of air at The top of the last layer, along the direction, x, perpendicular to the surface of the metal substrate (as shown in Figure 16).

[0135] For this example, the manufacturing and quality control procedure might follow the following steps (the quality control steps 3, 5, 7 and 9 are shown in Figure 17):

Manufacturing Steps Steps	Property Estimation for Quality Control
step 1	Estimate the complex permeability and conductivity of the metal plate (including any heat affected zone properties near the metal surface), using

the Inter-Meander Magnetometer in MQS mode.

step 2 Apply layer 1 (thickness Δ_1) to metal plate.

step 3 Estimate the complex permeability and conductivity of layer 1, using the Inter-Meander Magnetometer in MQS mode.

step 4 Apply layer 2 (thickness Δ_2) on top of layer 1.

step 5 Estimate the complex permeability and conductivity of layer 2, using the Inter-Meander Magnetometer in MQS mode, with an EQS capacitive correction

(i.e., a hybrid MQS/EQS mode).

step 6 Apply layer 3 (thickness Δ_3) on top of layer 2.

step 7 Estimate the complex permeability, complex permittivity, and conductivity of layer 3, using the Inter-Meander Magnetometer in EQS mode, with an MQS capacitive correction (i.e., a different hybrid MQS/EQS mode than used in step 5), or with the addition of a "push-pull" capacitive coupling drive as shown in Figure 15 (i.e., a third hybrid MQS/EQS mode).

step 8 Apply Layer 4 (thickness Δ_4) on top of layer 3.

step 9 Estimate the complex permittivity of layer 4, using the Inter-Meander Magnetometer in EQS mode.

[0136] The Inter-Meander Magnetometer is operated in EQS mode by applying a controlled voltage to the two secondaries 6, shown in Figure 15, which are now called the driven electrodes, and using the primary 4 as the sensing electrode. The voltage on the sensing electrode (formerly the primary winding) divided by the voltage applied to the driven electrodes (formerly the secondary windings) is now the gain of the sensor. The gain response is then used to estimate the complex dielectric properties, as in a standard interdigital-electrode-dielectrometer construct (M.C. Zaretsky, et al., Continuum Properties from Interdigital Electrode Dielectrometry, IEEE Transaction on Electrical Insulation, Volume 23, No. 6, Dec. 1985).

[0137] The MUT 12 shown in Figure 1 has two homogeneous layers of thickness Δ_1 and Δ_2, conductivity σ_1 and σ_2, and permeability μ_1 and μ_2. The height of the material of interest above the sensor windings is h.

[0138] In the preferred embodiments, pairs of properties can be estimated from a single transinductance measurement at the terminals of the sensor windings. The measurement apparatus in Figure 1 is capable of providing near-real time estimation of pairs of properties including: (1) σ_1 & Δ_1, (2) σ_1 & h, (3) σ_1 & μ_1, (4) Δ_1 & μ_1, (5) Δ_1 & σ_2, (6) μ_1 & h, and (7) $\mu^*_1 = \mu_1 + j\mu_1''$ = complex permeability. These property estimates could then be used to estimate other properties such as aging/fatigue in aluminum plates (e.g., conductivity measurement with lift-off compensation), or heat affected zone (HAZ) thickness, hardness and electrical properties.

[0139] Example measurement grids are provided later for $\sigma 1$ & Δ_1, σ_1 & h, and μ_1 & μ_1''. Also, an example of a single property measurement of the proximity to a highly permeable media is provided, and an example of conductivity-thickness product measurement on thin conducting layers.

Property Estimation Grid and Operating Point Response Curve Generation

[0140] Each parameter estimation application will require a set of property estimation grids 18 and operating point response curves. The number of grids and response curves required will depend on the application. The grids and response curves have several different uses throughout the parameter estimation process. These uses include the following:

1) Develop a measurement strategy and select the measurement operating points by evaluating the MUT property estimation grids and operating point response curves, at a variety of different operating points over the required dynamic range for the MUT properties of interest (step 3: of the generalized MUT property estimation procedure in Figure 3). Evaluating a property estimation grid includes investigating the sensitivity, selectivity and dynamic range for the MUT properties of interest. This is first accomplished by visually inspecting the grids. For example, a grid which provides a large variation in the magnitude and phase of the transinductance in response to relatively small variation in the MUT properties of interest would provide a good property estimation performance.

2) Graphical estimation of the MUT properties of interest (step 6: of the generalized MUT property estimation procedure in Figure 3).

3) Determination of the estimate tolerances, as a function of the estimated values for the MUT properties of interest (step 7: of the generalized MUT property estimation procedure in Figure 3). The tolerances at a given grid point are estimated by averaging the variation in transinductance magnitude and phase between that grid point and its neighboring grid points and dividing both the average change in magnitude and the average change in phase into the corresponding change in the MUT property of interest.

[0141] Property estimation problems requiring three or more MUT property estimates will always require more than one estimation grid or at least one additional operating point response curve, (e.g., in the case of three properties, at least one grid and one additional response curve is required).

[0142] Figure 18 provides a flow diagram describing the generation of a property estimation grid 18, using a continuum model 20. The same concepts described in this figure apply to the generation of operating point response curves. The only difference is that for property estimation grids the main loop is repeated for different MUT property pairs (e.g., conductivity & thickness, or conductivity & proximity), while for the generation of operating point response curves one operating point parameter is varied over a range of interest.

[0143] To generate a property estimation grid, first input at 96 the winding specifications and configuration, including the winding geometry, conductivity, back-plane conductivity and proximity, and substrate permeability. Also, input at 98 the operating point parameter set (i.e., h, ω, λ, α, x_s, y_s). A continuum model 20 is then used to compute the terminal relations at 106 for the first MUT property pair. The continuum model for the Inter-Meander Magnetometer is described in detail later. The terminal relations are translated into transinductance at 107 . To generate the complete property estimation grid for two MUT properties of interest (e.g. conductivity & thickness of a onducting layer), these properties are varied over The dynamic range of interest at 109. The continuum model is then used to compute the terminal relations for each new MUT property pair, and each new grid point is plotted at 108, until the property estimation grid 18 is complete for the dynamic range of interest.

[0144] A similar approach could be used to generate a property estimation grid when an accurate continuum model is not available. This would require the use of calibration test pieces with a variety of different property pairs covering the MUT property range of interest.

Sensor Design and Operating Point Selection/ Optimization

[0145] Singular value decomposition can be used for many aspects of sensor design and operating point selection/optimization. The distinction between selection and optimization is made here. Identification and selection of operating points and sensor designs which provide the desired performance does not require optimization.

[0146] Singular value decomposition is described in detail in later sections for specific examples including (1) the independent measurement of conductivity and thickness for metal foils, (2) the independent measurement of conductivity and air-gap height for metal plates, and (3) the measurement of air-gap height relative to a highly permeable media.

[0147] Figure 19 provides a basic flow diagram for optimization of sensitivity, selectivity and dynamic range using singular value decomposition on the Jacobian relating perturbations in the MUT properties of interest to changes in the value of the terminal relation measurements at the sensor windings.

Inter-Meander Magnetometer Design

[0148] The Inter-Meander Magnetometer sensor construct was intentionally configured to provide the symmetry necessary to permit accurate response prediction.

[0149] The proposed sensor is fabricated with "meandering" conductors confined to a single surface. The resulting periodic structure forms a transformer in the plane x = 0, as shown in Figures 10 and 20. The primary of the sensor has the terminals (i_1,v_1) and could be driven by an input current or voltage source. The secondary consists of a pair of conductors that meander to either side of the primary. The terminals of this pair of windings are connected in parallel so that their voltage, V_2, will reflect the flux produced by the driven winding. The return paths for the pair of secondary conductors are arranged, in Figure 10, so that each conductor will link flux over areas of the same size. The open circuit voltage or the current through a prescribed load at the secondary terminals could be the sensor output. This structure is represented in cross section in Figure 24(a), where what are shown as "wires" in Figure 20 are now shown to have widths c and d for the primary and secondary conductors, respectively. There are in wavelengths, λ, to the structure and the length, 1, is large enough compared to λ so that the fields can be regarded as two dimensional.

Optimization of Measurement Performance

[0150] A quantitative technique that permits the identification of regions of optimal measurement performance within the parameter space of interest is required. The measurement performance can be characterized by the following performance specifications:

(i) Performance bandwidth - range of frequencies over which accurate, uncalibrated, absolute measurement is possible with available instrumentation
(ii) Dynamic range - range of properties over which accurate parameter estimates can be obtained.
(iii) Sensitivity - variation in output signal produced by a variation in the measured property
(iv) Robustness - a measure of the ability to obtain accurate measurements at the limits of the sensor bandwidth

and dynamic range.

(v) Selectivity - a measure of the ability to differentiate between (1) the effects of two or more physical or geometric properties of interest (this definition is used throughout this document) (2) the effects of the estimated parameter and other modeled effects, (3) the desired signal and disturbances of other frequencies or phases, (4) the desired signal and noise (signal-to-noise ratio), (5) the desired signal and the effects of unmodeled dynamics.

(vi) Threshold level-the minimum output signal level required for accurate measurement of output magnitude and phase.

[0151] A typical measurement optimization procedure would follow the general procedure described below:

(1) Use the continuum model to numerically compute elements of the Jacobian relating differential variations in the vector of unknown quantities (e.g., conductivity and thickness of a metal foil) to the vector of measured quantities (e.g., The Inter-Meander Magnetometer Transimpedance, v_2/i_1, magnitude and phase)

(2) Determine the singular values and associated right singular vectors using Singular Value Decomposition for the Jacobian formulated in (1)

(3) Select the optimal frequency for the primary excitation and determine the performance bandwidth for an operating point at the center of the bounded parameter space for the application under consideration

(4) Determine the dynamic range by establishing the minimum acceptable selectivity, which relates to the condition number (= minimum singular value/maximum singular value), and the minimum sensitivity determined by the magnitude of the minimum relevant singular value

(5) Evaluate robustness by comparing the dynamic range to the application parameter space of interest, and by evaluating the relative observability for specific modes associated with the right singular vectors

(6) Confirm performance potential through proof of concept measurements and tune sensor geometry and geometric construct parameters if required.

Continuum Modeling

[0152] In the continuum models, two regimes of behavior are considered. In the first regime, the frequency ranges from low frequencies (currents are uniform with respect to the x and y directions throughout the conductors) to frequencies beyond the TDECF. In this range, span-wise diffusion is accounted for in the conducting windings, along the y direction, up until the currents in the conductors can no longer be assumed uniform with respect to the x direction. In the second regime, the frequency is assumed high enough that the magnetic vector potential can be approximated as constant, with respect to y, along the surface of the conducting windings.

[0153] The media above and below the windings are represented by surface inductance densities, L_n, which relate the Fourier amplitudes of the magnetic vector potential, A_n, to the Fourier amplitudes of magnetic field intensity, H_{yn}, in the planes just above (a) and below (b) the windings.

[0154] The preliminary objective is to predict the response of any particular circuit connected to the secondary for any excitation on the primary, with various neighboring media. This requires a detailed description of the windings that can be used with subroutines describing any particular neighboring media. A schematic representation of the response prediction algorithms is provided in Figure 22.

[0155] The neighboring media is represented as a multi-layered structure of P homogeneous layers above and/or below the winding plane, as shown in Figure 23. Representation of distributed properties can be achieved by introducing a large number of thin layers.

[0156] This approach permits a complete analytical solution for the field distributions in the direction perpendicular to the winding plane. A numerical solution using the subdomain method of weighted residuals (B.A. Finlayson, "The Method of Weighted Residuals and Variational Principles", Academic Press, NY, (1972)) is then introduced to incorporate the winding geometry, other relevant dynamics, and boundary conditions in the winding plane.

[0157] First, the specification of the meandering array 126 and the specifications of the MUT 128 are input to the continuum model 20. Then the collocation current densities, Kn, and vector potentials, An, are computed 130. The modeling effort is carried out in the following steps: (1) Fourier amplitudes are determined in terms of collocation current densities or vector potentials, (2) flux continuity and Ampere's continuity condition are introduced, (3) Faraday's law is evaluated to obtain the collocation conditions and subdomain integrals, and (4) equivalent circuit admittances are derived.

[0158] The result is a complete set of admittances 132 (Y_{11}, Y_{12}, Y_{21}, Y_{22}), as shown in Figure 22. These admittances are functions of the magnetometer geometry 126, the neighboring media properties 128, the primary excitation, and the secondary load. Predictions of the magnetometer responses are then obtained directly from the admittances using the standard two-port transfer relations 132.

Surface Inductance Density

[0159] The media above and below the windings are described by surface inductance densities, L_n, defined as the Fourier amplitudes of the normal flux density responses to single Fourier amplitudes of magnetic potential in the planes just above (a) and below (b) the windings. In the following, the magnetic field is assumed to be independent of z and is represented by the z component of the vector potential.

$$\vec{A} = A_z(x,y)\vec{i}_z \tag{3}$$

$$\vec{B} = \frac{\partial A_z}{\partial y}\vec{i}_x - \frac{\partial A_z}{\partial x}\vec{i}_y \tag{4}$$

Hence, with the Fourier series written in the form:

$$A_z(x,y) = \mathcal{R}e \sum_{n=-\infty}^{+\infty} \dot{A}_n(x) e^{-jk_n y} e^{j\omega t} \quad ; \quad k_n = \frac{2n\pi}{\lambda} \tag{5}$$

the surface inductance densities are given by

$$\dot{L}_n^a \equiv \frac{k_n^2 \dot{A}_n^a}{\dot{H}_{yn}^a} \quad ; \quad \dot{L}_n^b \equiv -\frac{k_n^2 \dot{A}_n^b}{\dot{H}_{yn}^b} \tag{6}$$

The first objective is to predict the response of any particular circuit connected to the secondary to any excitation on the primary for various neighboring media. This requires a detailed description of the windings that can be used with subroutines describing any particular linear neighboring media.

[0160] The neighboring media is accounted for by introducing the concept of a surface inductance density. Derivation of the appropriate surface inductance densities is required for each application considered. A generic representation suitable for many of these applications is developed in this section. This representation is then incorporated as a subroutine in the response prediction and parameter estimation algorithms.

[0161] Many applications can be represented using a media with multiple homogeneous layers. The required surface inductance densities can be conveniently obtained using transfer relations (J.R. Melcher, Continuum Electromechanics, Cambridge, MA, MIT Press (1981)). A medium with P layers (each of uniform conductivity, σ, and permeability, μ) is represented in Fig. 23

[0162] Layer j has the properties μ_j, σ_j and the thickness h_j. The upper surface of the j^{th} layer is designated by j. The transfer relation representing the solution of Laplace's equation for the magnetic vector potential in region j is given by

$$\begin{bmatrix} \dot{A}_n^{(j)'} \\ \dot{A}_n^{(j+1)} \end{bmatrix} = \begin{bmatrix} \dot{a}_{11}^{(j)} & \dot{a}_{12}^{(j)} \\ \dot{a}_{21}^{(j)} & \dot{a}_{22}^{(j)} \end{bmatrix} \begin{bmatrix} \dot{H}_{yn}^{(j)'} \\ \dot{H}_{yn}^{(j+1)} \end{bmatrix} \tag{7}$$

where

$$\hat{a}_{22}^{(j)} = -\hat{a}_{11}^{(j)} = \frac{\mu_j}{\gamma_j}\coth\gamma_j h_j \tag{8}$$

$$\hat{a}_{12}^{(j)} = -\hat{a}_{21}^{(j)} = \frac{\mu_j}{\gamma_j}\frac{1}{\sinh\gamma_j h_j}$$

$$\gamma j = \sqrt{k_n^2 + j\mu\sigma\omega}$$

and $F_n^{(j+1)}$ and $F_n^{(j)}$ represent the complex amplitude of the n^{th} Fourier component of a field quantity just above the lower and just below the upper interfaces of the j^{th} layer, respectively.

[0163] At the j^{th} surface, the boundary conditions are

$$\hat{A}_n^{(j)} = \hat{A}_n^{(j)'} \; ; \hat{H}_{yn}^{(j)} - \hat{H}_{yn}^{(j)'} = 0 \tag{9}$$

Surface current densities could also be considered at the interfaces but are not included in this example.

[0164] The surface inductance density above the j^{th} interface is given by

$$\hat{L}_n^{a(j)} = \frac{k_n^2 \hat{A}_n^{(j)}}{\hat{H}_{yn}^{(j)}} \tag{10}$$

The surface inductance density at x=0 is given by $L_n^{\ a} = L_n^{\ a(P+1)}$. L_n^a is obtained by progressing from the j=1 surface to the j=P+1 surface using the relation

$$\hat{L}_n^{a(j+1)} = k_n^2 \hat{a}_{22}^{(j)} + \frac{\hat{a}_{12}^{(j)}\hat{a}_{21}^{(j)}k_n^4}{\hat{L}_n^{a(j)} + k_n^2 \hat{a}_{22}^{(j)}} \tag{11}$$

The j=1 surface is generally at infinity so that $L_n^{\ a(2)} = k^2{}_n^{\ a}{}_{22}^{(1)}$.

[0165] An identical relation is obtained for the surface inductance density below the magnetometer interface, with L_n^b defined as in Eq. 6. (The details of the model are contained in "Uncalibrated, Absolute Property Estimation and Measurement Optimization for Conducting and Magnetic Media Using Imposed ω-k Magnetometry", by Neil Jay Goldfine, MIT Ph.D. Thesis, September 1990.)

Current and Vector Potential Distributions

[0166] Conduction in the windings at low frequencies is quasi-steady and the distribution of surface current density is uniform in both the x and y directions. The vector potential at low frequencies should exhibit a relatively smooth distribution since the presence of the conducting windings will not deflect the lines of magnetic flux at low frequencies. The symmetry of the Inter-Meander Magnetometer construct permits a qualitative prediction of the vector potential distribution. A sample distribution is shown in Fig. 25, where the surface current density and vector potential at a particular collocation point are designated by a circle or triangle, respectively. At the quarter wavelength point, the vector potential is zero due to symmetry assumptions. Consider the flux linked through a surface bounded by a line in the z direction at position y', between y=0 and y=λ/4, and a line at y=λ/4. Assuming the current in the primary is in the +z direction, as y' moves away from λ/4 toward the primary in the -y direction, more and more flux is linked until a maximum vector potential is reached at the center of the primary.

[0167] As the frequency is raised, the conductors tend to exclude the normal flux density, and the current redistributes over the widths of the conducting windings in the x and y directions. However, with the thickness of the conductors

in the x direction, Δ, much less than the widths c and d of the primary and secondary in the y direction, there will be a range of frequencies over which the current distribution remains essentially uniform in the x direction, but not in the y direction. The current begins to crowd out until it reaches a distribution with a 1/SQRT(r) dependence. The current density at The edge of the conducting windings goes to infinity and the vector potential distribution becomes uniform across the conducting intervals.

[0168] The simulated responses of the collocation on A and collocation on K approaches (described in "Uncalibrated, Absolute Property Estimation and Measurement Optimization for Conducting and Magnetic Media Using Imposed ω-k Magnetometry", by Neil Jay Goldfine, MIT Ph.D. Thesis, September 1990) are shown side by side in Fig. 25 for the parameters in the original construct of Figure 21. The (a) construct in Figure 21 provides increased TDES for some specific applications.

[0169] The collocation on A approach remains numerically well behaved until about 100 MHz for the original geometry in Figure 21. The collocation on K approach runs into numerical trouble at about 1 MHz, even with large numbers of collocation points.

[0170] The current distribution in the primary for the (a) construct of Figure 21 at 10 MHz using collocation on A is compared with the predicted 1/SQRT(r) distribution in Fig. 26. As the frequency is raised from 0.1 MHz to 10 MHz, the current distribution approaches the predicted 1/SQRT(r) distribution.

Measurement Optimization, Using Singular Value Decomposition (SVD)

[0171] The wide range of applications and the complex nonlinear parameter space common in nondestructive electromagnetic measurement applications necessitates the introduction of a generic tool for evaluating measurement performance. Properties such as sensitivity, selectivity, robustness, dynamic range and bandwidth must be quantified in order to provide a useful tool for optimization and comparison of sensor design and measurement performance.

[0172] A useful visualization which relates to the sensitivity of the measurement vector to perturbations in the unknown properties is provided by the "Generalized Sensitivity Ellipse" representation in Fig. 27. Such ellipsoids have been used to provide visual tools for design of mechanical linkages (H. Asada and K. Youcef-Toumi, Direct Drive Robots: Theory and Practice, MIT Press, 1987). The major axis of the ellipse is assigned the magnitude of the maximum singular value, σ_{max}, and the direction of its associated right singular vector, as shown. Similarly, the minor axis of the ellipse is assigned the magnitude of the minimum singular value and associated right singular vector. The left singular vectors can also be used to map perturbations of the unknown vector into the measured quantity space.

[0173] The ability to estimate two properties independently is called the selectivity. In the following sections, it is shown that the condition number, $\sigma_{min}/\sigma_{max}$, provides an excellent measure of selectivity for a two-property measurement application. For this definition of the condition number, a value of 1.0 provides the highest degree of selectivity, while a condition number of 0.0, a singularity point, implies that it is possible to perturb the unknown property vector in a manner that would be unobservable from the measured quantities. Each of these cases is demonstrated for actual measurement applications in the following sections.

Conductivity and Thickness Measurement for Thin Foils

[0174] Conventional methods for interpreting eddy current measurements using phaser diagrams often draw on first order approximations or lumped parameter representations. For example, it is common to introduce similarity conditions such as σf (the conductivity-frequency product) or $\sigma\Delta$ (the conductivity-thickness product). For many conventional eddy current sensor measurements, maintaining either of these products constant implies similitude (Nondestructive Testing Handbook, 2d Edition, vol. 4, Electromagnetic Testing, ASNT, 1986).

[0175] A limit frequency, f_g, can be defined. Below f_g, assumptions such as uniform current in the driven and sensing coils are accurate. It is quite reasonable under this condition to expect a degree of similitude associated with the σf product. This condition is derived from the skin depth or depth of penetration, which is defined by $\delta = SQRT(2/\omega\mu\sigma)$. Unfortunately, for the applications considered here it is of particular interest to go beyond this limit frequency.

[0176] One might also be tempted to normalize the frequency axis by the limit frequency. This is commonly called the frequency ratio (Nondestructive Testing Handbook, 2d Edition, Vol. 4, Electromagnetic Testing, ASNT, 1986). This may be a useful scaling but should not generally be used as a similarity criterion. The limitation of such a similitude assumption is apparent from a closer look at the parameter γ in the magnetic diffusion transfer relations presented in the surface inductance density section.

[0177] The excitation of higher order Fourier components ($n > 1$) would effect the relevant 2 magnetic diffusion time, $\tau_m = \mu\sigma l^2$. Of course in a continuum representation there are an infinite number of relevant magnetic diffusion times - one associated with each Fourier component in the infinite series of Eq. 14. The Inter-Meander Magnetometer was originally designed to impose a prescribed magnetic potential at a fixed wavelength. However, the excitation of shorter wavelength Fourier components is increased when span-wise diffusion in the conducting windings is significant, which

often occurs when the neighboring material is located a small fraction of the imposed wavelength above the sensor.

[0178] Fortunately, this additional complexity provides additional leverage and, consequently, improved selectivity, sensitivity, and dynamic range for many applications. In this section it is used to enable measurement of conductivity and thickness at a single temporal frequency.

[0179] In general, eddy current sensors provide only a measure of surface conductivity, $\sigma_s=\sigma\Delta$. This section demonstrates that the excitation of a wide range of Fourier components including short wavelengths enables the independent measurement of conductivity and thickness at a single temporal frequency.

[0180] Improved measurement performance results from the excitation of shorter spacial wavelength excitations.

[0181] First, a plot of the nonlinear parameter space for a wide range of conductivity and thickness is displayed. Second, the frequency responses over a range of foil conductivity and foil thickness are discussed and experimental validation of the span-wise diffusion continuum model is provided. Then SVD is performed to determine the optimal measurement range for two different metal foils. Finally, the actual measurement of conductivity and thickness is demonstrated for the two metal foils.

[0182] It is assumed in the remainder of this section that the height of the conducting foil is measurable by some other means as discussed in the next paragraph. It may be possible to measure the conductivity, height and thickness of a conducting layer at a single temporal frequency, but this is not attempted here.

[0183] One method for independent measurement of the foil height above the sensor is to use a temporal frequency at which the skin depth is smaller than the thickness of the metal foil but remains larger than the thickness of the conducting windings. The thickness of the conducting windings for the Inter-Meander Magnetometer used in the experiments is 25 μm. At 1.58 MHz the skin depth in copper (σ = 5.8E7 mhos/m) is about 50μm. The foils selected for the two examples must therefore be thicker than about 100 μm to permit independent measurement of the foil height at 1.58 MHz without knowledge of the foil thickness or conductivity. To demonstrate that this measurement can also be performed without knowledge of the foil conductivity, a plot of transinductance magnitude and phase is provided in Fig. 28.

[0184] From this figure it is clear that a gross estimate of the foil conductivity provides sufficient knowledge for independent measurement of the foil height. It is also clear that the foil thickness Δ, has only a small effect on the transinductance magnitude. As a result, the transinductance magnitude at 1.58 MHz will be used to adjust the height in the experimental setup. Note also that a good measure of the foil conductivity could be obtained from the phase measurement. Thus, the independent measurement of conductivity and height is possible at frequencies meeting the prescribed limitations with regard to skin depth.

[0185] The nonlinear parameter space for the transinductance magnitude and phase is plotted in Fig. 29. Lines of constant conductivity are plotted for foil conductivity, σ, ranging from 3.2×10^7 mhos/m to 6.0×10^7 mhos/m in increments of 2.0×10^6 mhos/m. Lines of constant foil thickness are plotted for foil thickness, Δ, ranging from 0.1 mm to 0.6 mm in increments of 0.0125 mm.

[0186] Several observations can be made from this plot. First, and most interesting, there is a wide range of thickness and conductivity values for which a small increase in thickness at a constant conductivity actually results in a larger transinductance magnitude.

[0187] An experimental demonstration is provided in Fig. 31 and Fig. 32. The experimental measurements are indicated by crosses and squares for the two different copper foils. The micrometer measured thickness, Δ, is indicated for each foil; and a conductivity of 5.49E7 mhos/m was used in the simulations that are indicated by solid lines. This value of conductivity is the actual value measured for the thinner foil - a demonstration of this measurement will follow. Excellent agreement is demonstrated for frequencies above the impedance analyzer 14 threshold frequency at about 100 KHz. Magnitude measurements are possible below this frequency, but accuracy is limited for transinductance magnitudes below 0.05 Ω. Figure 32 shows the unanticipated behavior. Better agreement for the thicker foil would be possible if its conductivity were also estimated and used in the simulations.

[0188] The last observation from the plot of the nonlinear parameter space in Fig. 29 relates to the top of the curve, where increasing the thickness actually causes a reversal in the phase.

[0189] Now, SVD is performed on the Jacobian for foils at a prescribed height of 0.4 mm, a drive frequency of 1.58 kHz, and for an Inter-Meander Magnetometer wavelength, λ=12.7 mm. The results are summarized in Fig. 58 and Fig. 59 for aluminum and copper foils, respectively.

[0190] As stated earlier, the condition number, c, provides a measure of the selectivity for a two-parameter estimation application. It also indicates the relative sensitivity of the two orthogonal modes associated with the singular vectors. For very thin layers (below 0.1 mm), the conditional number approaches Zero for both copper and aluminum foils. This implies that an unobservable mode exists. This mode is associated with the minimum singular value, σ_{min}, and has the associated right singular vector $[0.7\ -0.7]^T$. This is exactly what physical intuition would have predicted. For foils that are very thin compared to the imposed wavelength, a perturbation in the unknown vector along the indicated right singular vector would produce no change in the surface conductivity, $\sigma_s=\sigma\Delta$ of the foil. The next section provides a demonstration of surface conductivity estimation using a multiple frequency nonlinear least squares algorithm.

[0191] It is important to note, however, that the largest sensitivity to measurement of either foil conductivity or thick-

ness, when the other property is given, occurs at Δ=0.12 mm, where σ_{max} reaches a maximum - for aluminum foils with conductivity near 3.72E7 mhos/m, and at Δ=0.07 mm - for copper foils with conductivity near 5.8E7 mhos/m.

[0192] For thick layers, Δ above 0.6 mm, the singular vectors indicate that the thickness of the foil is essentially unobservable. However, excellent sensitivity to foil conductivity is sustained indefinitely, as the thickness increases. This is consistent with the observation that when the upper surface of the foil is farther and farther away from the sensor, the measured transinductance should become insensitive to thickness variations.

[0193] The transition between singular modes indicated by the right singular vectors is gradual between $[0.7\ -0.7]^T$ and $[1.0]^T$, and between $[0.7\ 0.7]^T$ and $[0\ 1]^T$. The crossing of the two singular modes associated with constant conductivity-thickness product, $[0.7\ -0.7]^T$, and maximum sensitivity of the conductivity-thickness product $[0.7\ 0.7]^T$ is also associated with a shifting in dominant behavior from the imposed wavelength to the shorter wavelength excitations.

[0194] The singularity points at 0.39 mm for aluminum and 0.32 mm for copper are coincident with the reversal in the variation of the Transinductance phase indicated in Fig. 29.

[0195] Two actual measurements are now demonstrated for copper and aluminum foils with thicknesses near the peak in the condition number. An expansion of the parameter space about a preliminary estimate of The operating point is provided for the two measurements in Fig. 35 and Fig. 26. The estimated foil conductivity and thickness are indicated. As a rough check of the foil thickness measurement, a micrometer measurement is provided for comparison. The error in the micrometer measurement is about 15 µm. The estimated values for foil thickness are in excellent agreement with the micrometer measured values in both cases. The conductivity estimates are also reasonable for copper and aluminum.

[0196] Note that effective thickness of a diffusion layer near the surface of a material can also be estimated using this approach. For example, a conductivity and effective thickness grid could be generated to detect and characterize titanium α-case properties or carburized steel case properties.

Multiple Frequency Measurement of Conductivity-Thickness Product

[0197] A demonstration of the measurement of the surface conductivity and height of a thin metal foil above the sensor is provided for several foils using a multiple frequency nonlinear least squares parameter estimation algorithm. This demonstration addresses applications for which $\delta >> \Delta$ and the selectivity (condition number) for conductivity and thickness is much less than one 1. No attempt is made to optimize this multiple frequency measurement.

[0198] The parameter estimation programs incorporate a package developed by Argonne National Laboratory, Minpack Project in 1980. This package uses a modified Levenberg-Marquardt method (also called Marquardt method) in which the steepest descent method is used far from the minimum and then smooth transition to the inverse Hessian method occurs as The minimum is approached (L. Ljung, System Identification: Theory for the User, Prentice-Hall NH (1987); W.H. Press et al., Numerical Recipes, The Art of Scientific computing, Cambridge U. Press (1986)).

[0199] The results for six different foils are presented in Fig. 37 and Fig. 38. For the thicker foils, the condition number has increased sufficiently to require a more robust estimation approach. In other words, for the thicker foils, it is necessary to adjust σ and Δ independently to achieve better agreement between the simulated and experimental response.

[0200] At this point it is important to emphasize that all measurements described here are both uncalibrated and absolute. The consistent agreement between simulated and experimental data provides further support for this claim. The capability to measure absolute physical and geometric properties without calibrations will provide significant cost and performance benefits to many applications.

Conductivity and Height Measurement for Thick Conducting Plates

[0201] The independent measurement of conductivity and height is a common requirement in eddy current sensors applications. However, the extremely high sensitivity of measurements to the height of a MUT often prevents accurate conductivity measurements. This is especially the case when calibration must be used and accurate location of the sensor is difficult.

[0202] In this section, the SVD-based measurement optimization techniques presented earlier are used to provide accurate independent measurement of the conductivity and height (lift-off) for relatively thick metal plates.

[0203] First, a comparison of simulated and experimental data is provided in Fig. 39 for a brass plate at various heights above the sensor. In this case, the conductivity was adjusted in the simulations to obtain visual agreement with the experimentally measured phase.

[0204] SVD is now performed on the new Jacobian. Plots of the condition number and associated singular values and singular vectors as a function of height and conductivity are provided in Figs. 40, 41 and 42. For good conductors, such as brass, aluminum and copper, the measurement shows excellent dynamic range and would permit sorting of a wide range of conducting materials located for this example at an unknown height between 0.03 mm and 0.5mm.

[0205] Finally, the independent measurement of height and conductivity is demonstrated in Figure 43 for an aluminum and brass plate with no calibration. The experimental data points for each plate trace out a line of constant conductivity. This provides strong support for the claims of absolute uncalibrated measurement of conductivity.

[0206] It is important to note that the multiple height measurement provides a single frequency multiple measurement approach. This will enable accurate measurement of conductivity in applications for which the conductivity is dispersive (i.e., σ varies with frequency). This should have direct application in crack detection and aging/fatigue monitoring in metal plates, foils and pipes. This provides a simple alternative to the multiple wavelength approach (J. R. Melcher, Application Serial No. 325,695 (1989), allowed, for a continuation of patent) to property estimation and can also be applied to magnetic media.

Height Measurement for High Permeability Layer

[0207] In this section, a brief evaluation of measurement performance and design issues is provided for the measurement of height for a high permeability layer.

[0208] SVD results are provided in Fig. 44 for a highly permeable layer at various heights above the sensor. In this example, the condition number is always zero. This is consistent with the fact that the phase is zero with no ground plane and zero bulk conductivity, so that only the magnitude provides useful measurement information. With a back-plane it may be possible to estimate both the height and the permeability. The optimal sensor position for measurement of small variations in layer height is approximately 0.2 mm for this example.

[0209] A wide range of potential sensor design variations is possible to enhance the sensitivity to height measurement. For demonstration purposes, a conducting back-plane (ground-plane) is introduced at 0.5 mm below the sensor. The proximity of this back-plane to the winding plane could be optimized using the SVD-based methods described earlier. This optimization is not provided here. The variation in the magnitude of the Transinductance with and without this ground plane for different heights of the highly permeable layer is demonstrated in Fig. 45a and 45b.

[0210] The measurement of transimpedance, $v_2/j\omega i_1$, is demonstrated at 1 MHz for an infinite half space of a highly permeable material (χ_m = 1E3, σ = 0.1 mhos/m - for example, a sintered powder) at the height h_a (2) above the magnetometer surface. A significant increase in sensitivity for close proximity height measurement is apparent when the ground plane is present. Measurements are possible with the HP LF 4192 Impedance Analyzer at 1 MHz; however, with the back-plane, these measurements could not easily be made below 100 KHz. Without the back-plane, measurements can typically be made as low as 20 KHz with the available instrumentation for the original winding construct from Figure 21.

[0211] It is always a good idea to check the performance of the computer simulations by plotting the spatial variations of current and vector potential. These plots are provided in Fig. 47, Fig. 48 and Fig. 49. Variations in the distribution of the currents in the secondary, and more subtly in the primary, are shown in these three figures. The current at each collocation point is denoted in these figures by o, and the vector potential by Δ.

Single Frequency Estimation of Complex Permeability

[0212] The estimation of complex magnetic susceptibility is demonstrated in this section for dispersive media with no significant bulk conductivity. The span-wise diffusion continuum model provides predictions of the response for any layered media with completely specified properties. The media selected for this demonstration is a thick layer of granular aluminum (= 1 mm particle radius) placed at two different heights above the sensor windings. This measurement is ideal for parameter estimation, since with no ground plane and no significant bulk conductivity, the universal transinductance plot in Fig. 50 can be used to graphically estimate the complex magnetic susceptibility for the granular aluminum layer. The universal plot and the fact that the transimpedance is an analytic function of the complex magnetic susceptibility permit graphical estimation at any frequency from a single "universal" plot.

[0213] In this plot, the magnetometer response, $v_2/j\omega i_1$, is plotted for a grid of complex permeability values ($\chi_n = \chi' - j\chi''$). The lines of constant χ' and χ'' are always orthogonal because $v_2/j\omega i_1$ is an analytic function of χ_m. This orthogonality is exhibited in the figure by consistently scaling the magnitude and phase axis in accordance with the logarithm of the complex transimpedance (M. C. Zaretsky, et al. Continuum properties from Interdigital Electrode Dielectrometry, IEEE Transactions on Electrical Insulation, Vol. 23, No. 6, Pp. 899-917, Dec. 1988).

[0214] The parameter estimation methodology is initiated with a first guess obtained visually from the universal transinductance plot. The secant method is then used in a root searching procedure to minimize the error, $e^*(\theta^*)$, between the experimentally measured transimpedance, $v_2/j\omega i_1$, and the predicted transimpedance (M. C. Zaretsky, et al. Continuum properties from Interdigital Electrode Dielectrometry, IEEE Transactions on Electrical Insulation, Vol. 23, No. 6, Pp. 899-917, Dec. 1988; L. Lying, System Identification: Theory of the Use, Prentice Hall, Inc., NH, 1987). The parameters, θ^*_i, are updated by $\Delta\theta^*_i$ by forming a secant using The most recent two guesses. The fact that the transimpedance is an analytic function of the complex magnetic susceptibility permits the direct use of the secant method with

parameter updates determined from (M. C. Zaretsky, et al. Continuum properties from Interdigital Electrode Diolectrometry, IEEE Transactions on Electrical Insulation, Vol. 23, No. 6, Pp. 899-917, Dec. 1988).

$$\Delta\theta_i^* = \frac{\epsilon^*(\theta_i^*)}{\left(\frac{\epsilon^*(\theta_i^*) - \epsilon^*(\theta_{i-1}^*)}{\theta_i^* - \theta_{i-1}^*}\right)} \qquad (12)$$

[0215] Parameter estimation of dispersive complex permeability is now demonstrated for the diamagnetic granular aluminum layer. The initial estimate of the derivative is obtained by simulating a second guess with a 2% variation in the real and imaginary parts of χ_m. The magnitude and phase of the transimpedance, $v_2/j\omega i_1$, is obtained experimentally using the HP LF 4192 Impedance Analyzer. In order to demonstrate absolute measurement for layered media, a 2 cm layer of granular aluminum is measured for two different heights, $h_a(3)=0$ and $_a(3)=0.8$ mm, above the magnetometer windings. Figure 51a provides the experimental measurement of transimpedance magnitude and phase at each frequency and height (note: the precision of the phase measurement with the HP LF 4192 Impedance Analyzer increases incrementally with the magnitude of the transimpedance). The input to the parameter estimation is the first guess for the real and imaginary parts of χ_m at each frequency. The program then provides updated predictions for the χ_m determined from Eq. 12. The first guess and resulting estimates for this example are provided in Figure 51b.

[0216] The estimated χ_m in Figure 51b are now used to predict the response of the sensor with the granular aluminum layer at 0.8 mm above the sensor (note: the estimated aggregate setup error is about 10% for the height above the sensor and possible variations in coverage of the active sensor region with a consistent layer of granular aluminum). Fig. 52 shows the experimental and predicted responses for the two cases ($h_a(3)=0$ and $h_a(3)=0.8$ mm) using the estimated values of χ_m from Figure 51c. Of course, the predicted and measured responses are identical for $h_a(3)=0$ since the parameter estimation routines were run for this MUT height. For $h_a(3)=0.8$ mm, the predicted response is well within the estimated 10% setup error. This result provides solid verification of the algorithms and parameter estimation methodology.

[0217] Further verification is obtained by comparison with an analytical model of conducting spheres built up from a magnetic dipole representation. If the effects of contact between the spheres is neglected, a model derived by Inkpen and Melcher (S. L. Inkoen and J. R. Melcher, Smoothing the Electromagnetic Heating Pattern In Polymers," Mid-April 1985, Vol. 25, No. 5, Pp. 289-294) applies directly. This model also neglects the effect of the fields induced in one sphere on the fields induced in neighboring spheres. Thus, some disagreement between this model and the actual measurements is expected.

[0218] The examples discussed in this section demonstrate the capability of the Inter-Meander Magnetometer and associated parameter estimation algorithms to estimate complex magnetic susceptibility for diamagnetic materials. This methodology can be applied directly to applications involving layered ferrous media. Care must be taken in that case to ensure the universality of the transimpedance plots. If universal plots are not obtainable the only adjustment in the methodology is the required use of frequency dependent transimpedance plots to obtain a first guess at each frequency.

Conductivity and Permeability Estimation for Homogeneous Infinite Half Space

[0219] The bulk conductivity introduces shape variance into the magnitude-phase plots as a function of drive frequency. Although it is possible that universal plots may exist for a properly normalized transimpedance in specific examples, obtaining a general universal plot is unlikely. Furthermore, unlike the real and imaginary parts of the complex permeability, the transimpedance can not be represented over the entire relevant parameter space as an analytic function of a complex parameter incorporating both the permeability and the conductivity (e.g., for electroquasistatics such a parameter is $\varepsilon^* = \varepsilon' - j\varepsilon'' = \varepsilon - j\sigma/\omega$). However, there are regions of practical importance over which the transimpedance exhibits some of the same properties of an analytic function. This implies that all derivatives exist and are continuous at all points in the region; satisfaction of the Cauchy-Riemann equations is also a necessary condition for analyticity (R. V.Churchill, and G. W. Brown, "Complex Variables and Applications", McGraw-Hill, NY, 1984; F. B. Hildebrand, "Advanced Calculus for Applications", Prentice-Hall, N5, 1976). The graphical analog states that in regions of analyticity with respect to a complex parameter space the magnitude vs. phase plot will always exhibit orthogonality between lines of constant real part and lines of constant imaginary part. In the case discussed here, the magnitude vs.

phase plot for conductivity and permeability does approach this property for certain parameter space regions.

[0220] This is demonstrated in Figures 54 and 55 for 1 KHz and 10 MHz. Clearly, even by scaling these plots in accordance with Eq. 51 the desired orthogonal characteristic is not exhibited over the entire relevant parameter space. The double-valued nature of the magnitude vs. phase plot at 10 MHz and The saturation of the magnitude for large values of μ,σ are related to magnetic diffusion in the MUT. Two characteristics are most apparent. First, as the permeability, μ, increases, the transimpedance magnitude generally increases at a given conductivity, σ. This is the result of an increased inductive coupling between the primary and secondary windings. Second, as The conductivity increases for a given permeability, the transimpedance magnitude decreases. This is the result of a reduction in inductive coupling to the secondary due to increased shielding associated with decreasing magnetic skin depth in the measured media. In the double valued region, the skin depth, decreases significantly with μ at 10 MHz resulting in increased shielding. The result is a region over which different combinations of permeability and conductivity result in the sane transimpedance magnitude and phase. The independent estimation of μ and σ could also be optimized using the SVD-based method described earlier. This is not shown here.

Increased Selectivity

[0221] The region of high selectivity (i.e. the region where the grid lines are nearly orthogonal) can be expanded by using a meandering (figure 10 or 11) or single turn (figure 4, 5, 6 or 7) (not embodying the invention) winding with a spatial wavelength, λ, that is on the same order or smaller than the skin depth at the selected operating frequency. This is apparent from Eg. 8, where the parameter, γ, indicates the tradeoff between the wavenumber, k, and the term $\omega\sigma\mu$ which can be rewritten as $2/\delta^2$, where δ is the skin depth. This permits the independent measurement of conductivity and permeability for homogeneous plates and the measurement of conductivity and permeability distributions near the surface of heat treated or carburized steel parts. A near real-time measurement of the conductivity and permeability distribution near the surface of a carburized steel part would provide significant economic savings and quality enhancement potential for many applications, such as bearing manufacturing, which currently use destructive means to measure properties such as percent carbon content near the surface of carburized parts.

[0222] As in the prior Melcher Patent, U.S. Patent No. 5,015,951, May 14, 1991, with any of the above applications we can use multiple primaries.

Double-Sided Measurement

[0223] Two new configurations are now proposed for measurement of geometric and physical properties of a layer of conducting or magnetic media. The proposed apparatus might incorporate a winding construct similar to the previously discussed Inter-Meander Magnetometer structure shown in Fig. 10.

[0224] The measurement of complex permeability, for example, might be accomplished with a new construct that incorporates a set of two identical Inter-Meander Magnetometer structures located above and below the layer of magnetic media. The inherent symmetry of the resulting apparatus provides for two modes of operation. Schematics of these two operating modes are provided in Fig. 56. The odd mode is generated by applying the excitation currents or voltages a half wavelength out of phase, as shown in the figure. In this mode, the magnetic flux normal to the center line (in the x direction) of the thin layer is exactly zero for all y. In the even mode, the excitation is in phase, as shown, and the magnetic field intensity in the y direction at the center line of the layer is exactly zero for all y.

[0225] Information obtained from measurements in each of these modes is then combined to obtain estimates of the property of interest. The variation of these properties as a function of an external bias field could also be considered, since the measurement is based on a perturbation of the excitation fields.

Equivalents

[0226] While the invention has been particularly shown and described with reference to preferred embodiments thereof, it will be understood to those skilled in the art that various changes in form and details may be made therein without departing from the spirit and scope of the invention as defined by the appended claims.

Claims

1. A magnetometer for measuring a geometric property and the conductivity of a material comprising:

   an electromagnetic winding structure capable of imposing a magnetic filed in the material when driven by an electric signal and sensing an electromagnetic response;
   an analyzer for applying the electric signal to the winding structure to define a spatial wavelength associated

with the imposed magnetic field in the material, the electric signal having a preselected temporal excitation frequency; and

a property estimator coupled to the winding structure for receiving sensed responses, the property estimator accessing a property estimation grid for translating sensed responses into substantially independent geometric property and conductivity estimates at the single preselected temporal excitation frequency.

2. The magnetometer as claimed in claim 1 wherein the estimation grid includes magnitude and phase values of impedance responses of the winding structure computed from a model of the electromagnetic winding structure and the sensed responses are translated into independent geometric property and conductivity estimates through interpolation within the property estimation grid.

3. The magnetometer of claim 2 wherein the impedance responses are transimpedance responses.

4. A magnetometer as claimed in claim 2 wherein the impedance responses are transinductance responses.

5. A magnetometer as claimed in any preceding claim wherein the geometric property is the actual or effective thickness of a surface layer of the material.

6. A magnetometer as claimed in any of claims 1-4 wherein the geometric property is the proximity of the winding structure to the material.

7. A magnetometer as claimed in any of claims 1-4 wherein the geometric property is the thickness of a surface region with different electrical properties than the core material.

8. A magnetometer as claimed in any preceding claim wherein the property estimator generates the property estimation grid by successively implementing a model, which for each implementation provides a prediction of an electromagnetic response for a geometric property and conductivity based on a set of parameters characterizing the winding structure and the material.

9. A magnetometer as claimed in any preceding claim wherein the winding structure is formed of a plurality of electromagnetic winding elements arranged into a meandering pattern.

10. A magnetometer as claimed in any preceding claim wherein the winding structure is capable of being adapted to conform to a curved surface of the material.

11. A magnetometer as claimed in any preceding claim wherein the analyzer applies multiple electric signals each having a single preselected temporal excitation frequency to the winding structure for measuring the dependence of conductivity on temporal excitation frequency.

12. A method of measuring a geometric property and the conductivity of a material comprising:

imposing a magnetic field in a material by driving an electromagnetic winding structure with an electric signal to define a spatial wavelength associated with the imposed magnetic field in the material, the electric signal having a preselected temporal excitation frequency;

sensing an electromagnetic response of the electromagnetic winding structure; and

accessing a property estimation grid for translating sensed responses into substantially independent geometric property and conductivity estimates at the single preselected temporal excitation frequency.

13. The magnetometer as claimed in claim 12 wherein the estimation grid includes magnitude and phase values of impedance responses of the winding structure computed from a model of the electromagnetic winding structure and the sensed responses are translated into independent geometric property and conductivity estimates through interpolation within the property estimation grid.

14. The magnetometer of claim 13 wherein the impedance responses are transimpedance responses.

15. A magnetometer as claimed in claim 13 wherein the impedance responses are transinductance responses.

16. A magnetometer as claimed in any of claims 12-15 wherein the geometric property is the actual or effective thick-

ness of a surface layer of the material.

17. A magnetometer as claimed in any of claims 12-15 wherein the geometric property is the proximity of the winding structure to the material.

18. A magnetometer as claimed in any of claims 12-15 wherein the geometric property is the thickness of a surface region with different electrical properties than the core material.

19. A magnetometer as claimed in any of claims 12-18 wherein the property estimator generates the property estimation grid by successively implementing a model, which for each implementation provides a prediction of an electromagnetic response for a geometric property and conductivity based on a set of parameters characterizing the winding structure and the material.

20. A magnetometer as claimed in any of claims 12-19 wherein the winding structure is formed of a plurality of electromagnetic winding elements arranged into a meandering pattern.

21. A magnetometer as claimed in any of claims 12-20 wherein the winding structure is capable of being adapted to conform to a curved surface of the material.

22. A magnetometer as claimed in any of claims 12-21 wherein the analyzer applies multiple electric signals each having a single preselected temporal excitation frequency to the winding structure for measuring the dependence of conductivity on temporal excitation frequency.

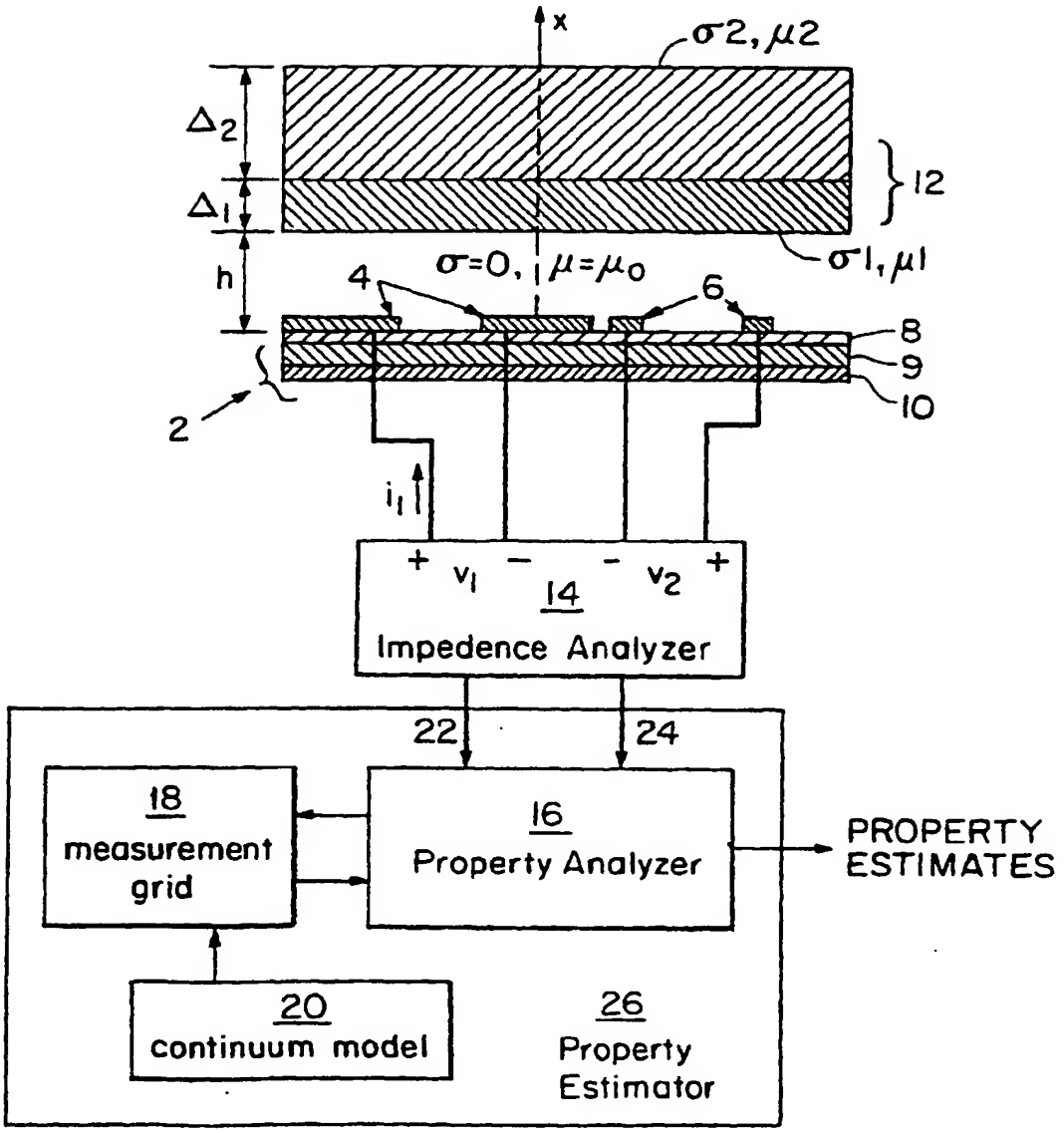

FIG. 1

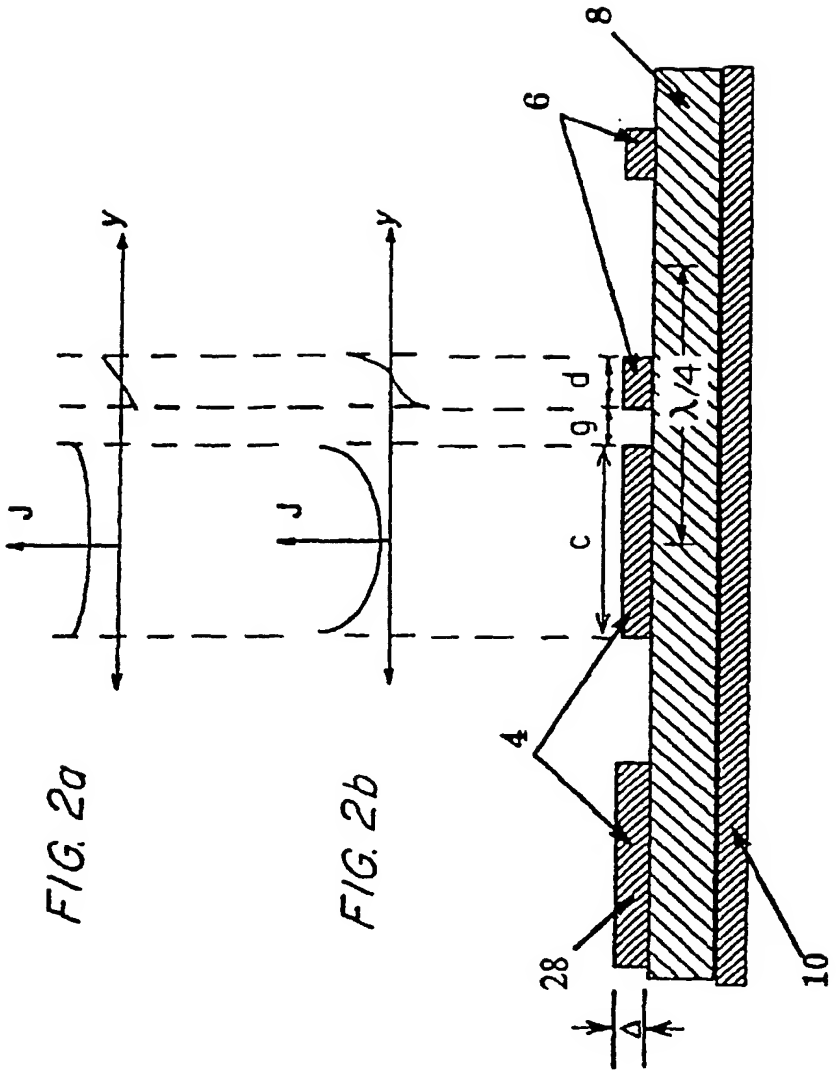

FIG. 2a

FIG. 2b

FIG. 2c

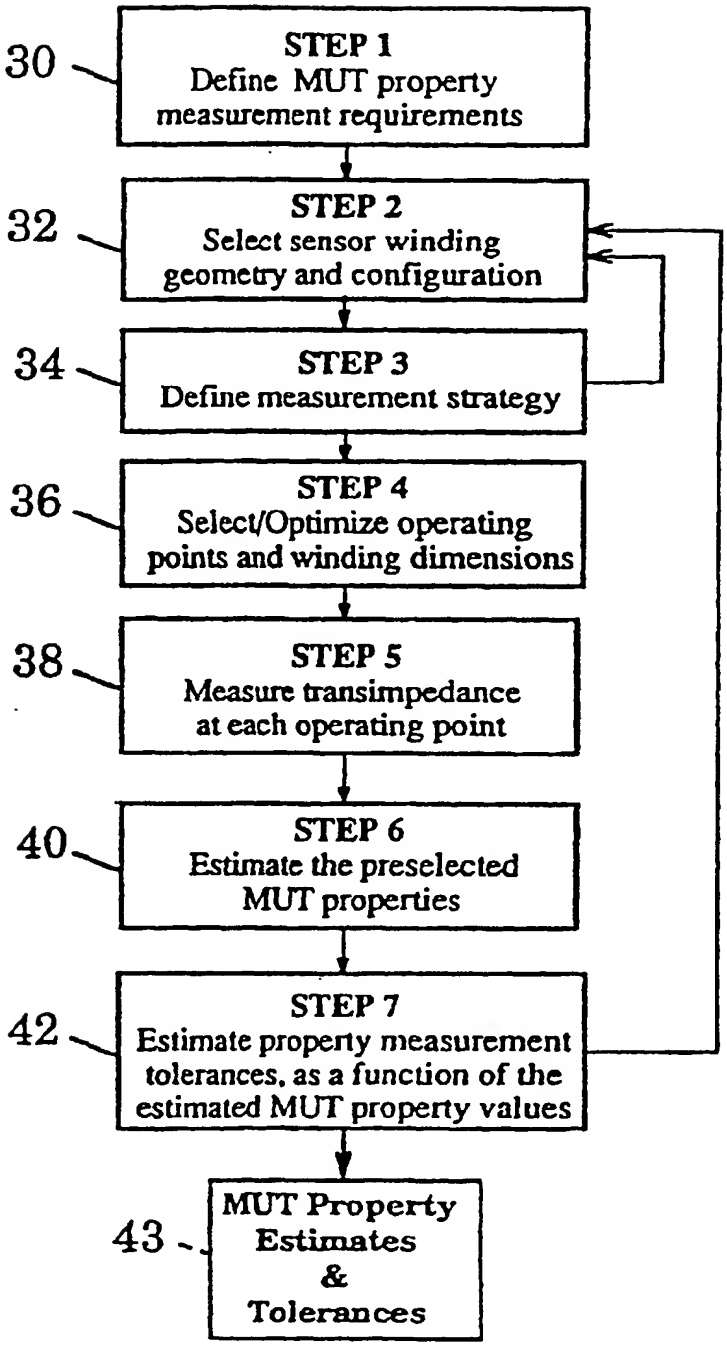

FIG. 3

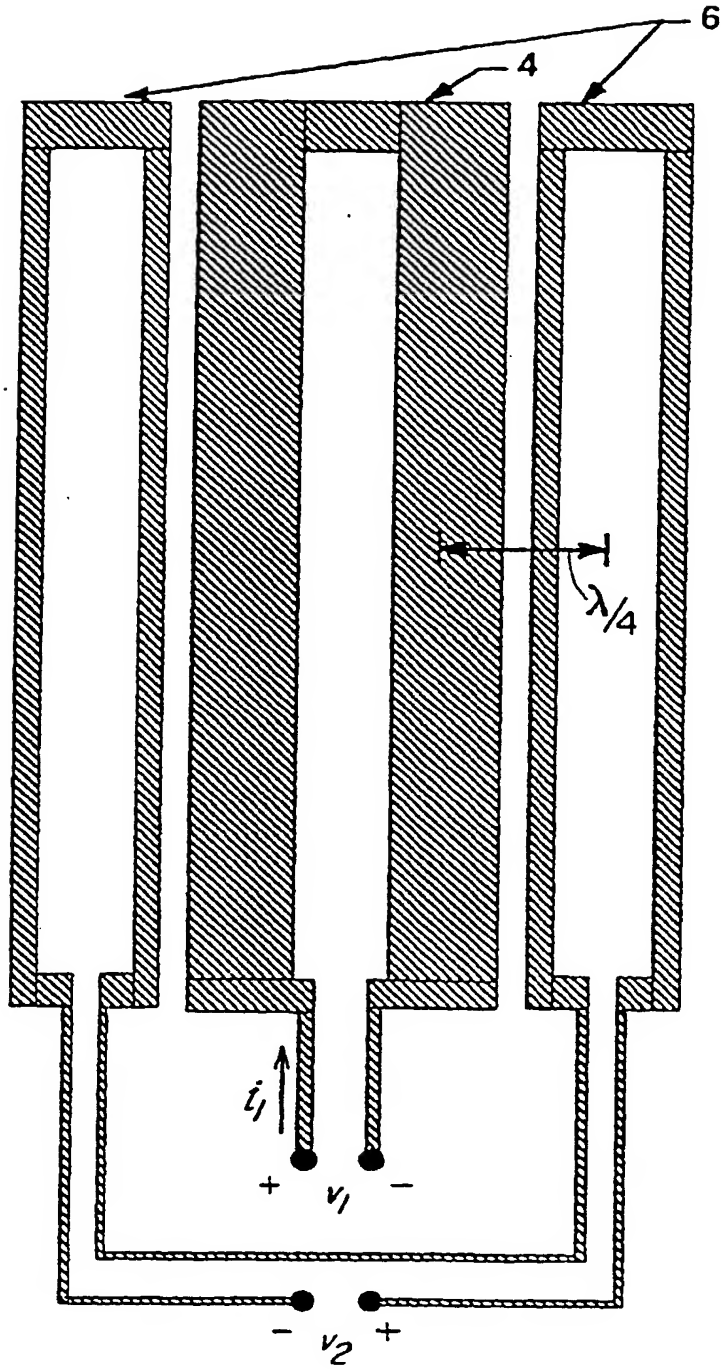

FIG. 4

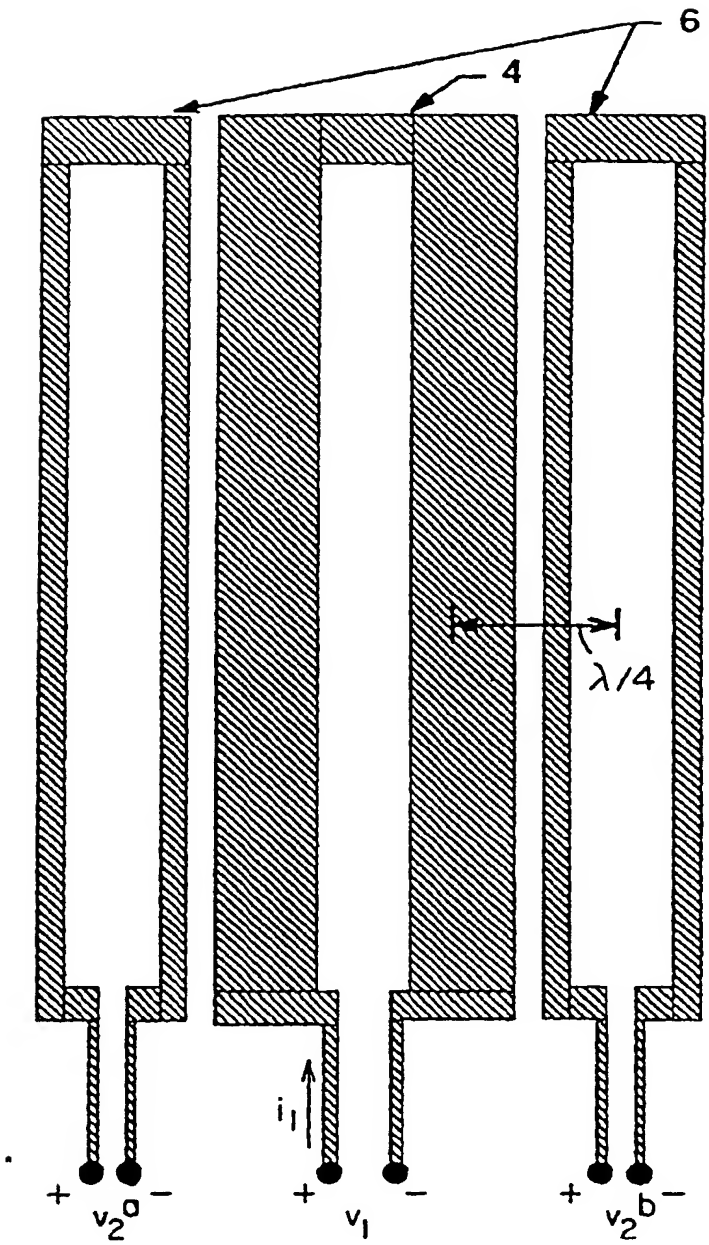

FIG. 5

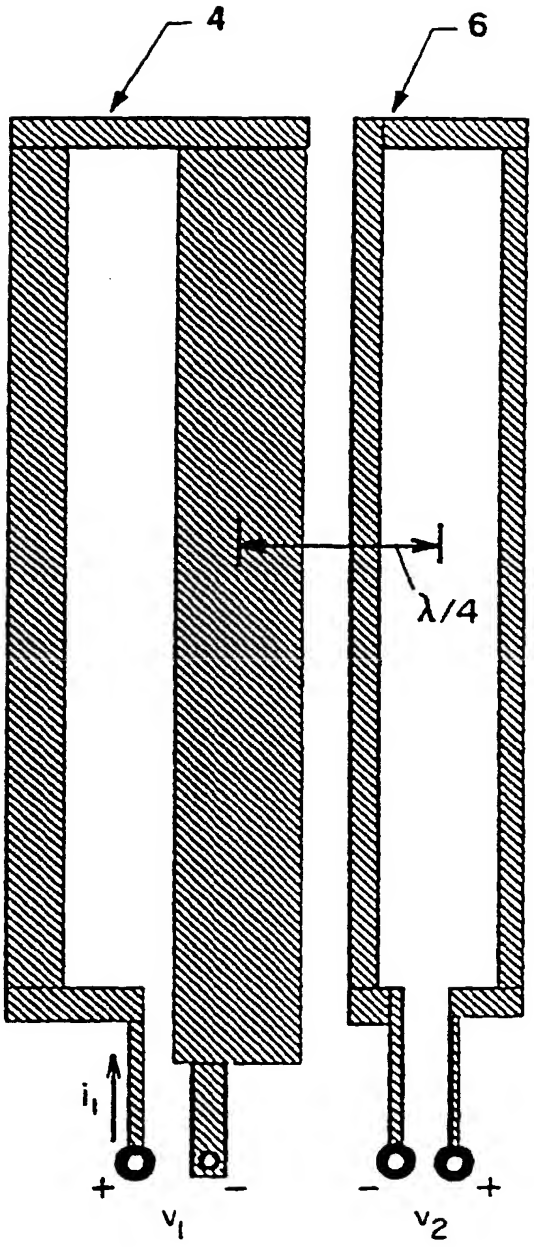

FIG. 6

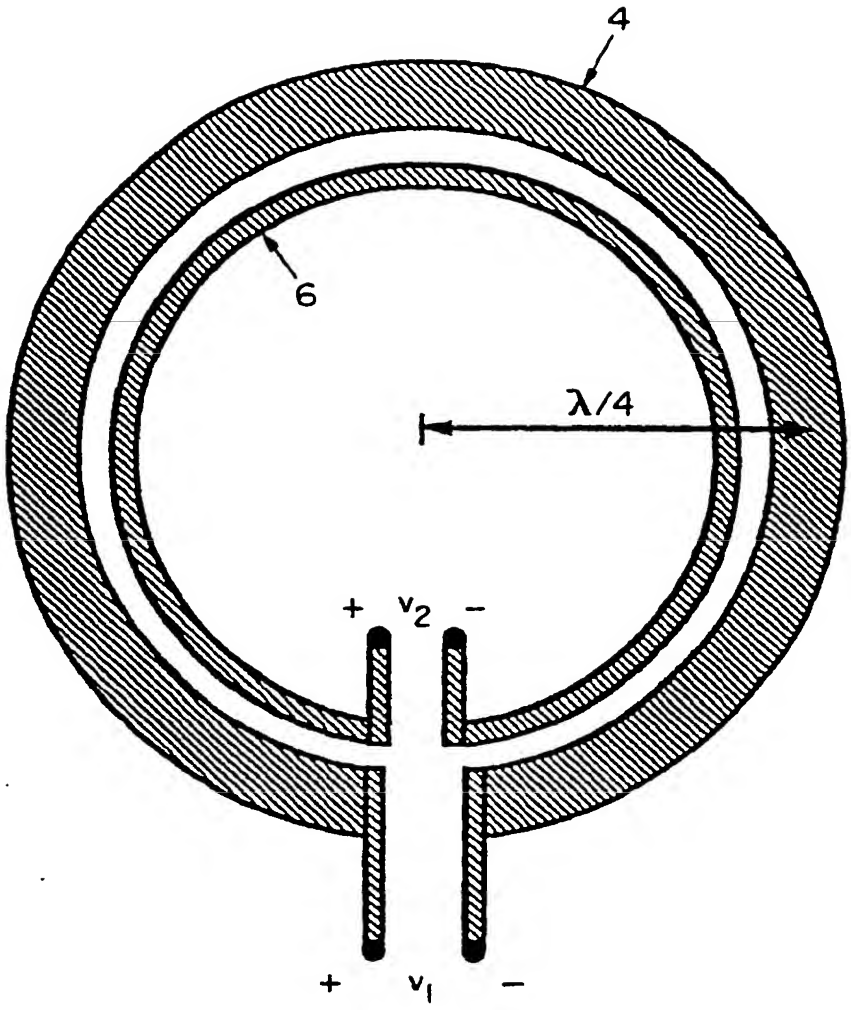

FIG. 7

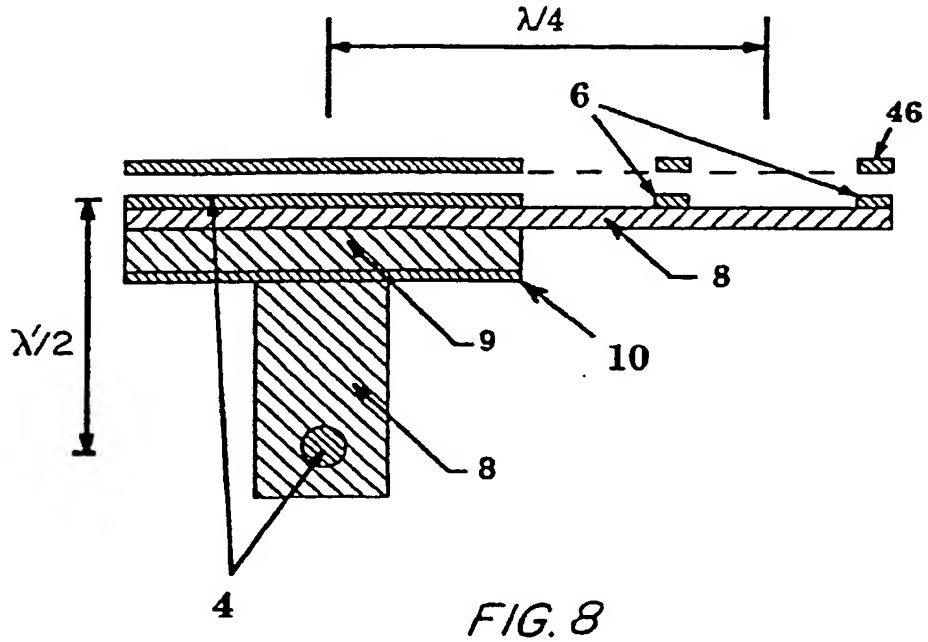

FIG. 8

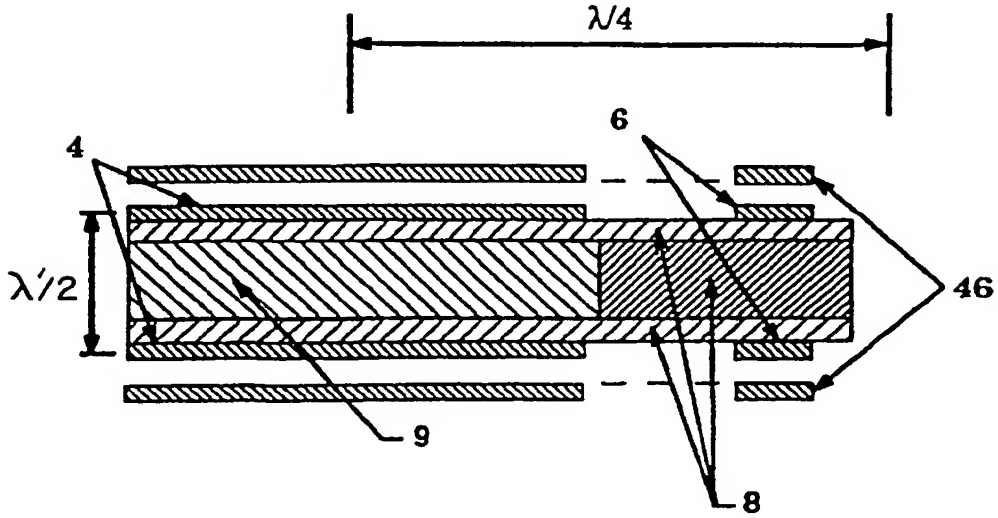

FIG. 9

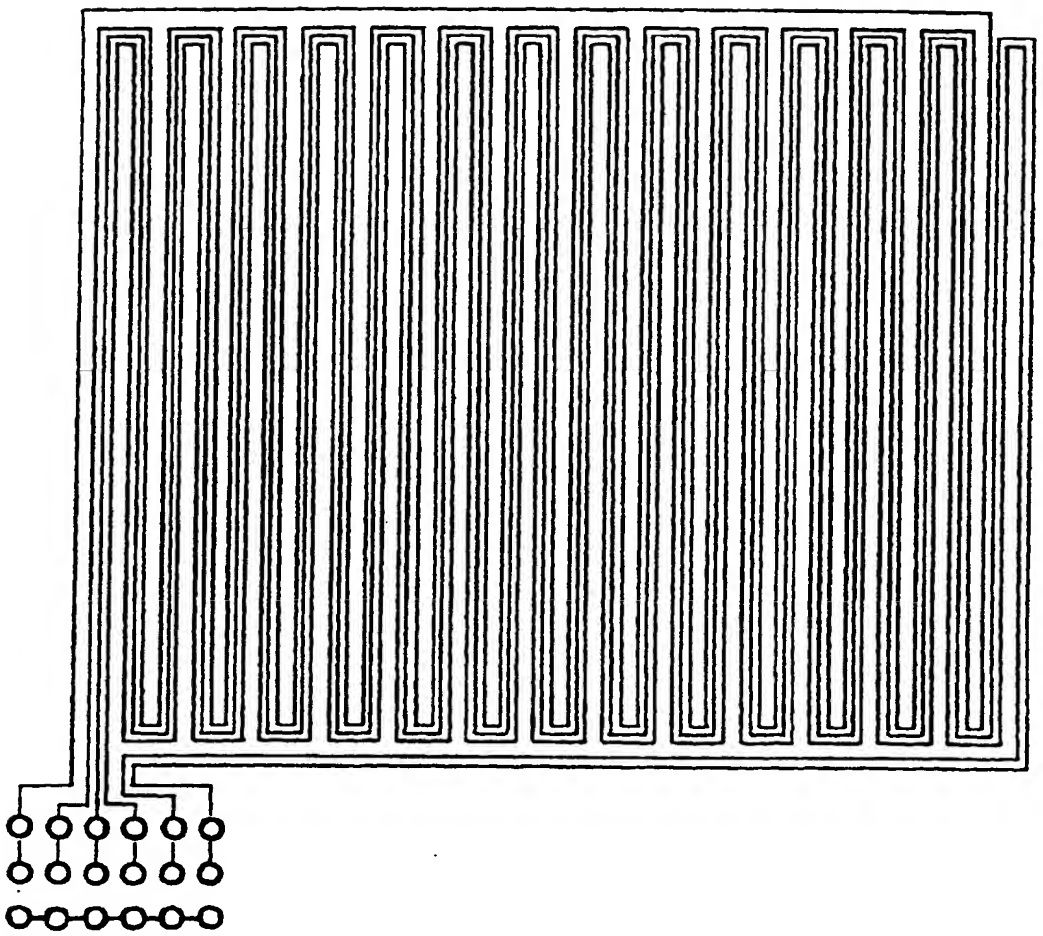

FIG. 10

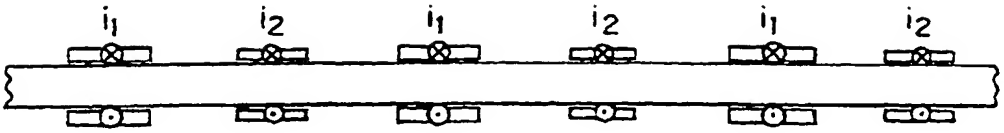

FIG. 11a

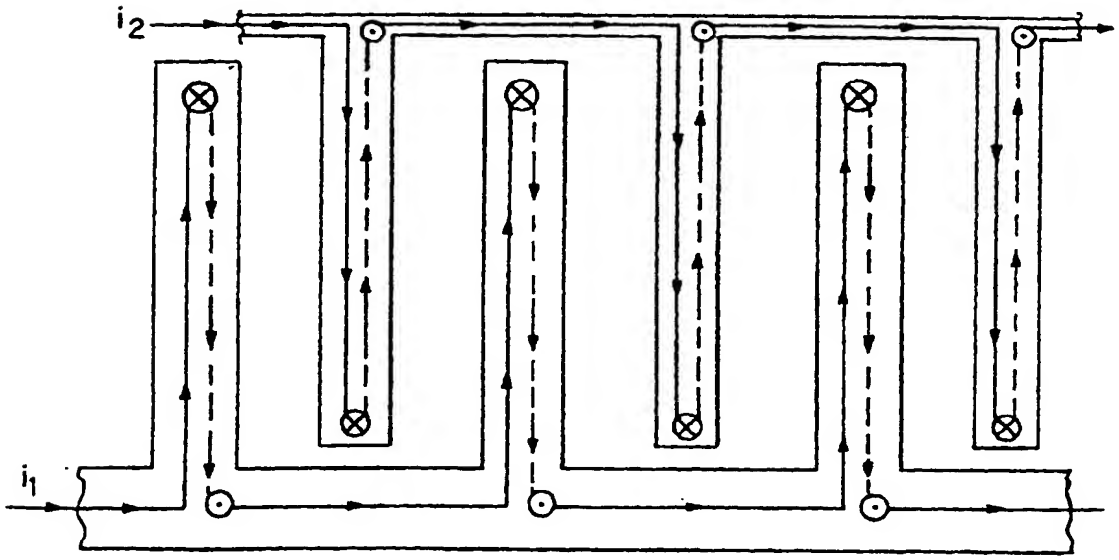

FIG. 11b

Large Radius Parts

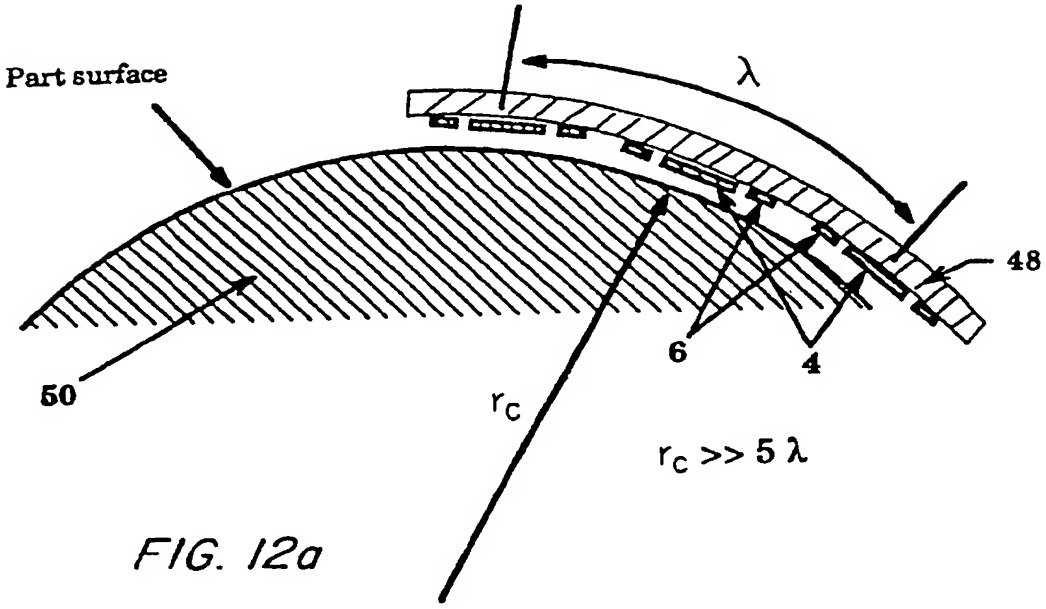

FIG. 12a

Small Radius Parts

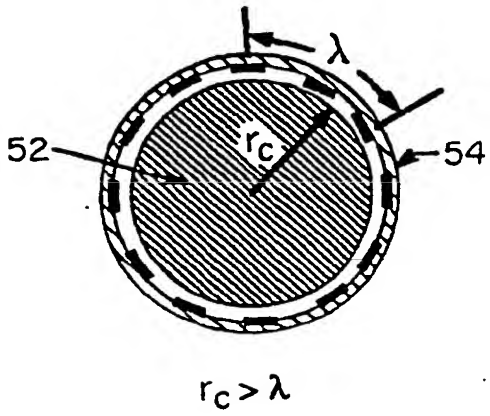

FIG. 12b

Spiralled Sensor Construct

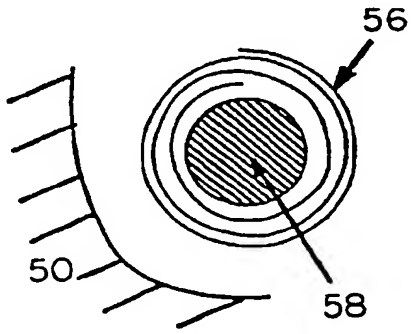

FIG. 12c

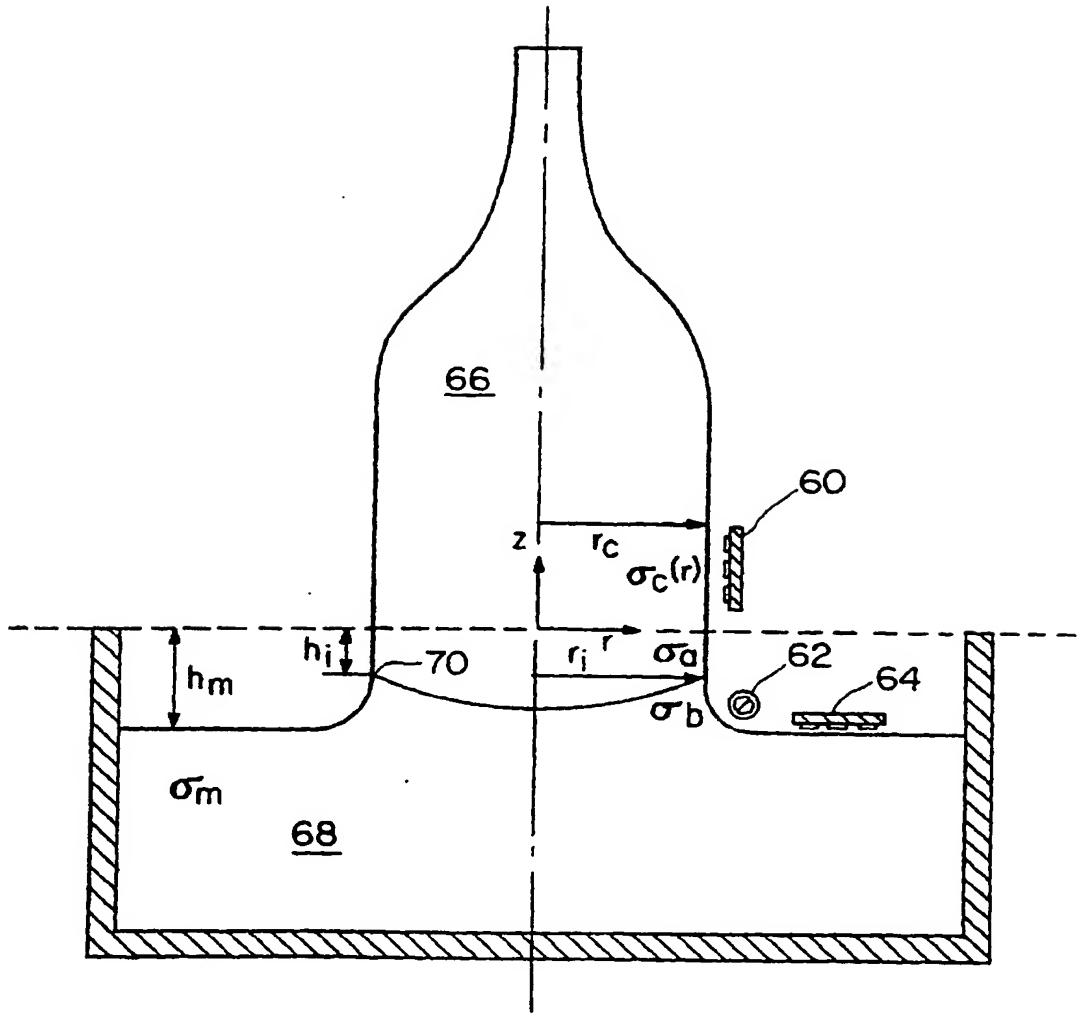

FIG. 13

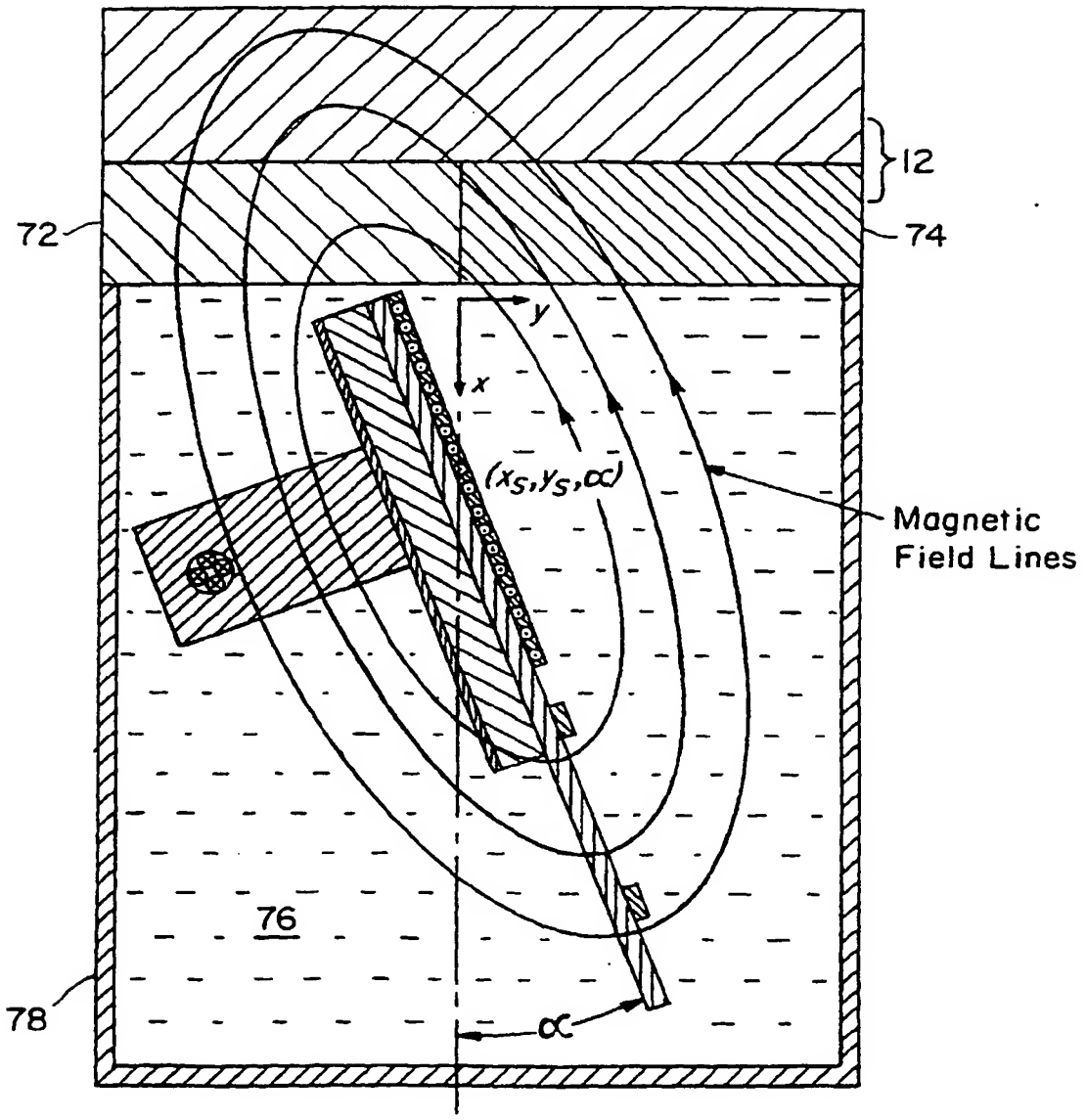

FIG. 14

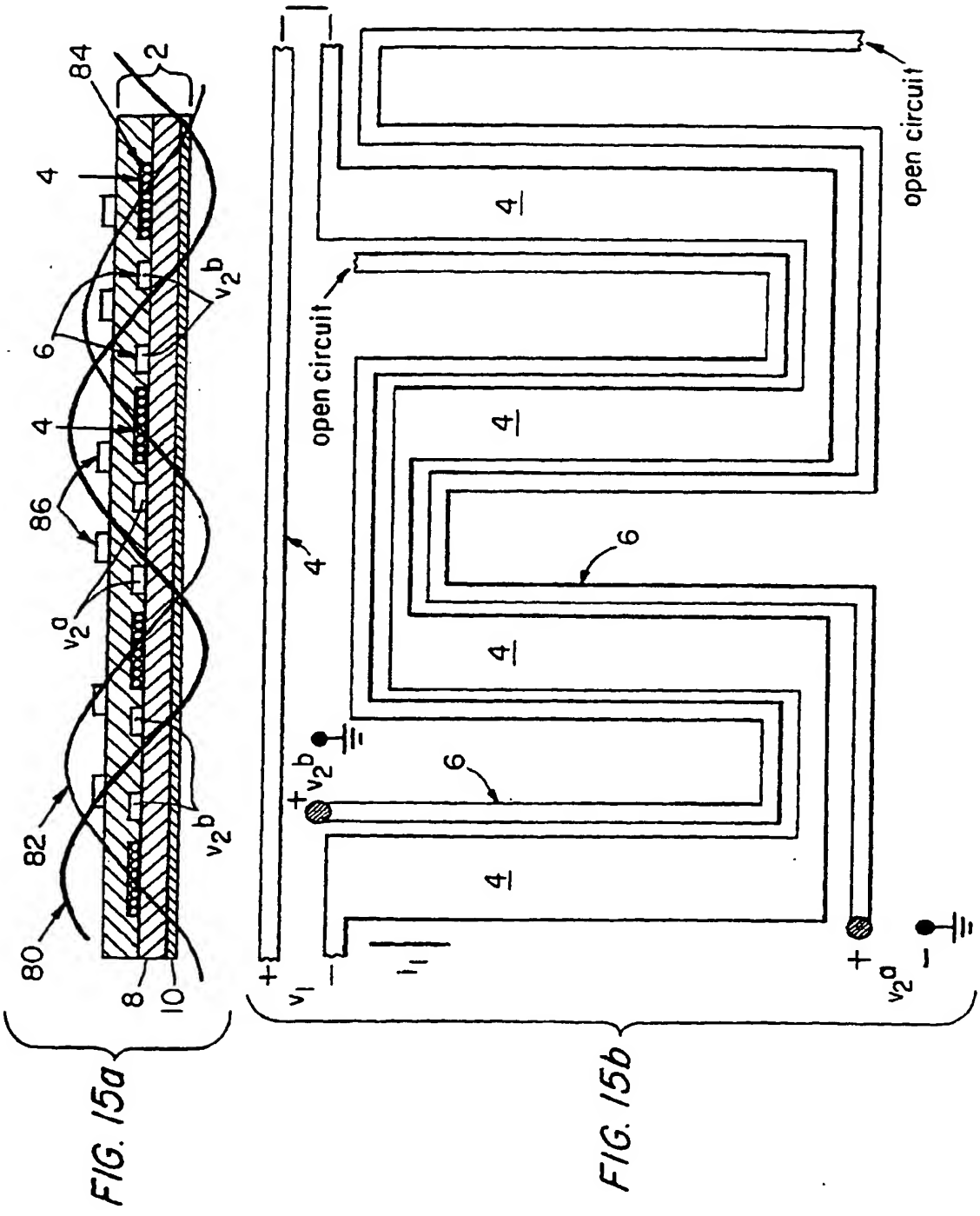

FIG. 15a

FIG. 15b

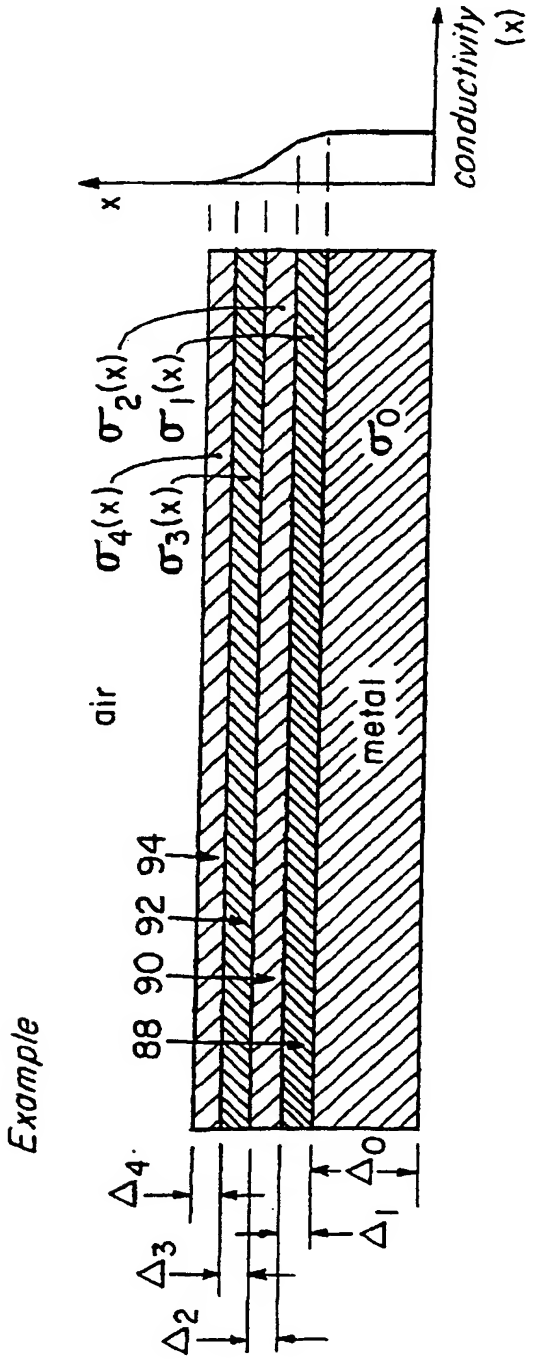

FIG. 16

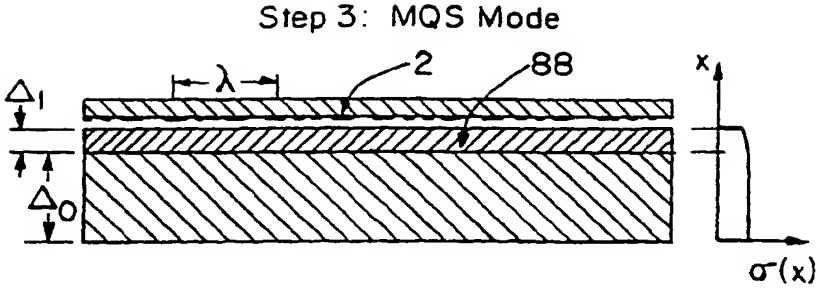

FIG. 17a

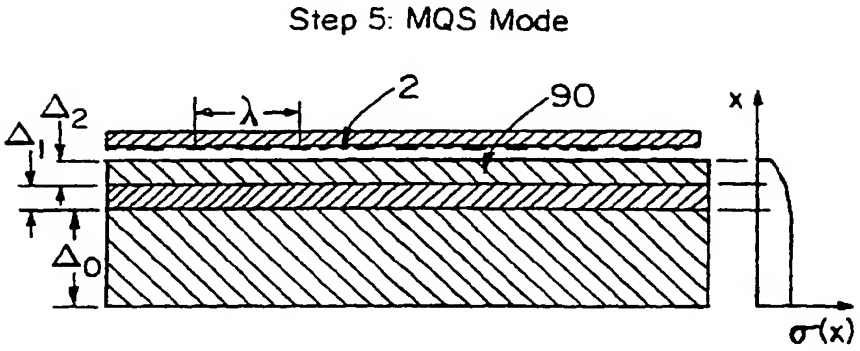

FIG. 17b

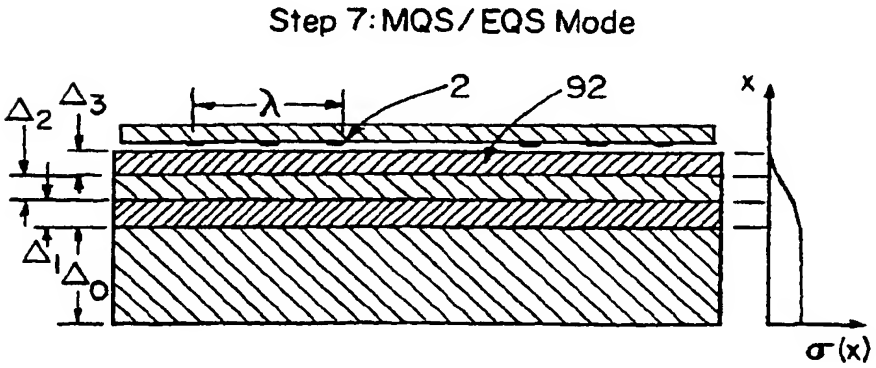

FIG. 17c

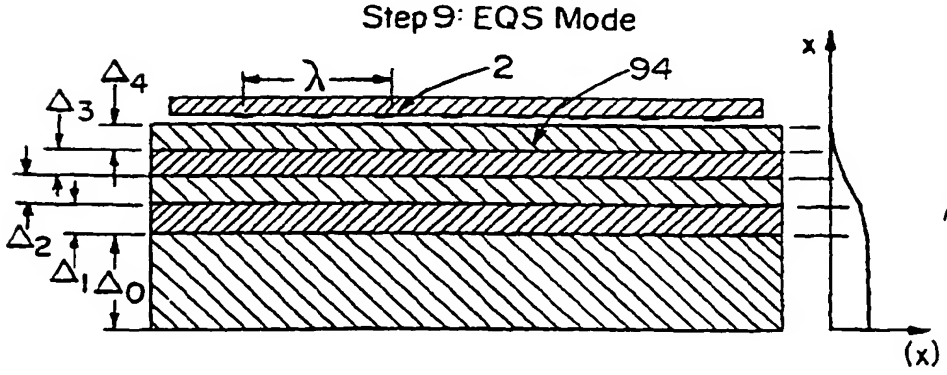

FIG. 17d

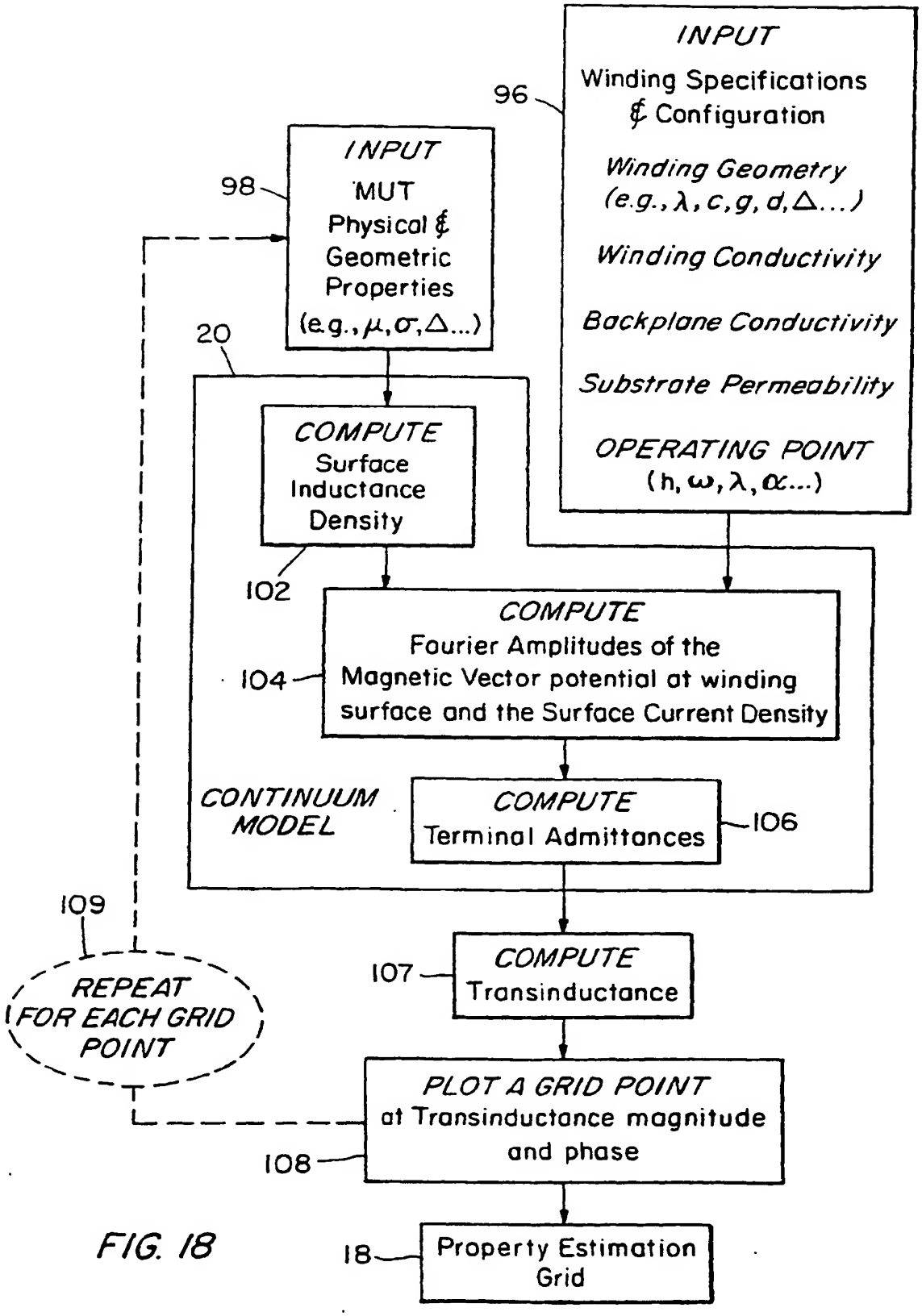

FIG. 18

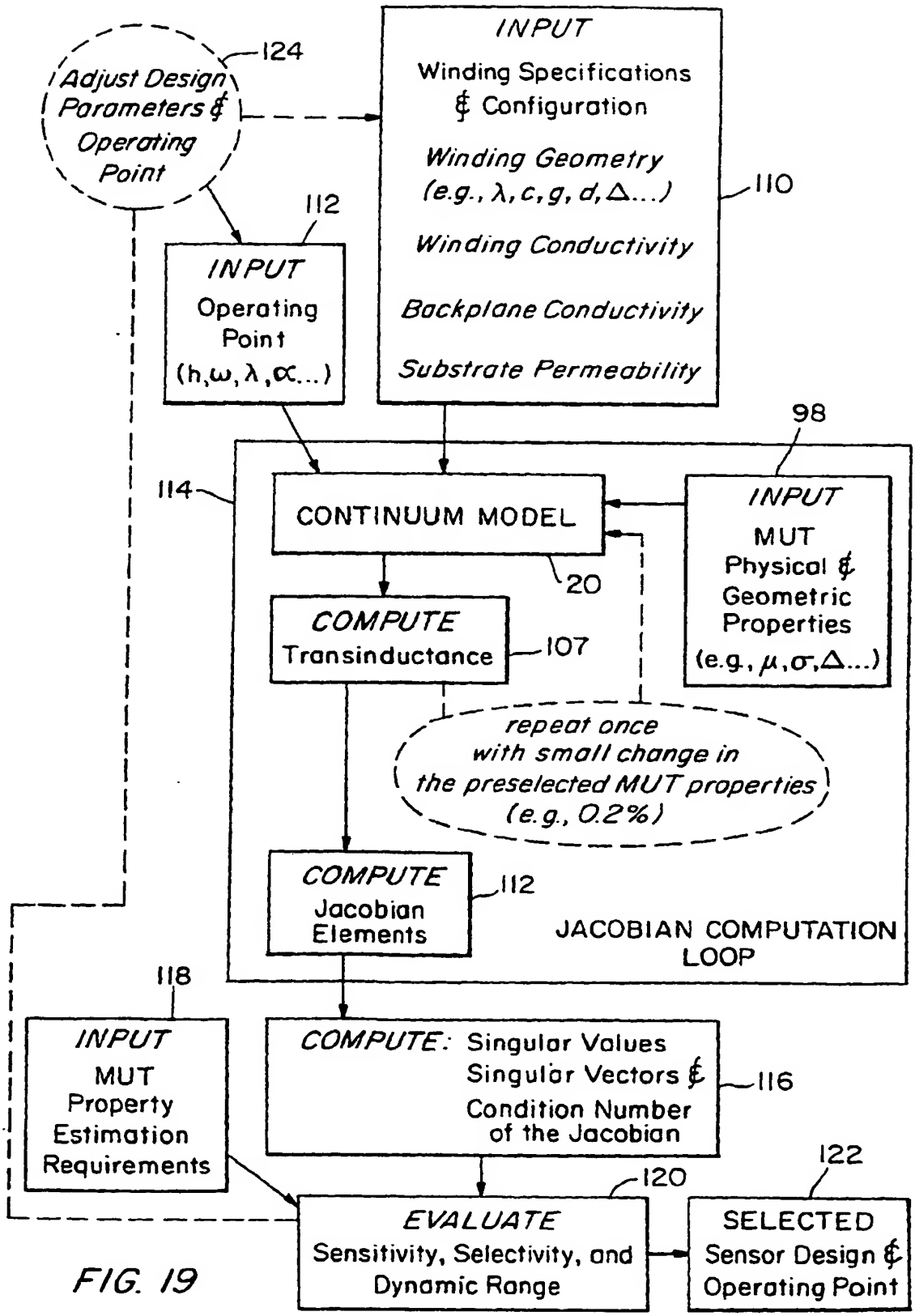

FIG. 19

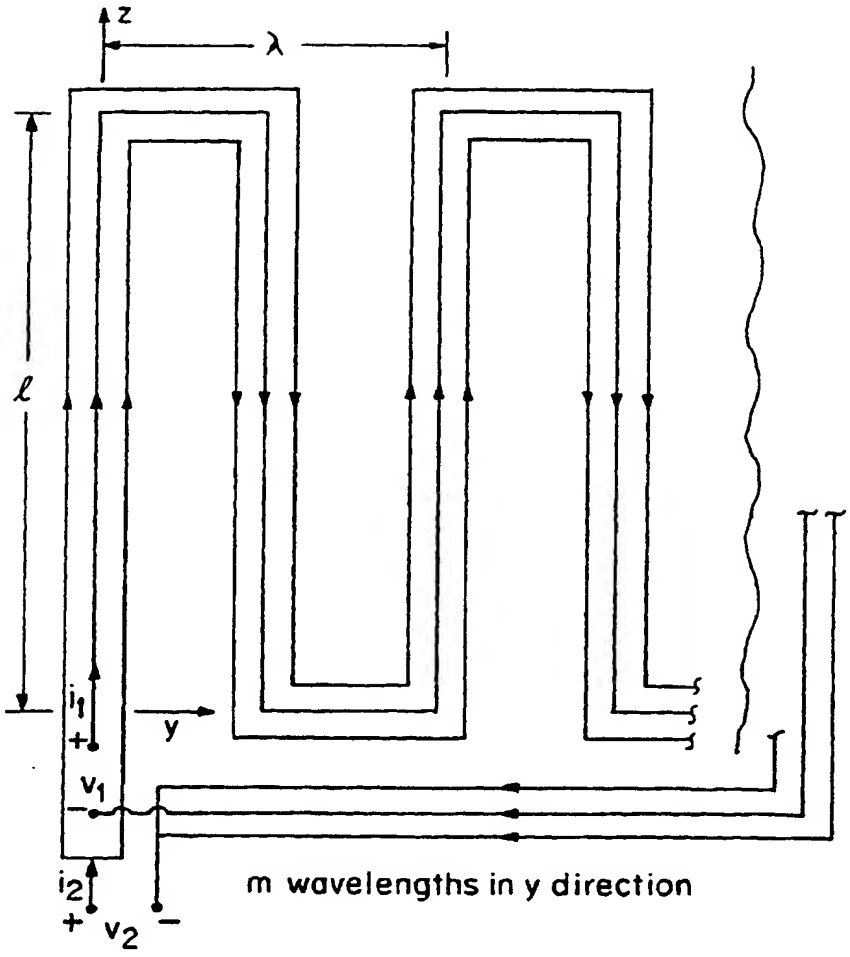

FIG. 20

MAGNETOMETER PARAMETERS										
	Geometric (lengths in mm)									
Construct	λ	Δ	c	d	g	l	m	σ(mhos/m)	z_l	freq
original	12.7	0.025	1.27	0.65	0.6	100	10	5.8E7	∞	scan
(a)	10.0	0.05	2.00	0.100	0.100	100	10	5.8E7	∞	scan

FIG. 21

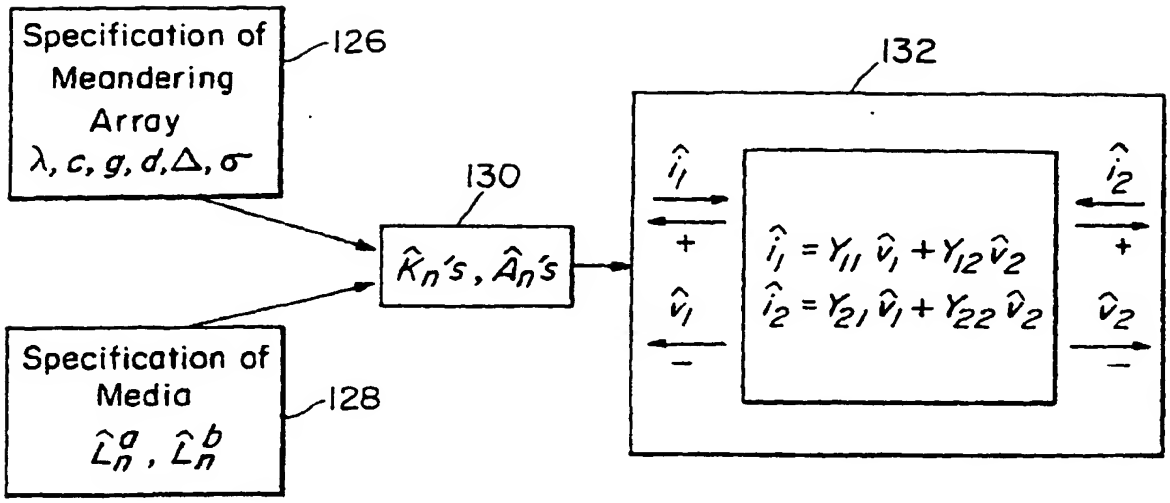

FIG. 22

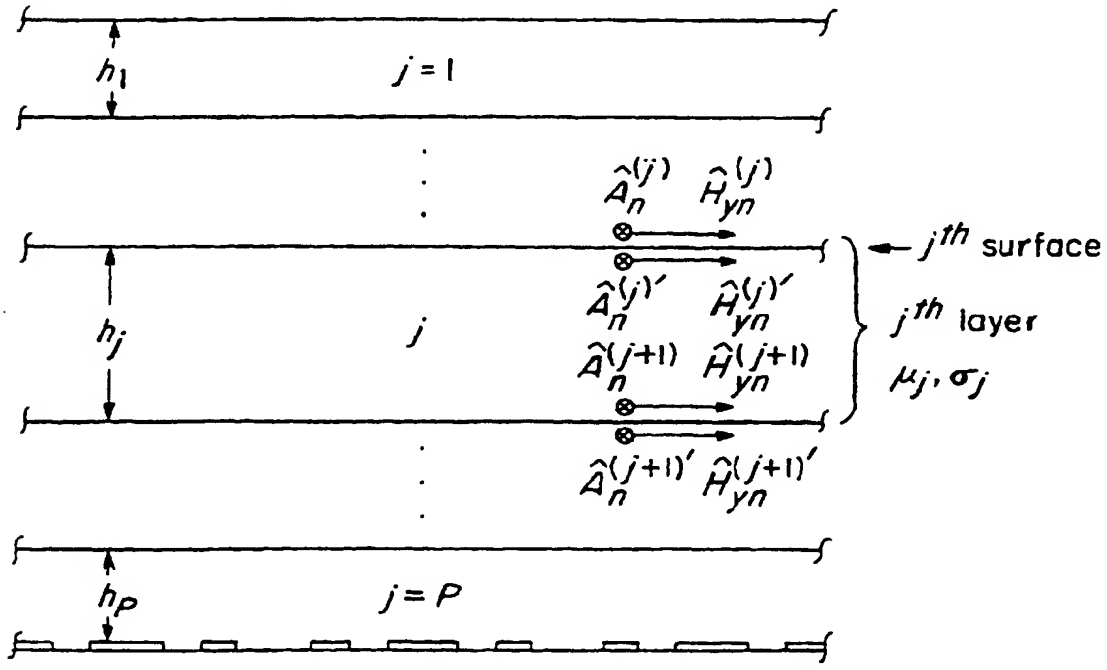

FIG. 23

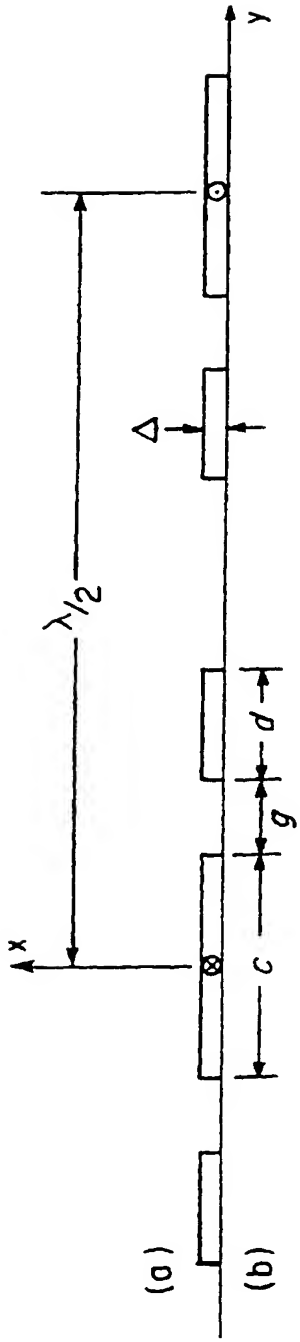

FIG. 24a

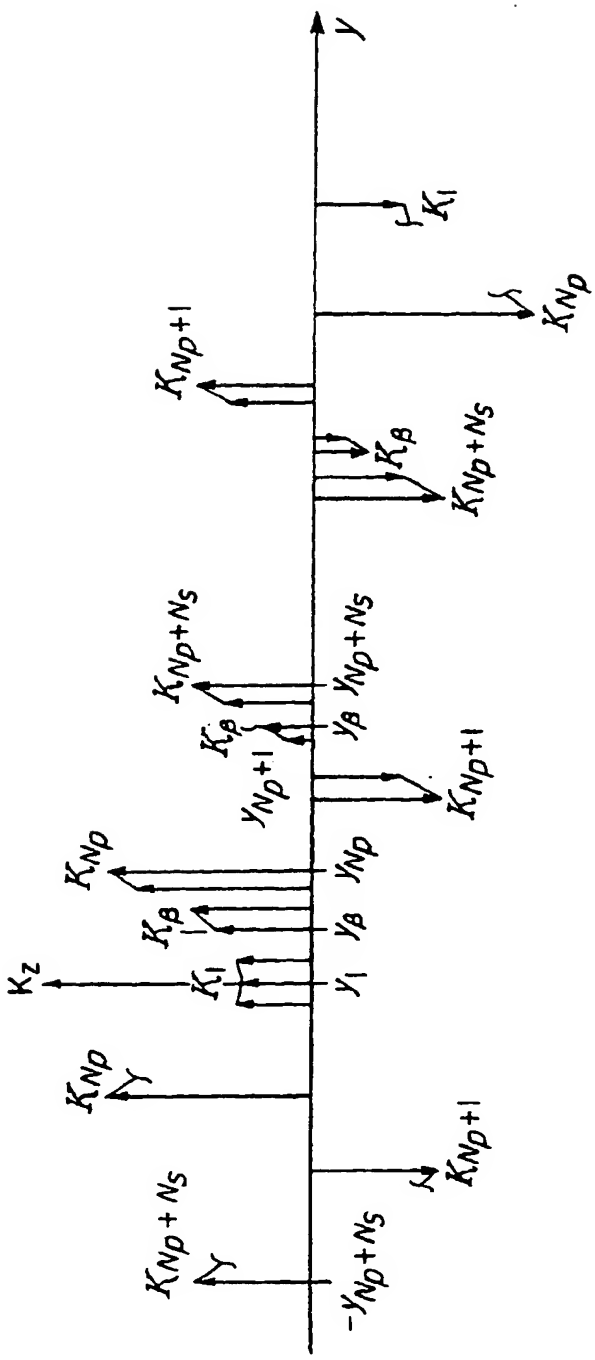

FIG. 24b

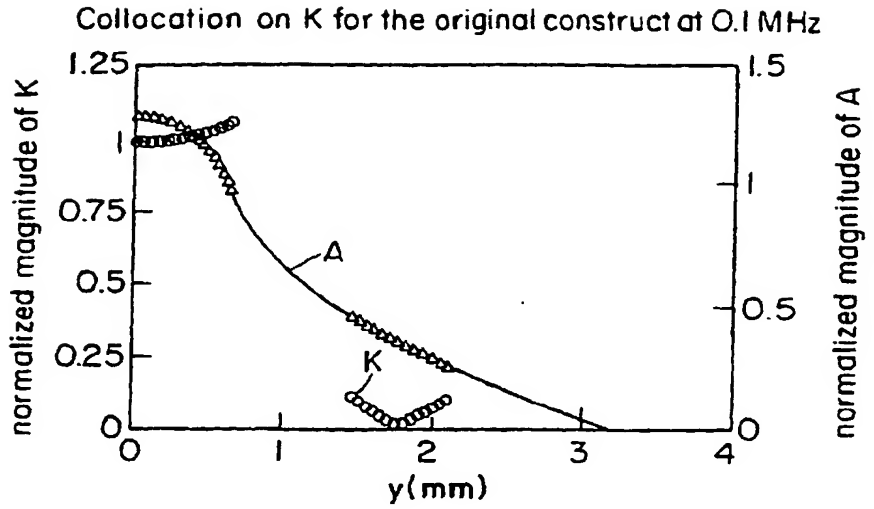

FIG. 25d

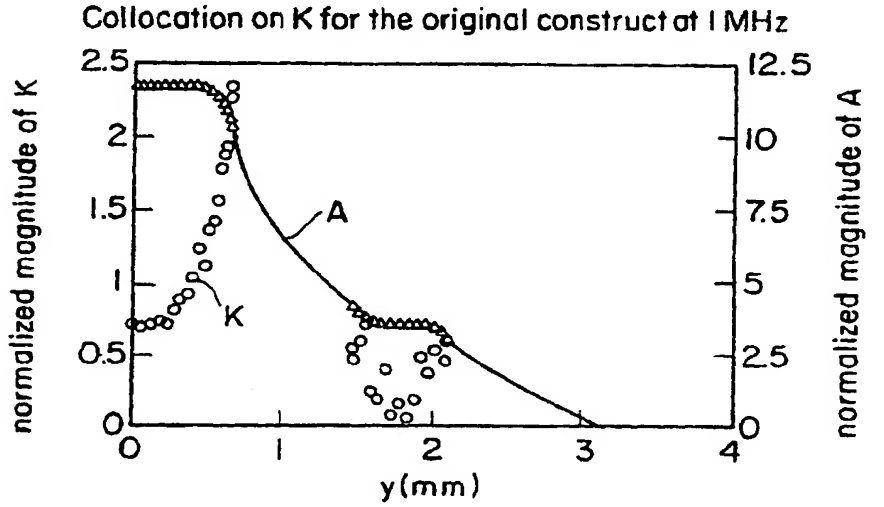

FIG. 25e

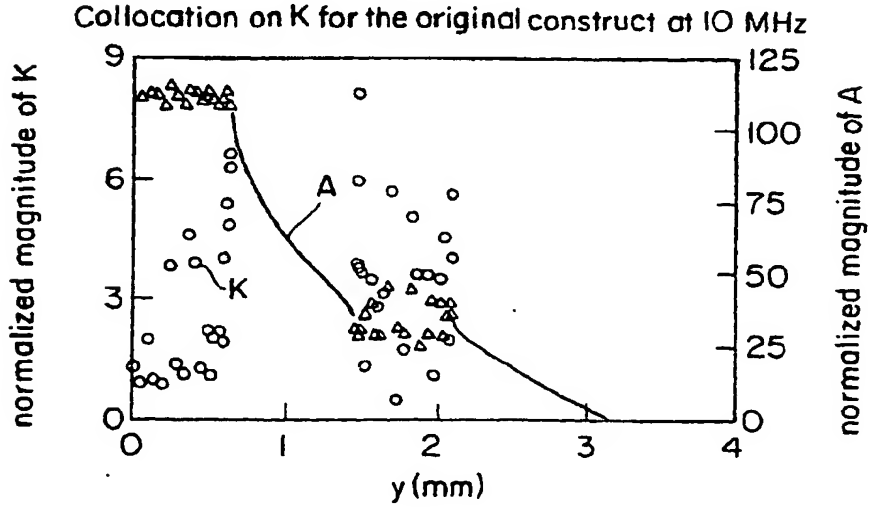

FIG. 25f

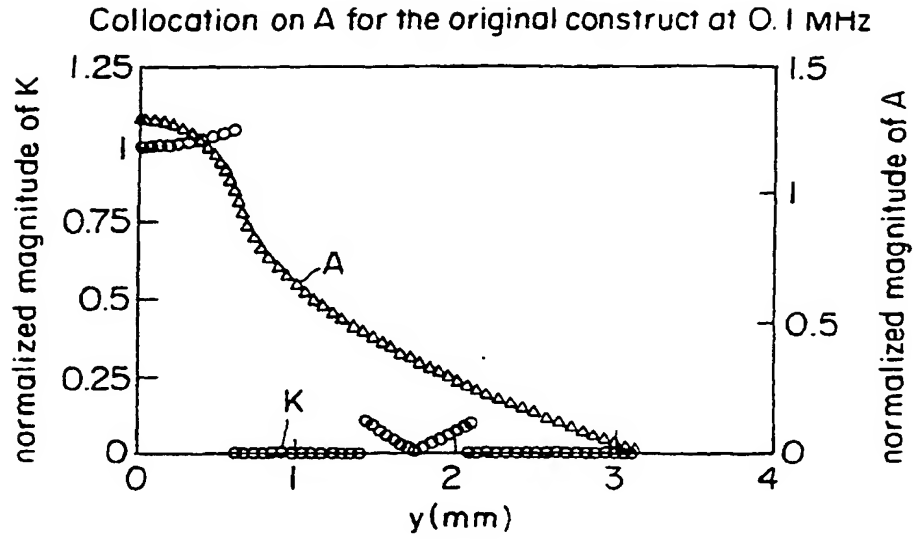

FIG. 25a

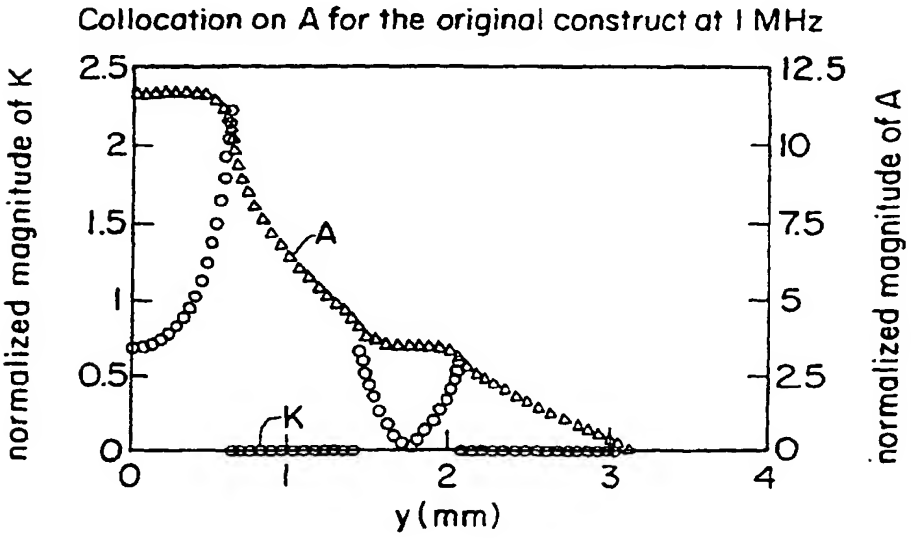

FIG. 25b

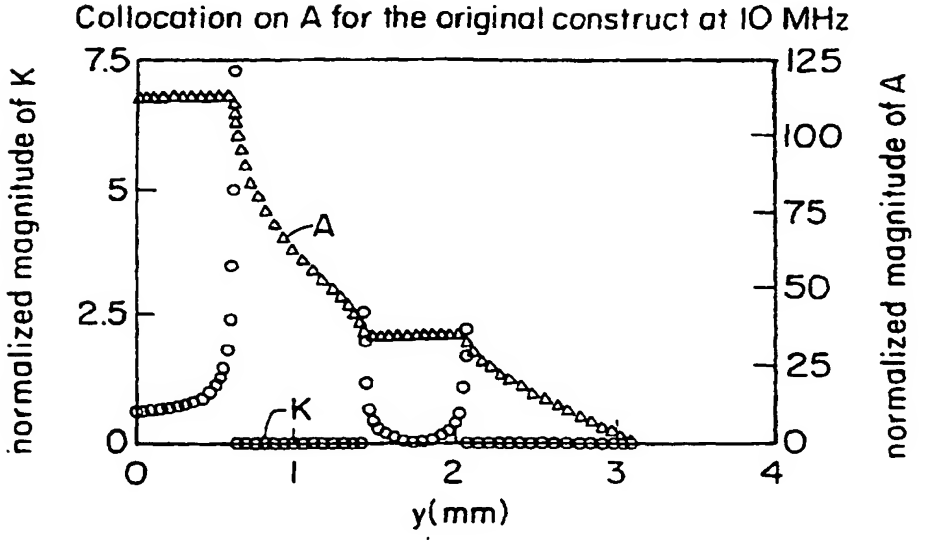

FIG. 25c

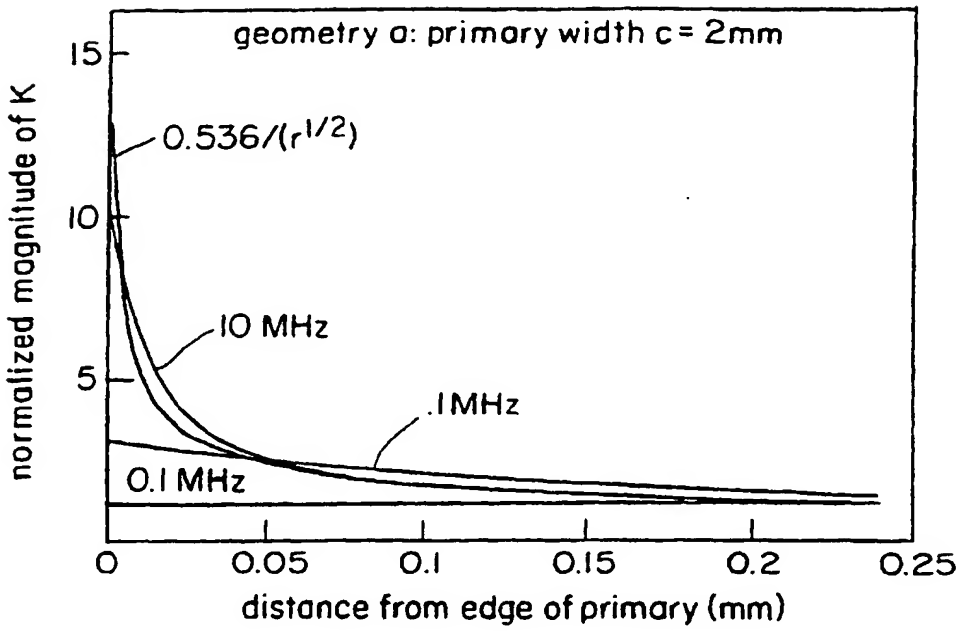

FIG. 26

FIG. 27a

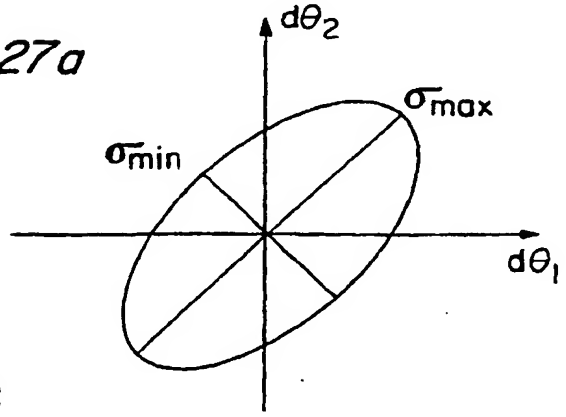

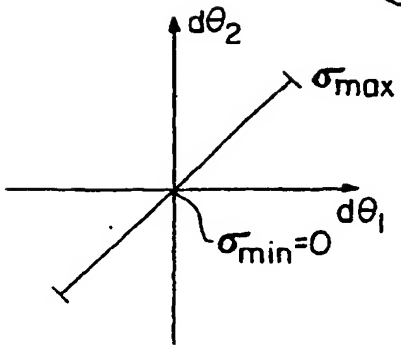

FIG. 27b

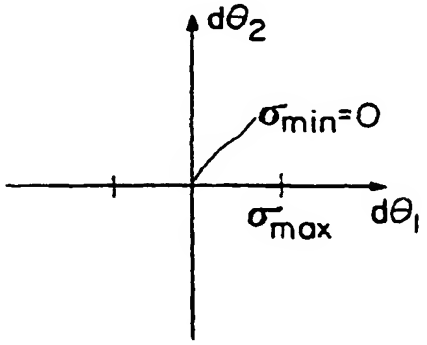

FIG. 27c

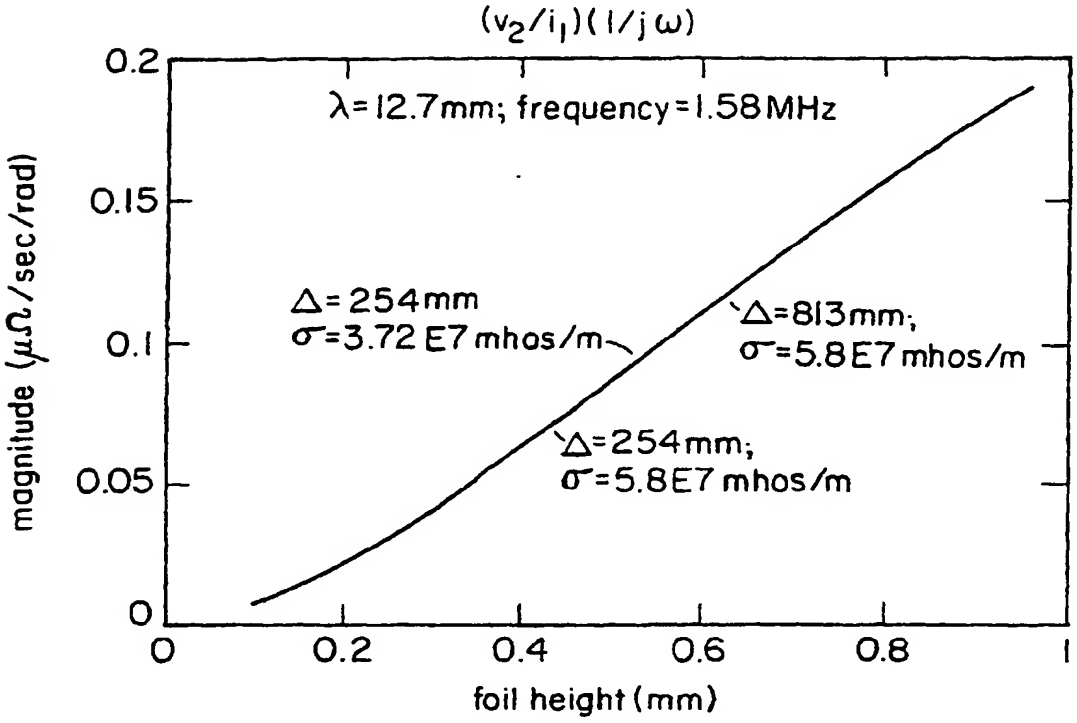

FIG. 28a

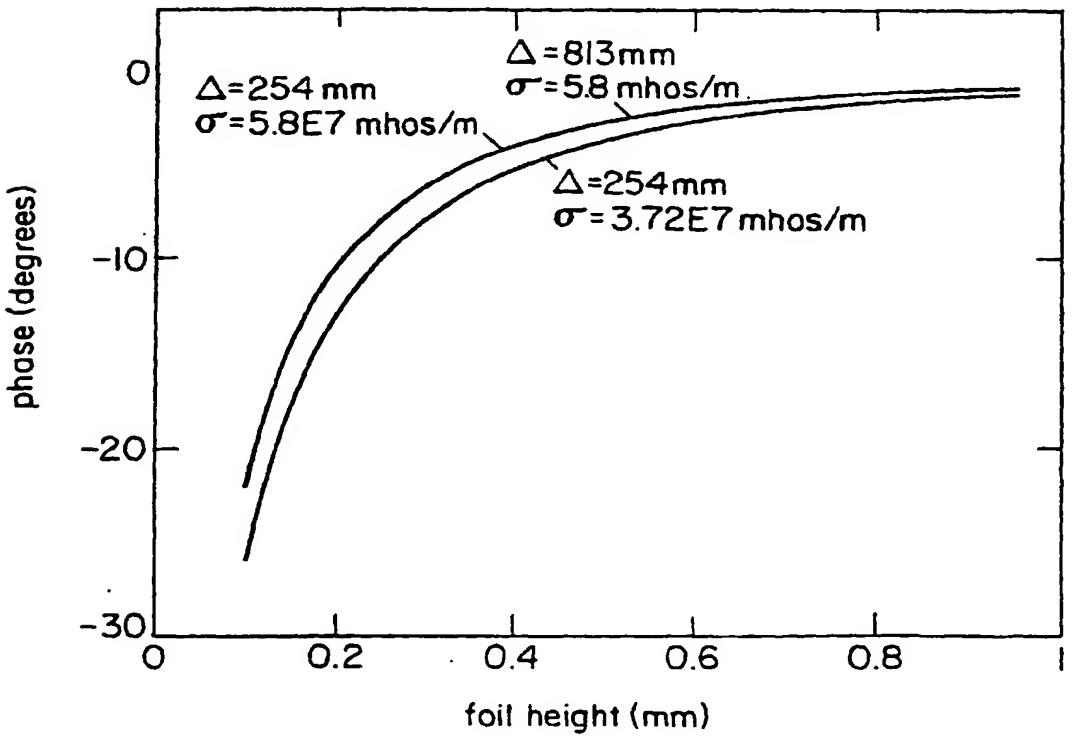

FIG. 28b

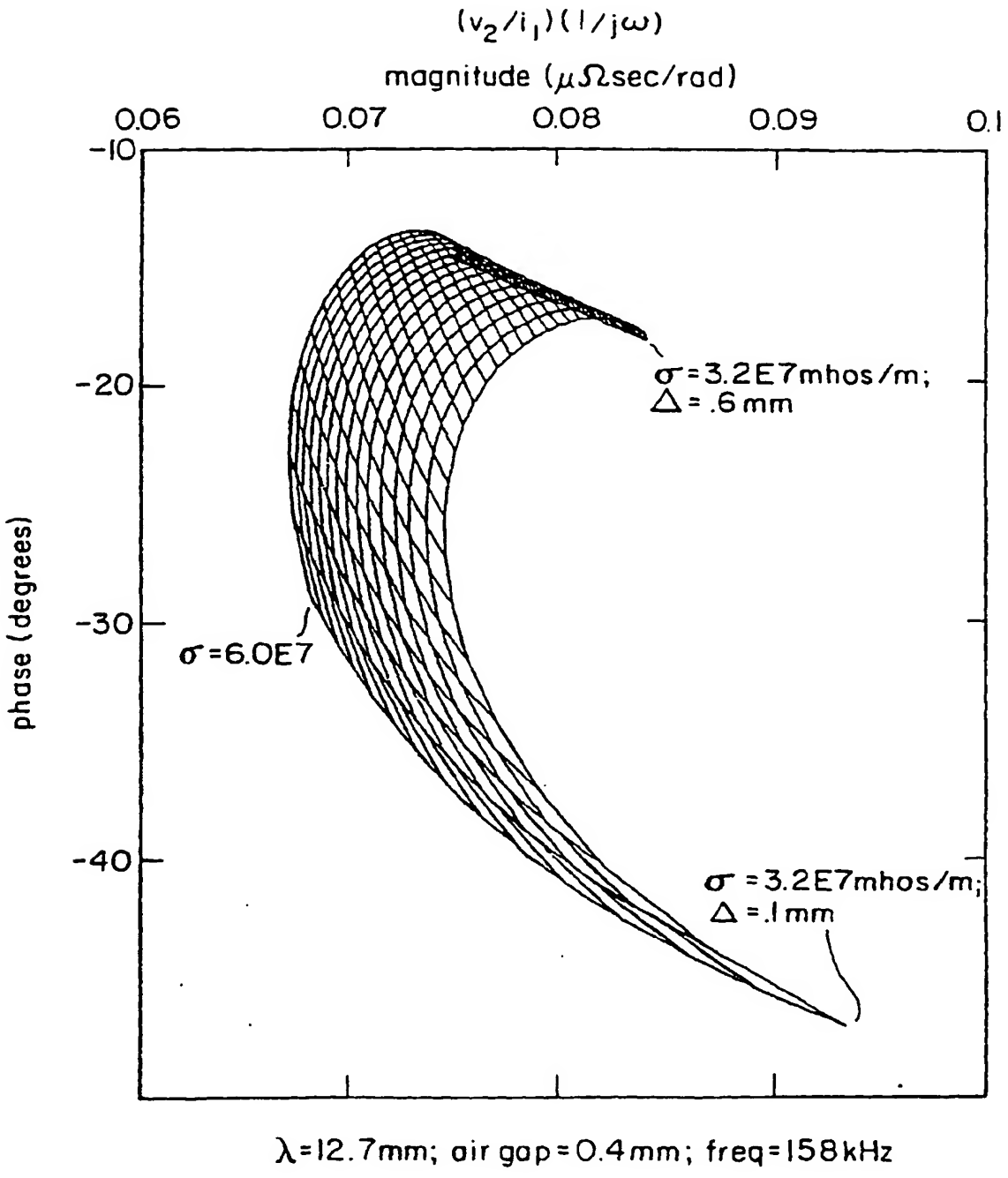

FIG. 29

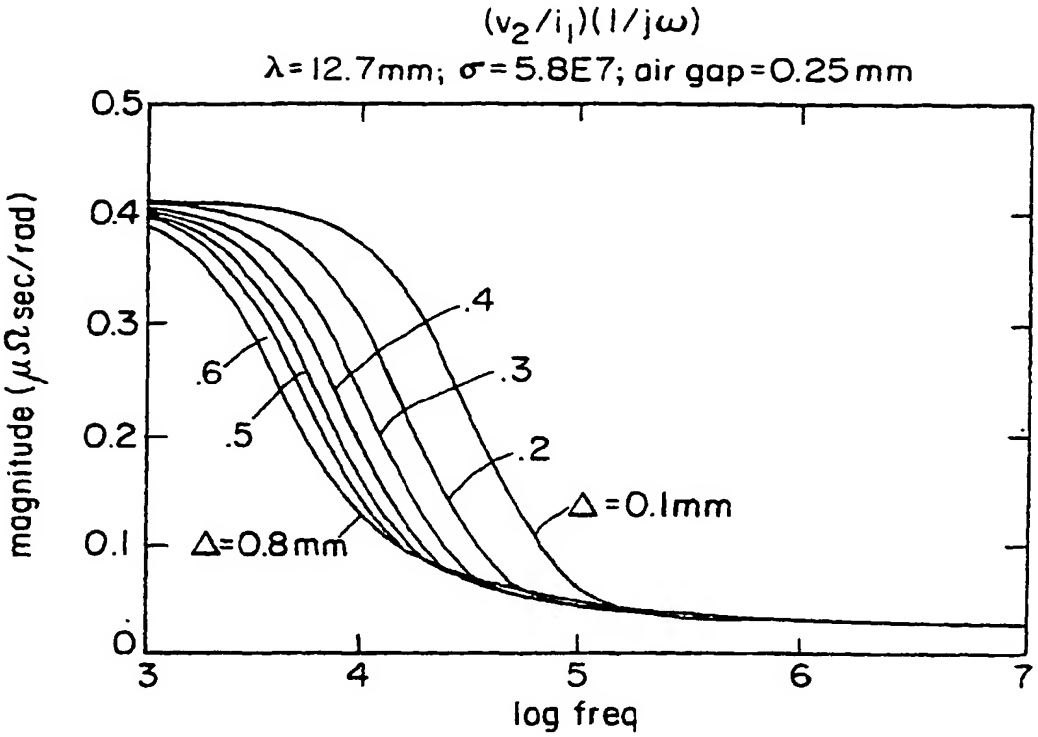

FIG. 30a

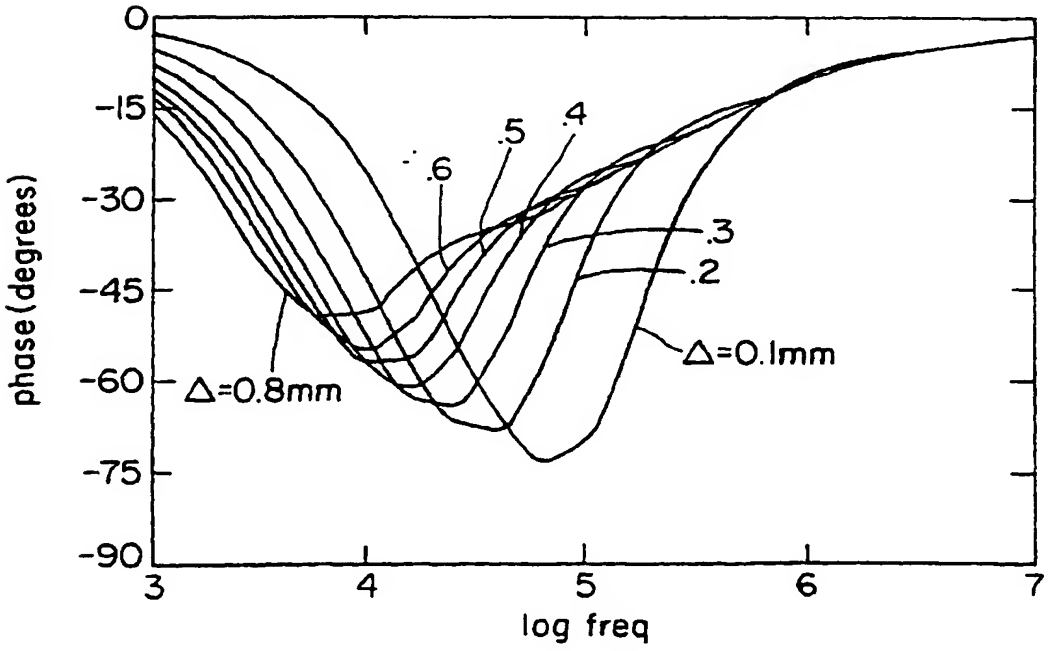

FIG. 30b

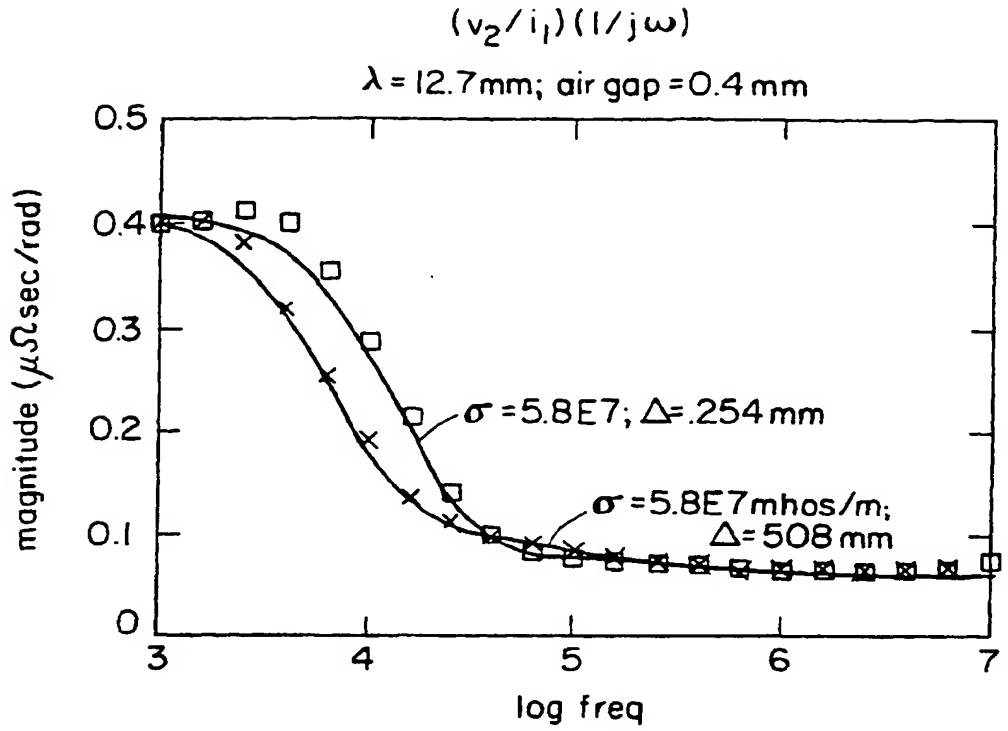

FIG. 31a

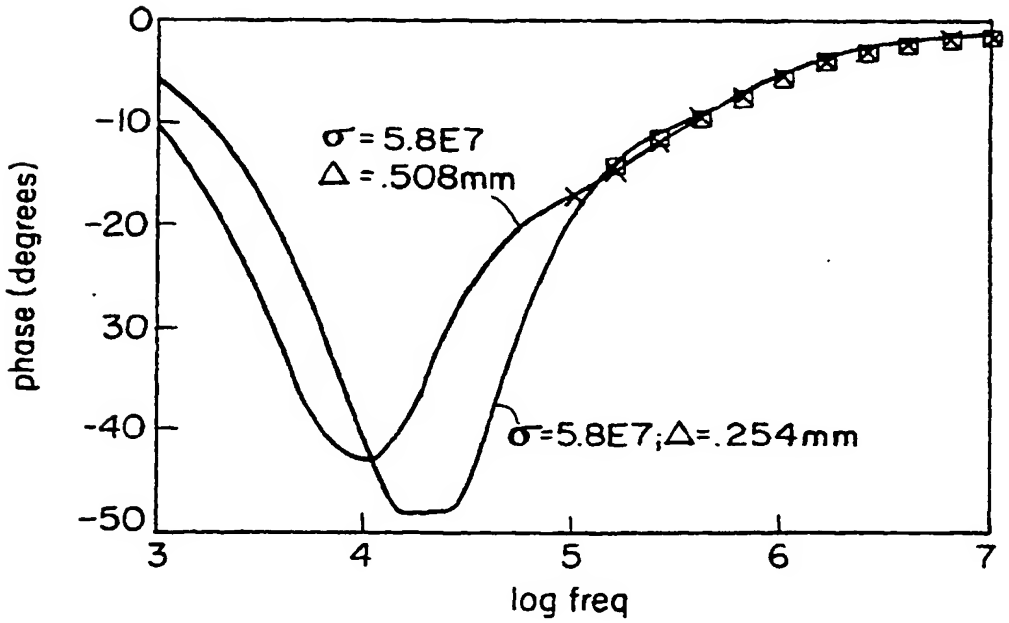

FIG. 31b

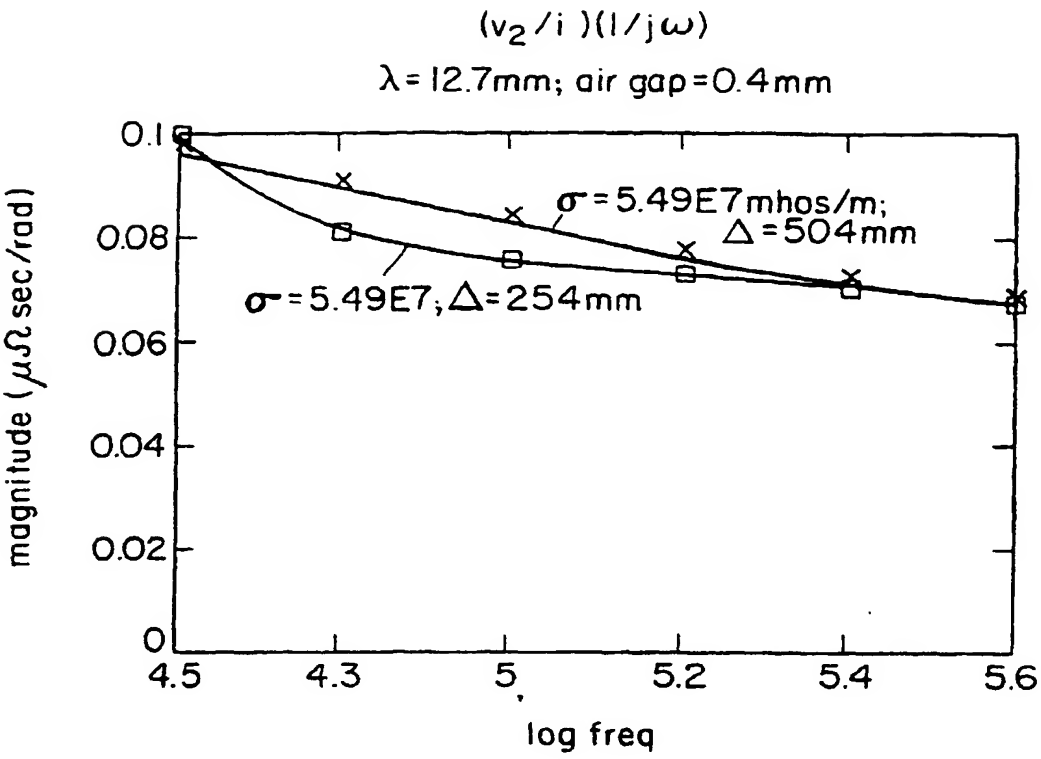

FIG. 32a

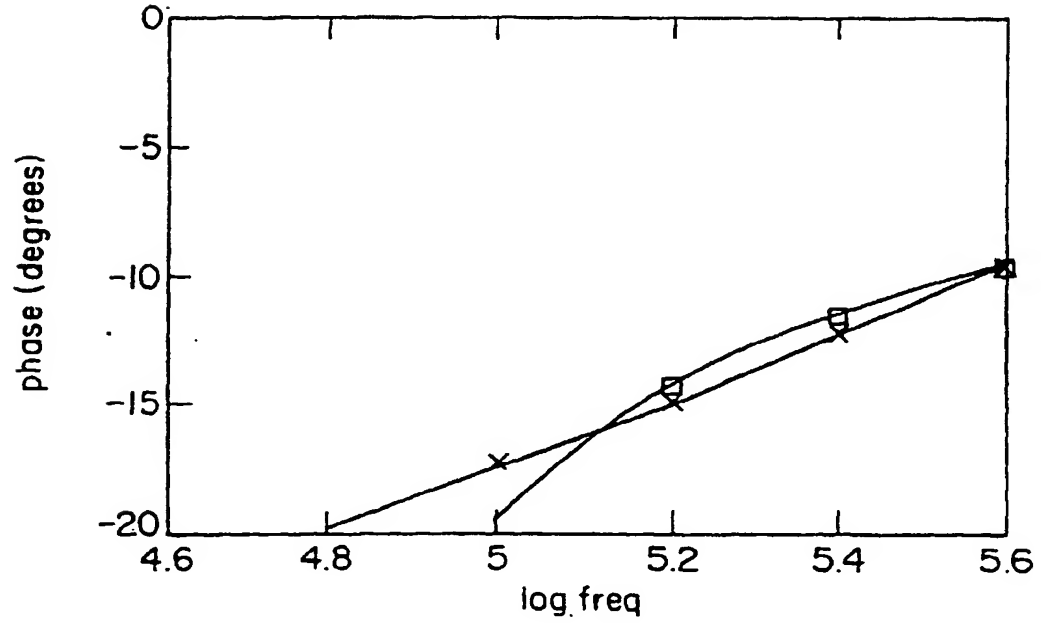

FIG. 32b

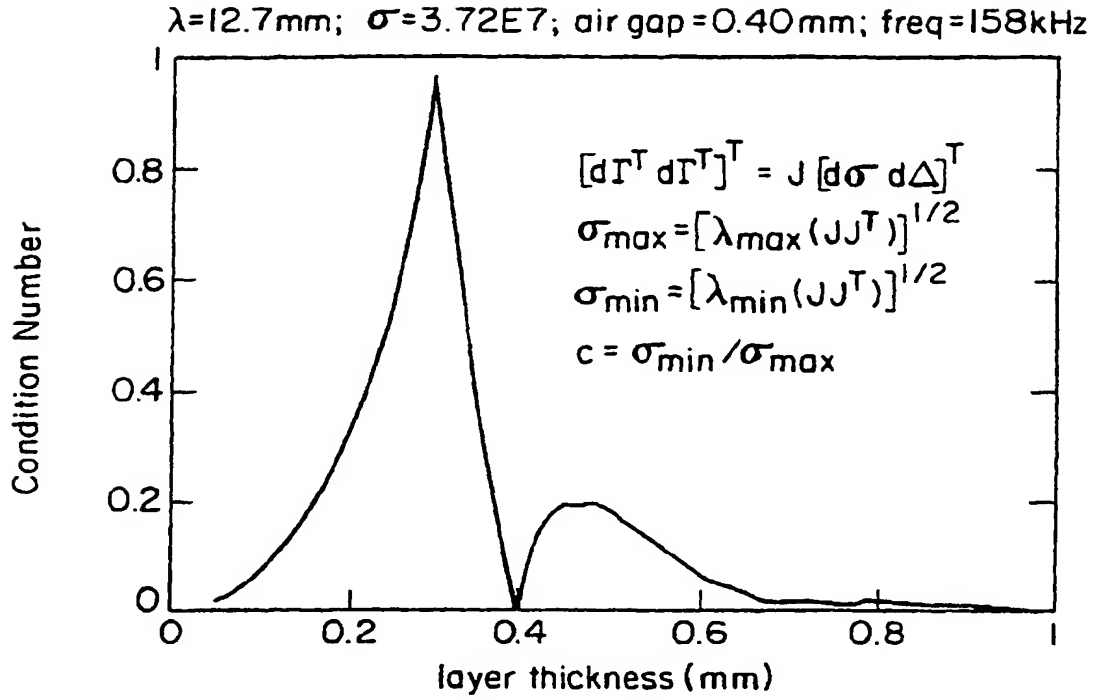

FIG. 33a

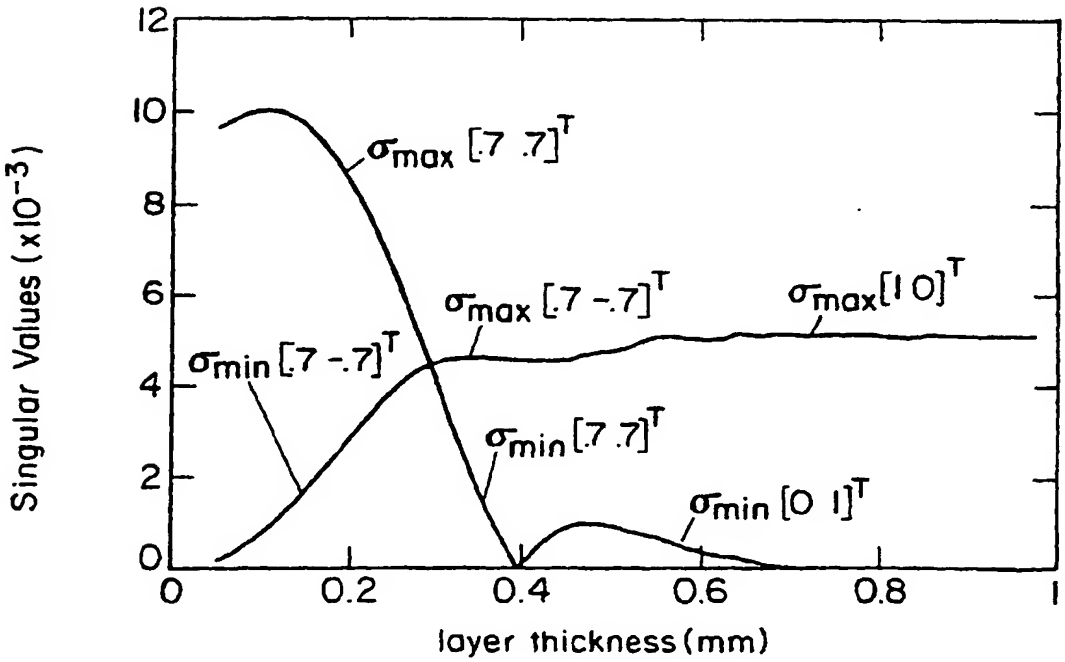

FIG. 33b

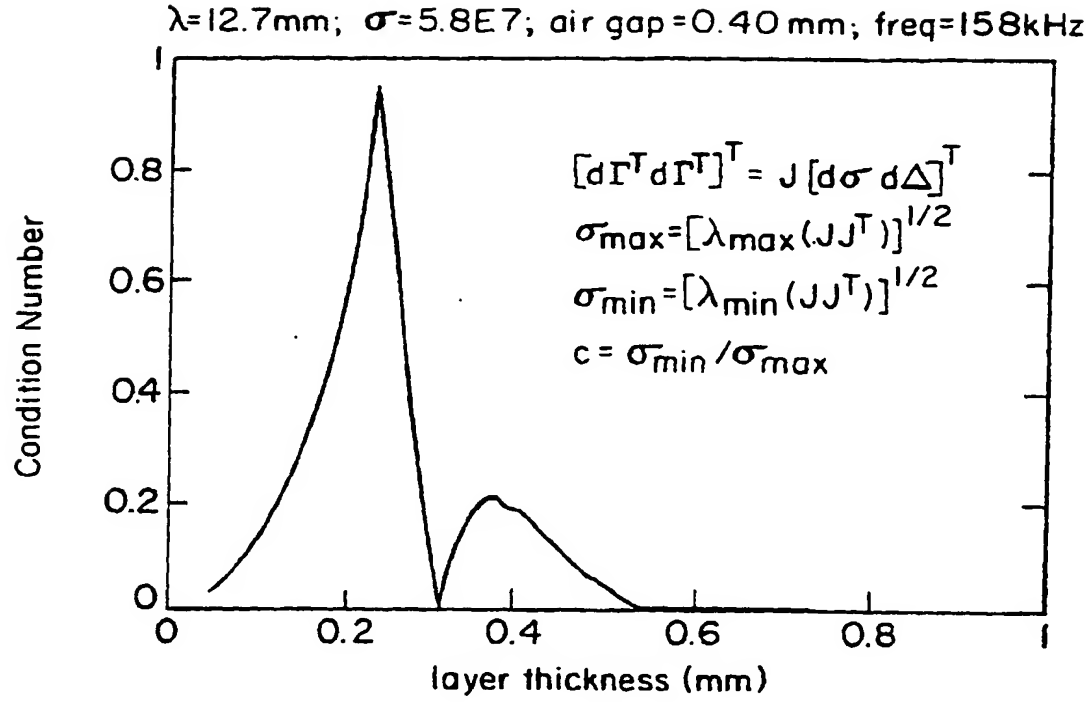

FIG. 34a

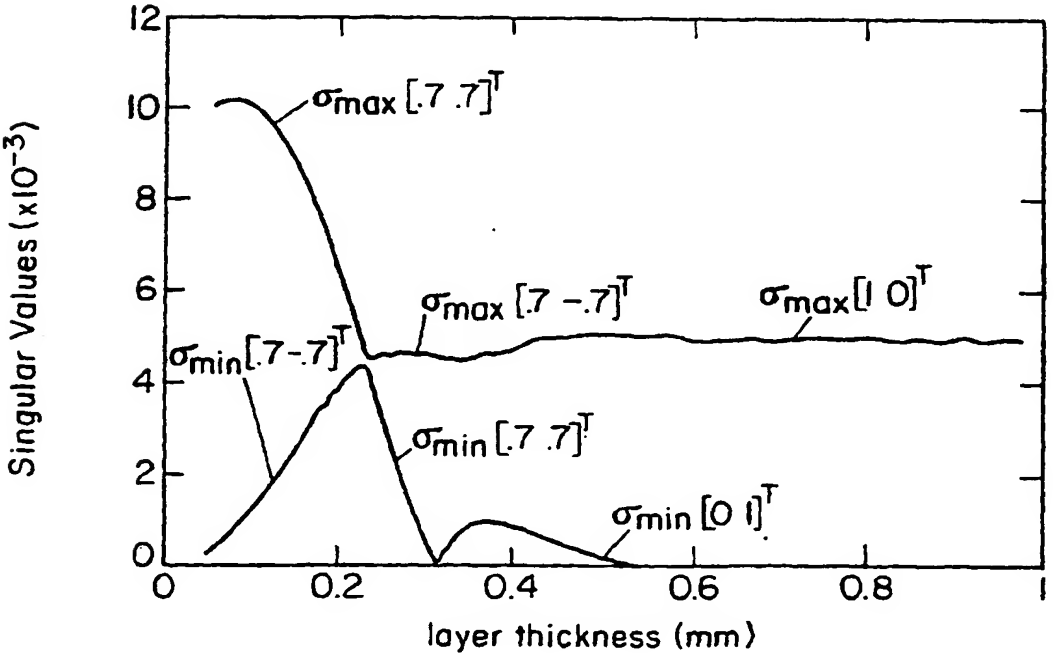

FIG. 34b

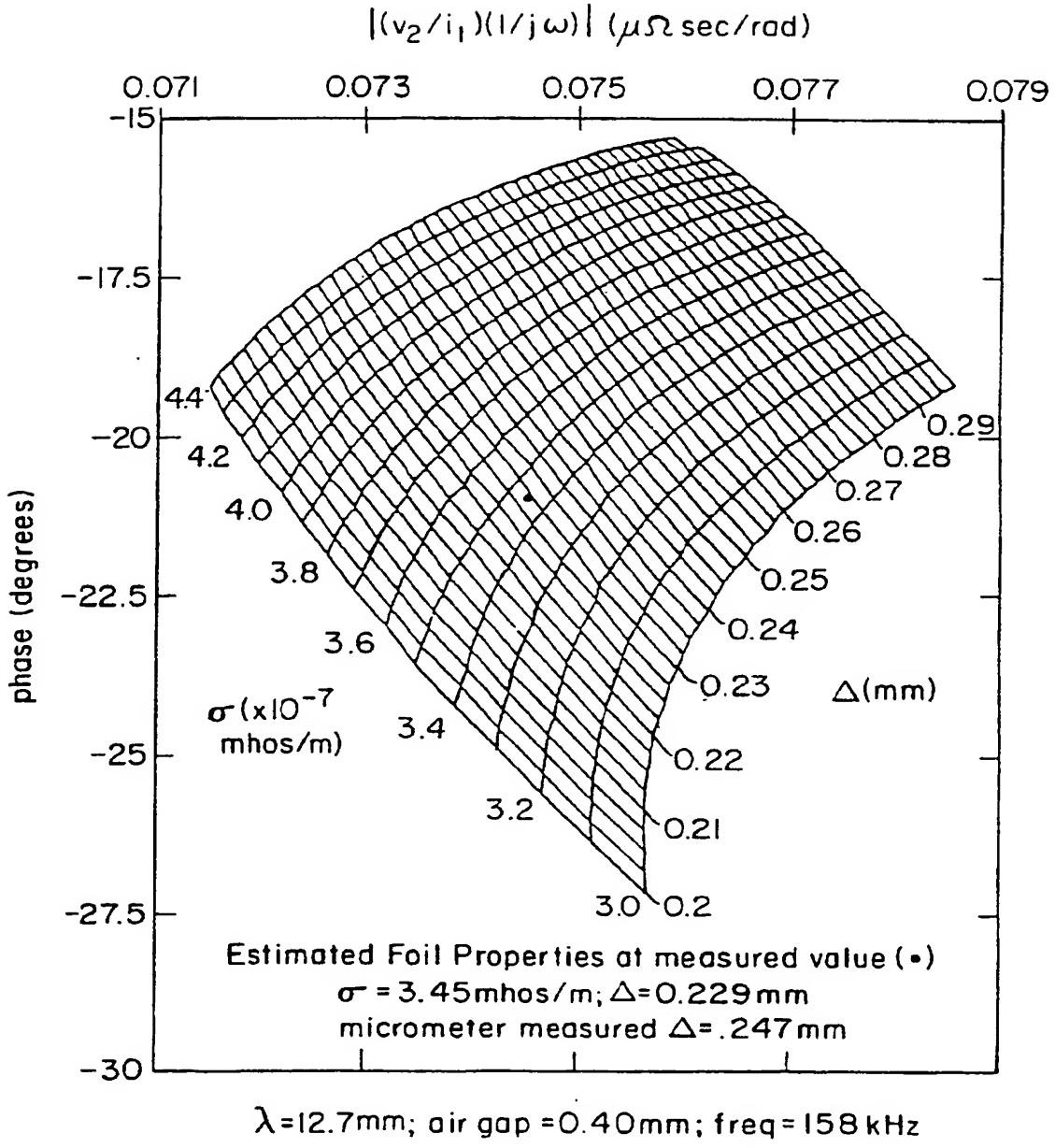

FIG. 35

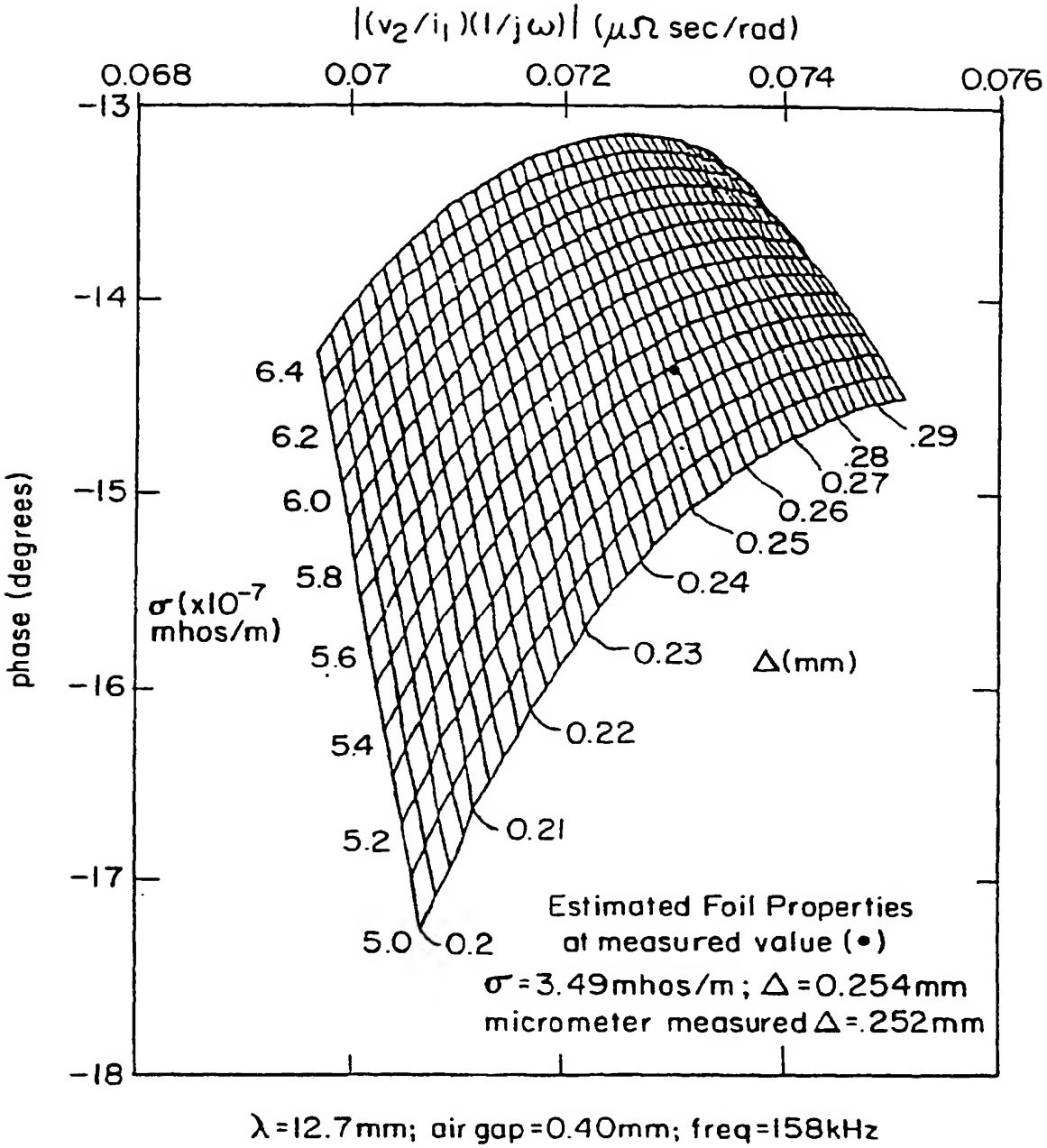

FIG. 36

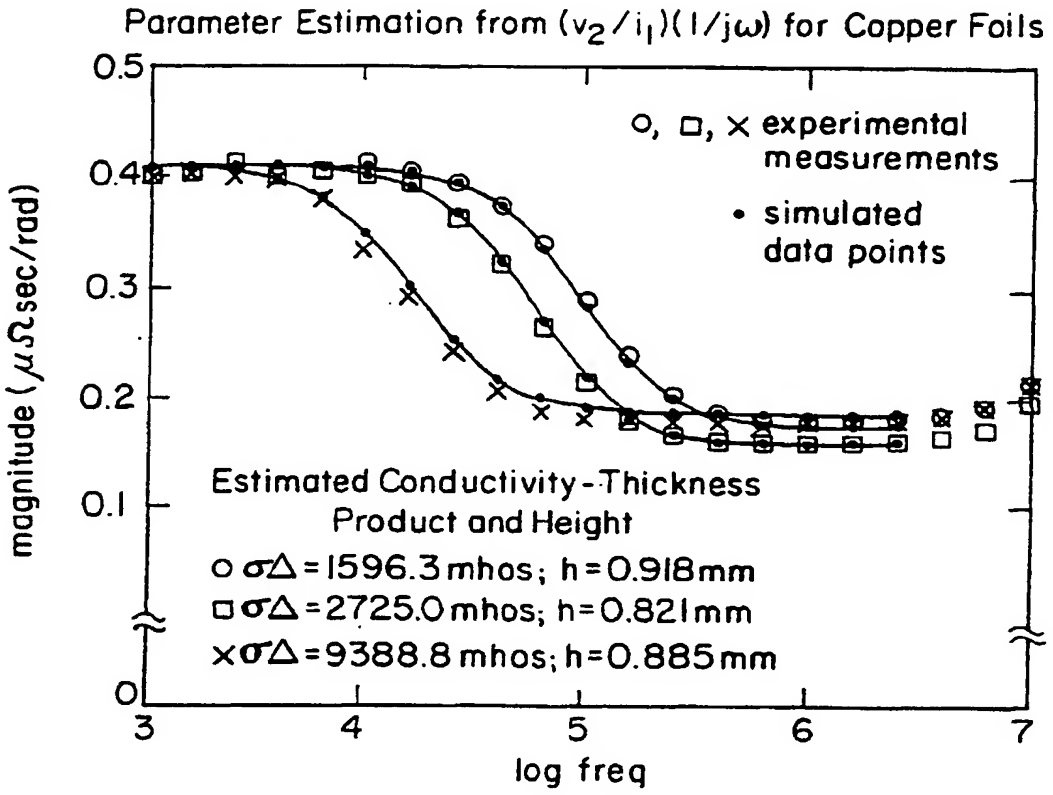

FIG. 37a

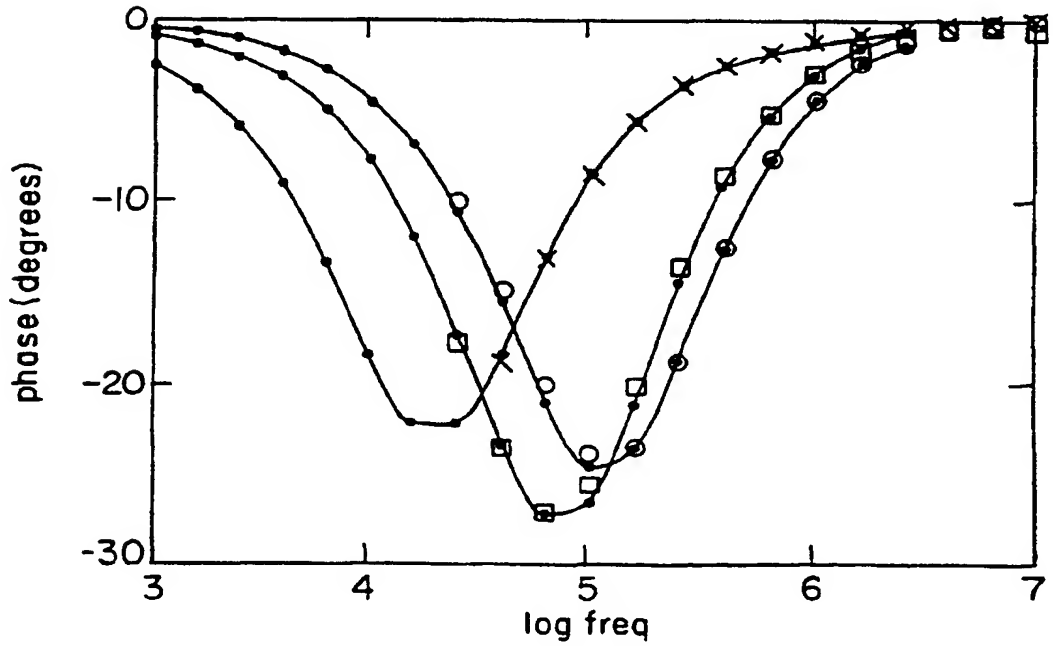

FIG. 37b

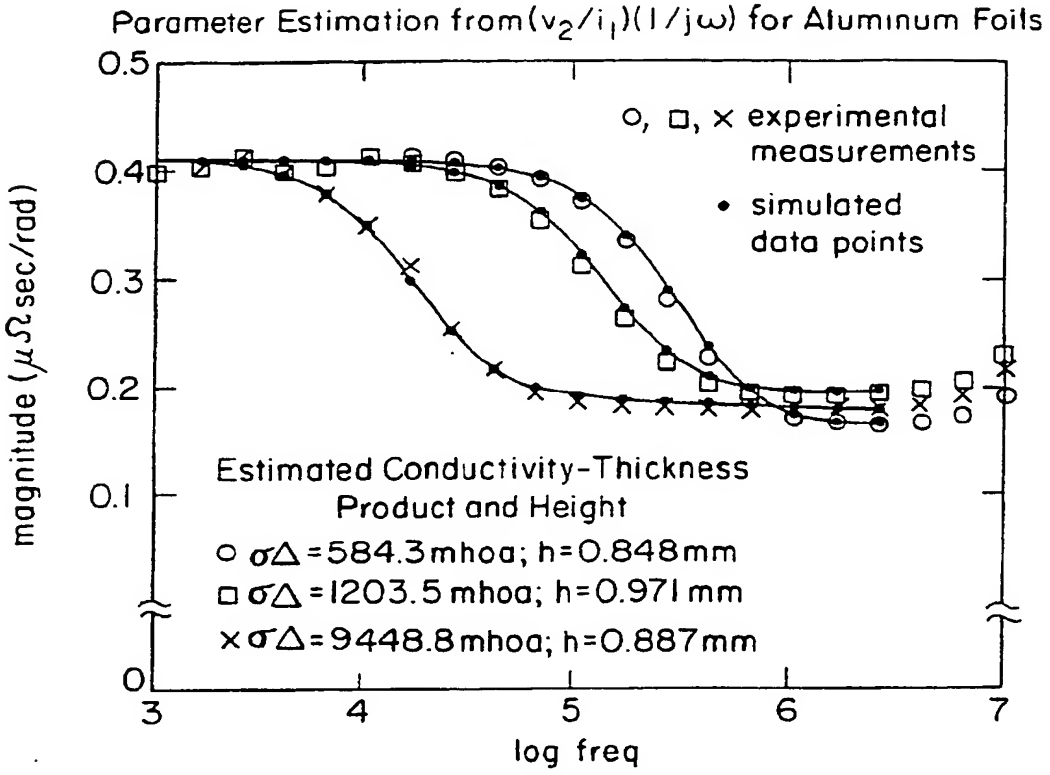

FIG. 38a

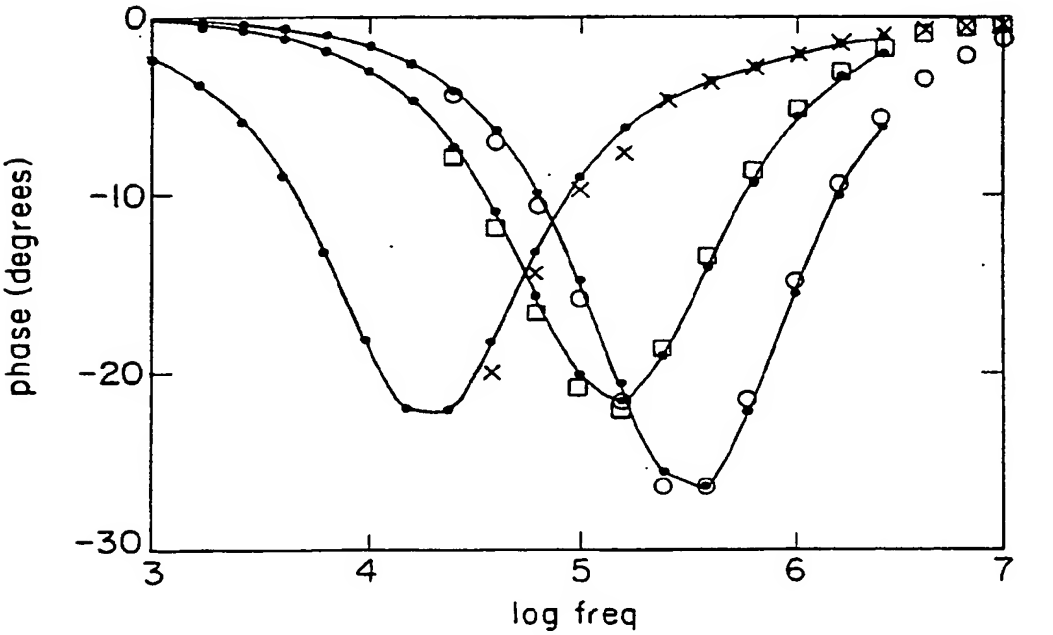

FIG. 38b

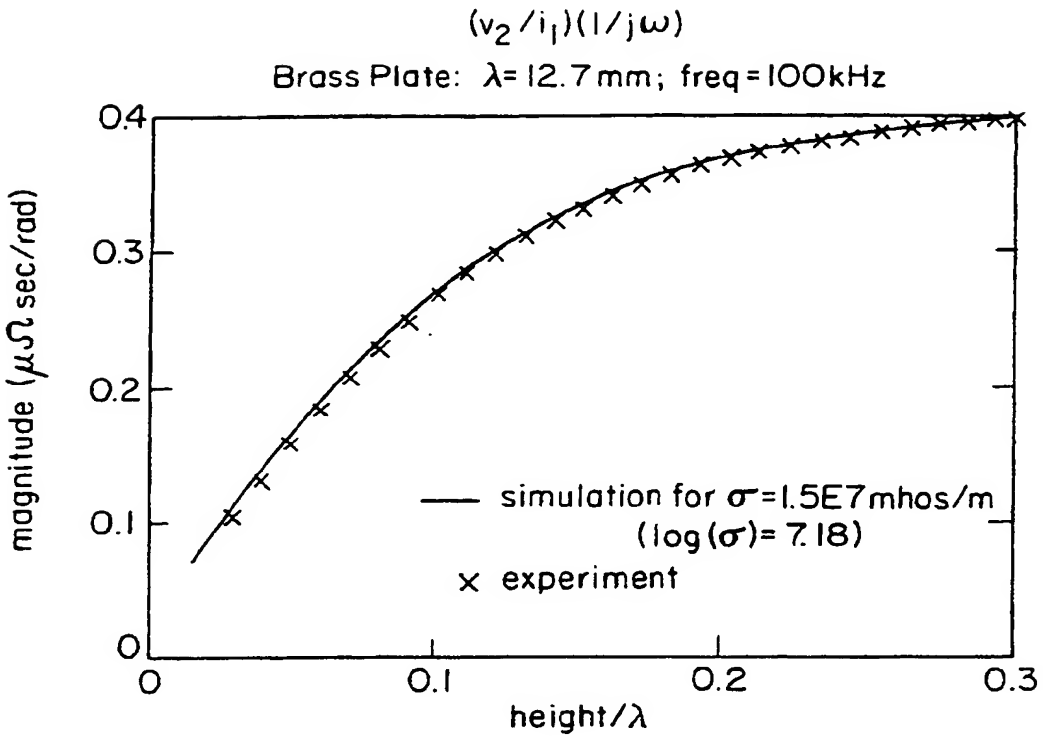

FIG. 39a

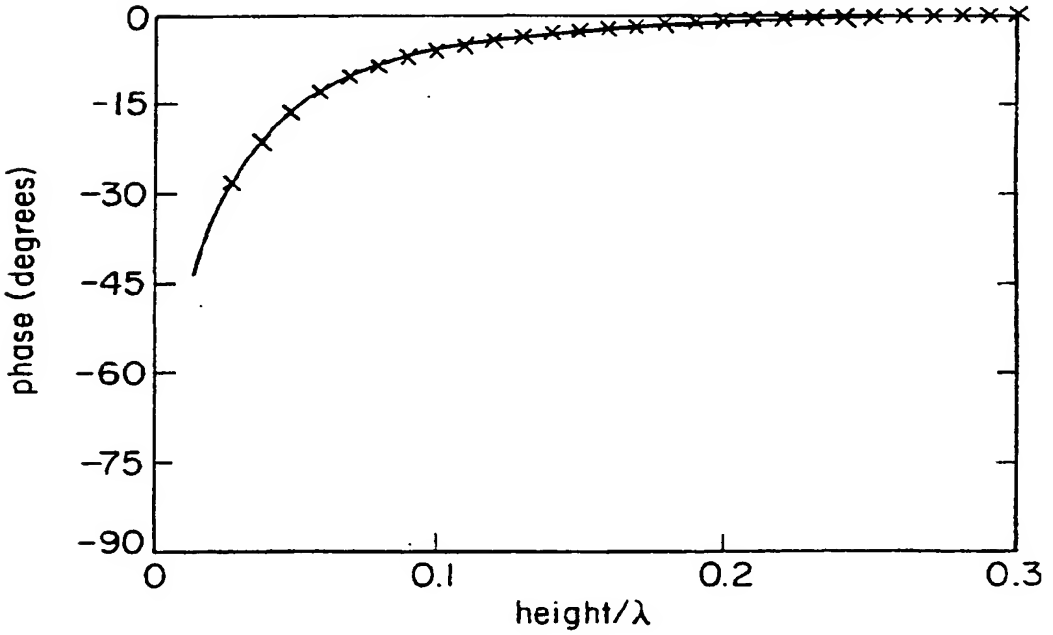

FIG. 39b

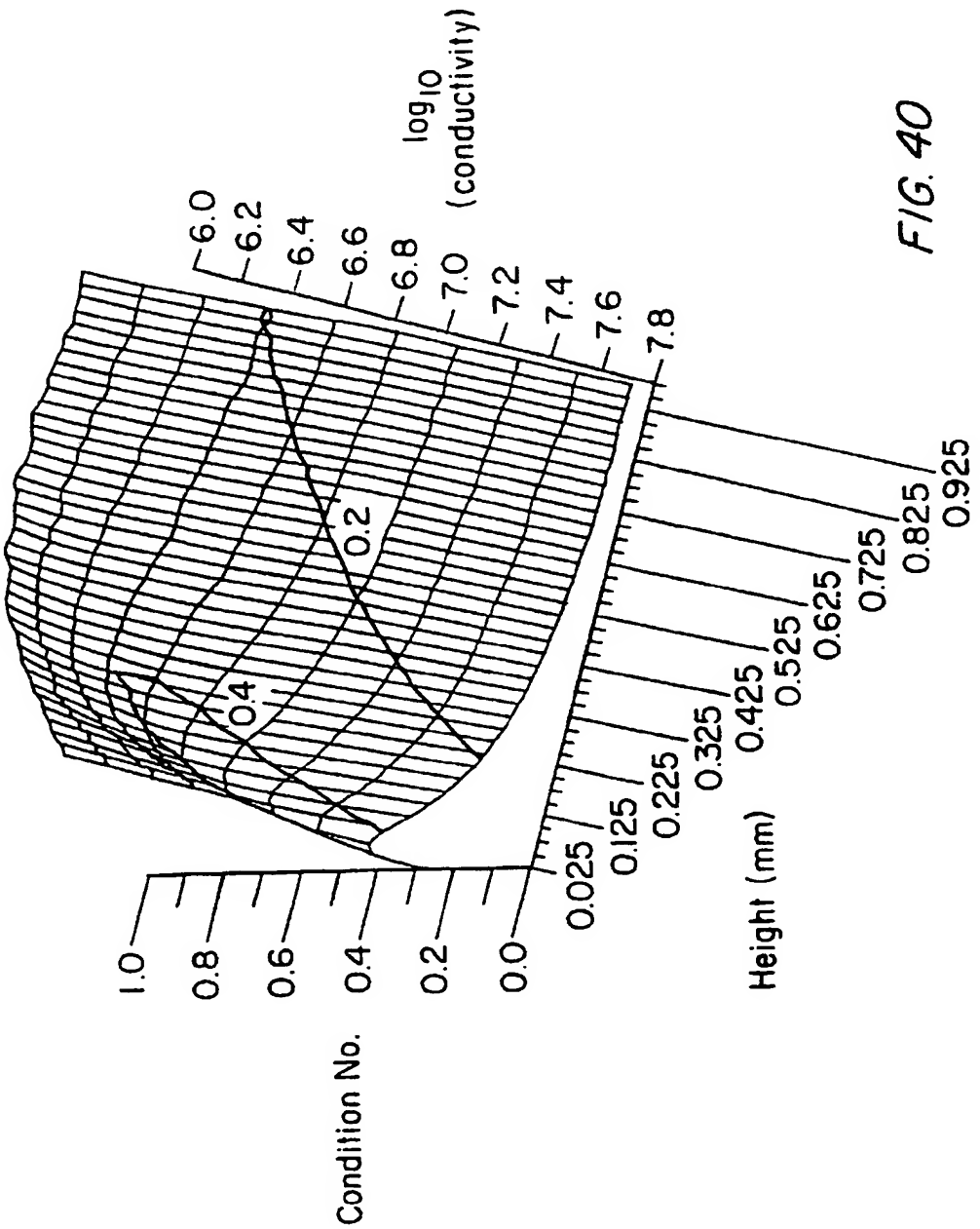

FIG. 40

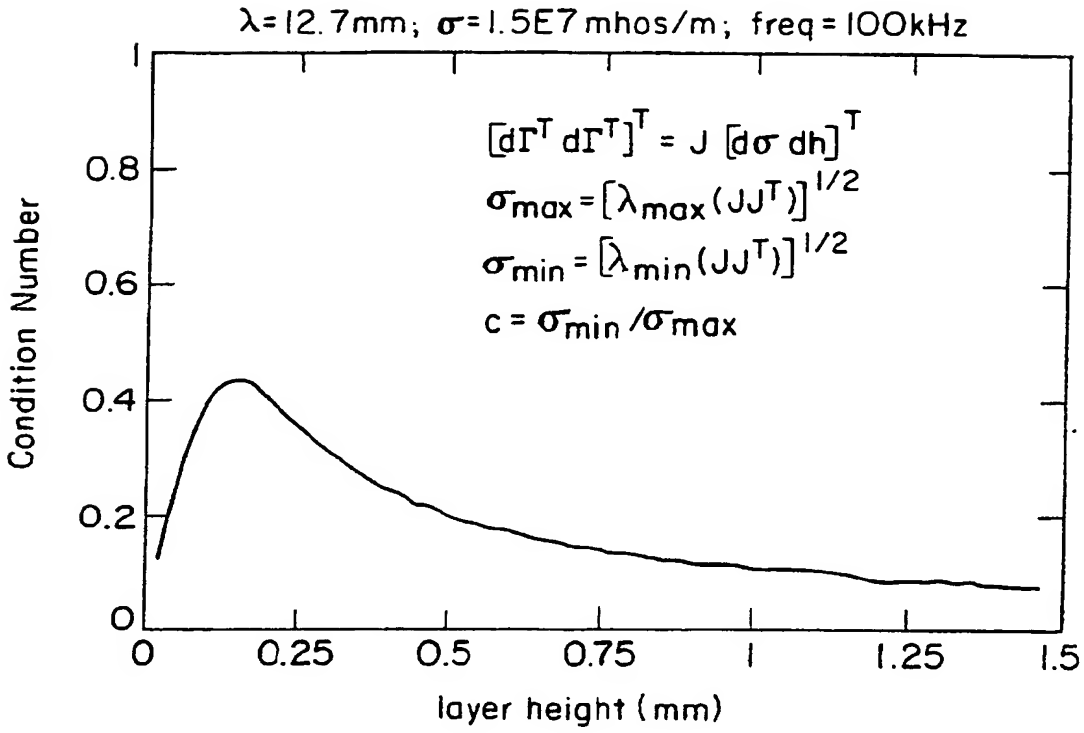

FIG. 41a

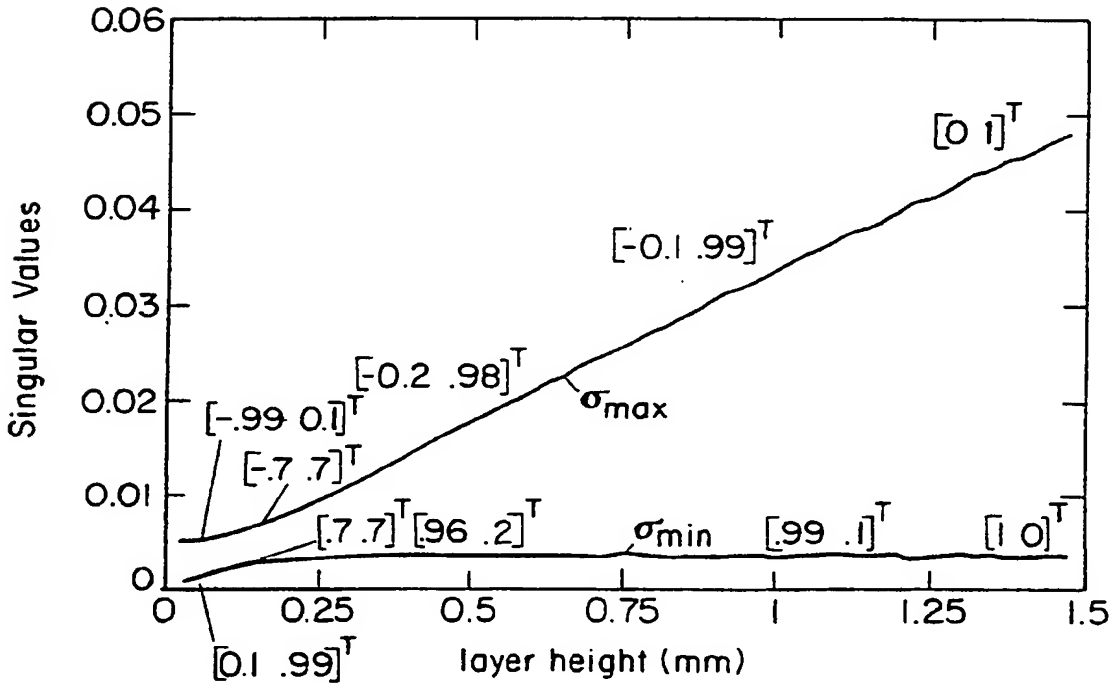

FIG. 41b

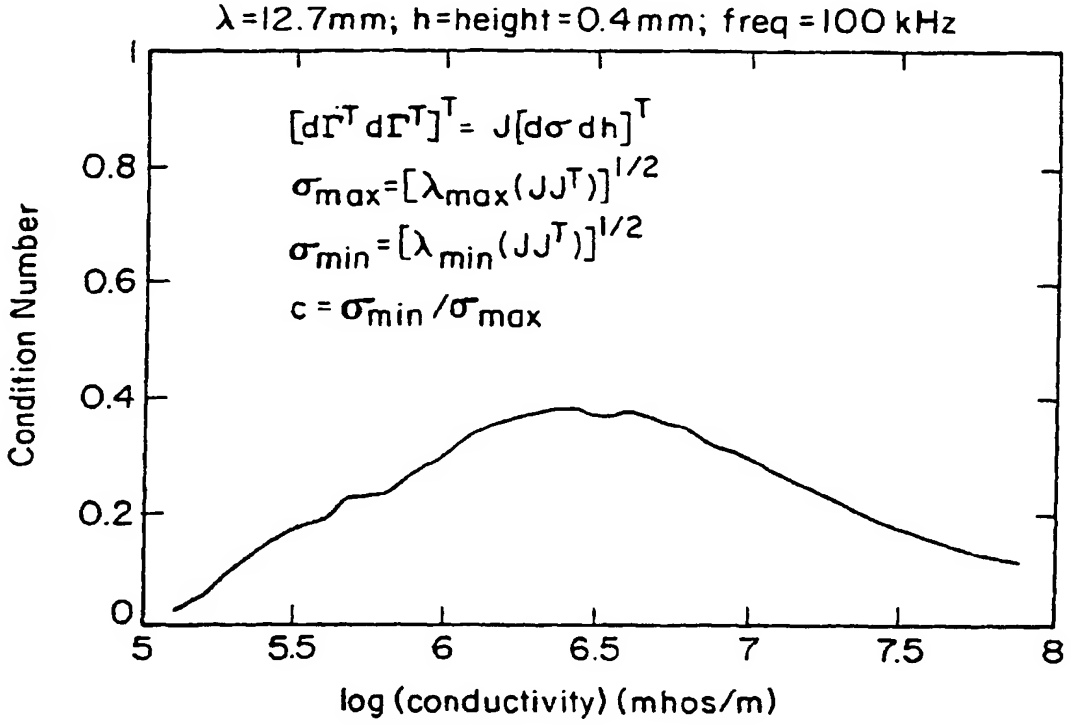

FIG. 42a

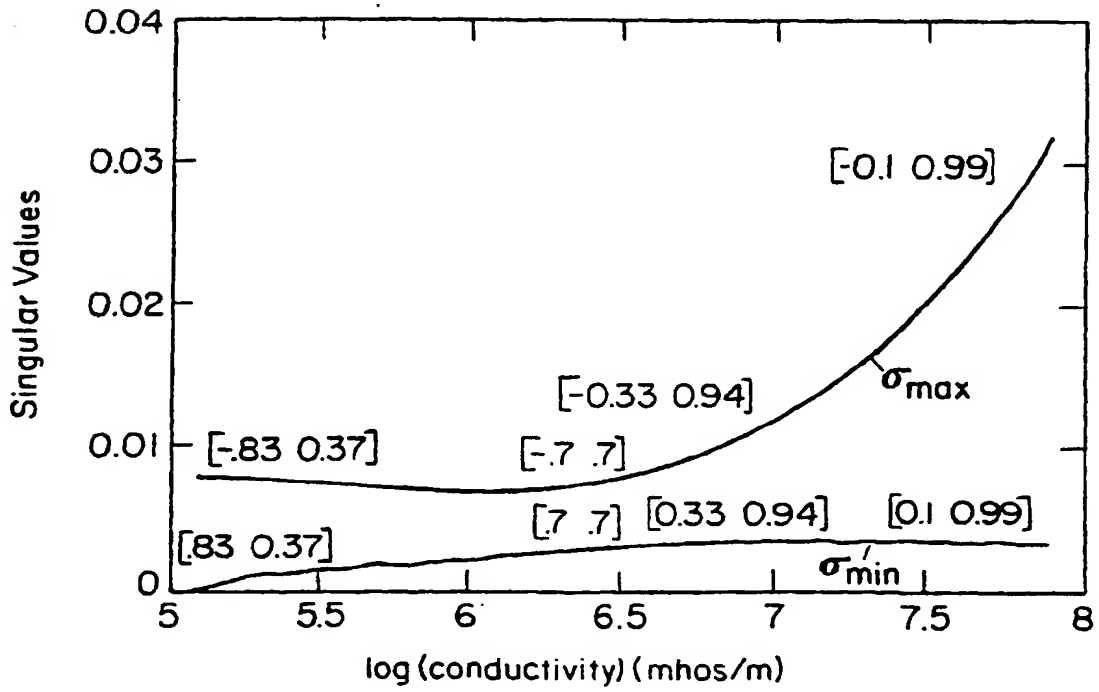

FIG. 42b

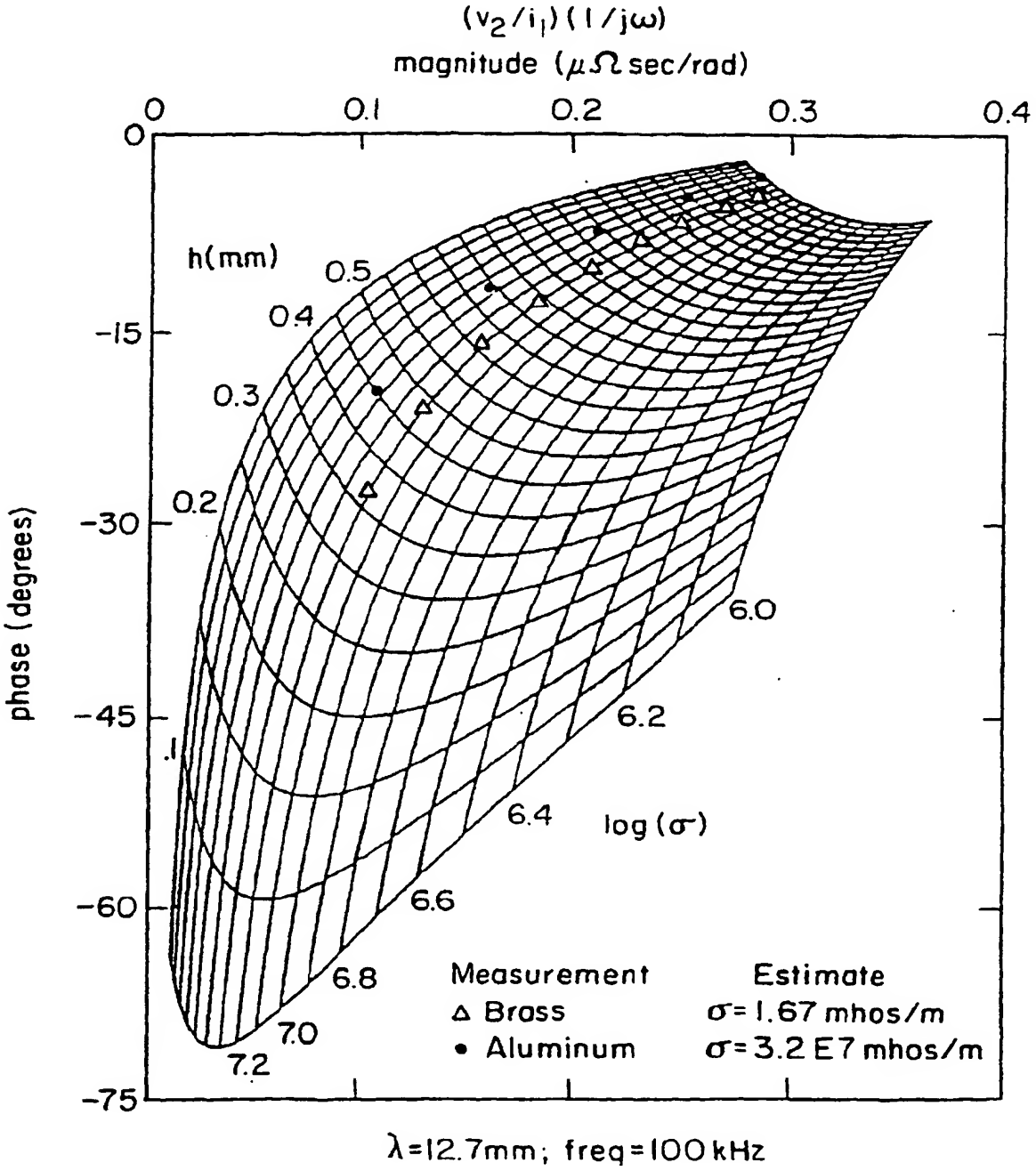

FIG. 43

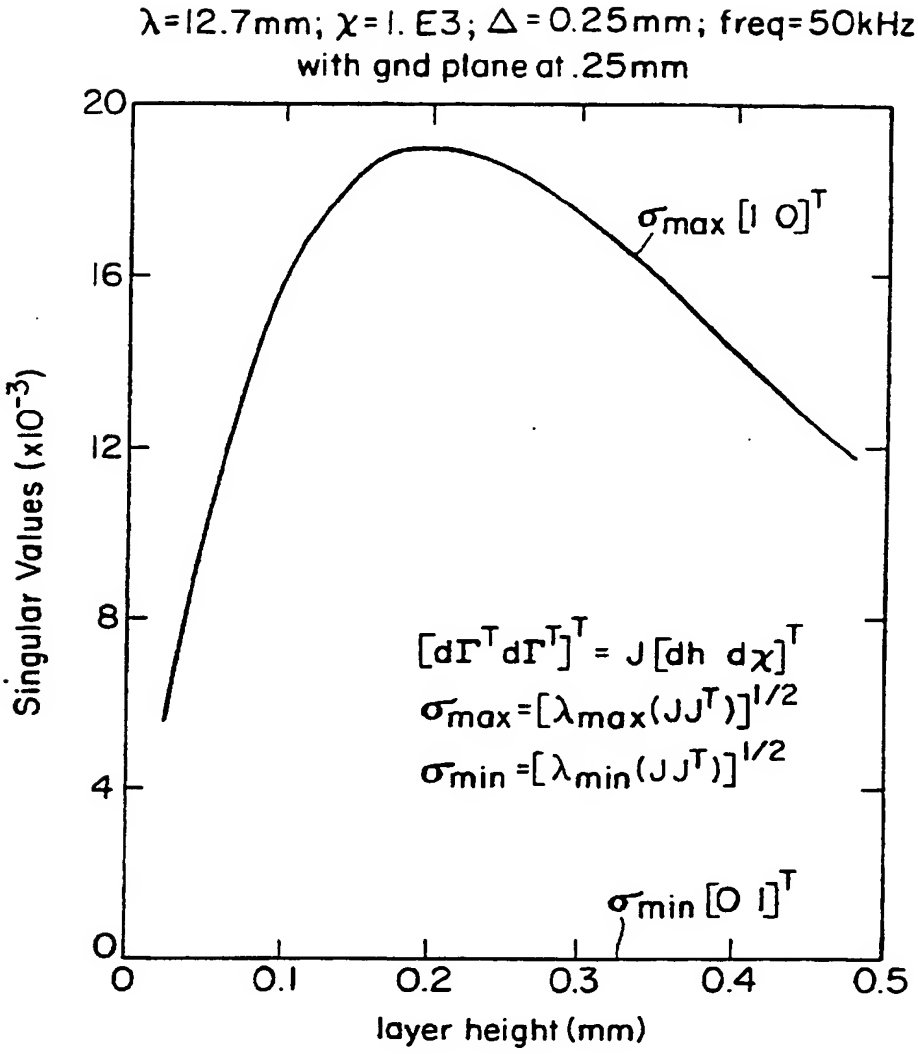

FIG. 44

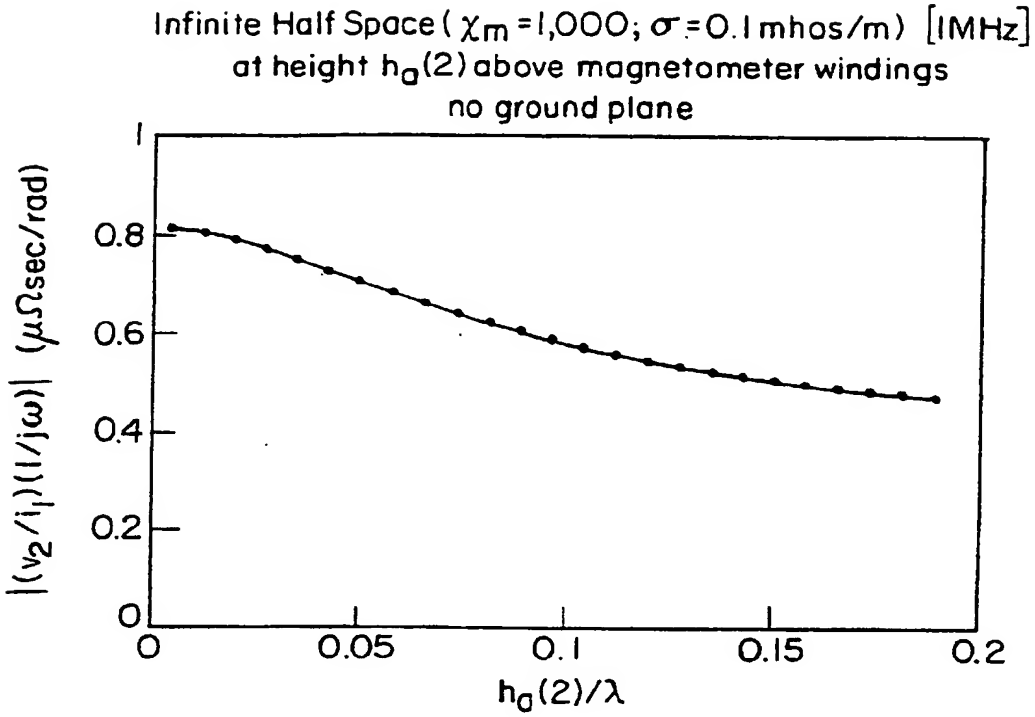

FIG. 45a

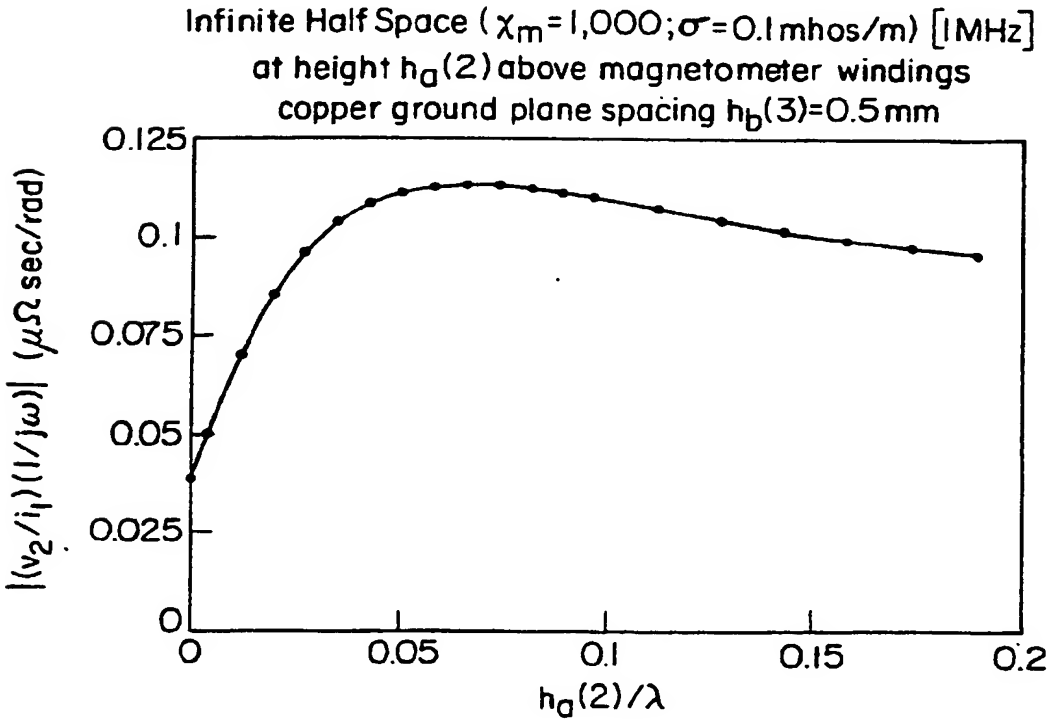

FIG. 45b

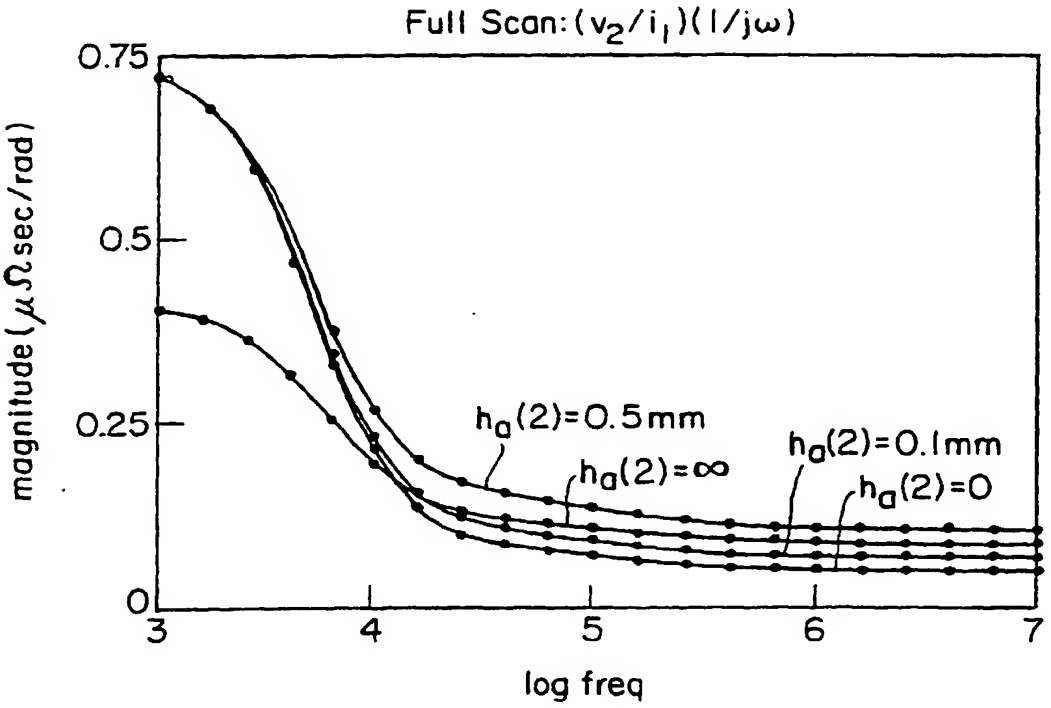

FIG. 46a

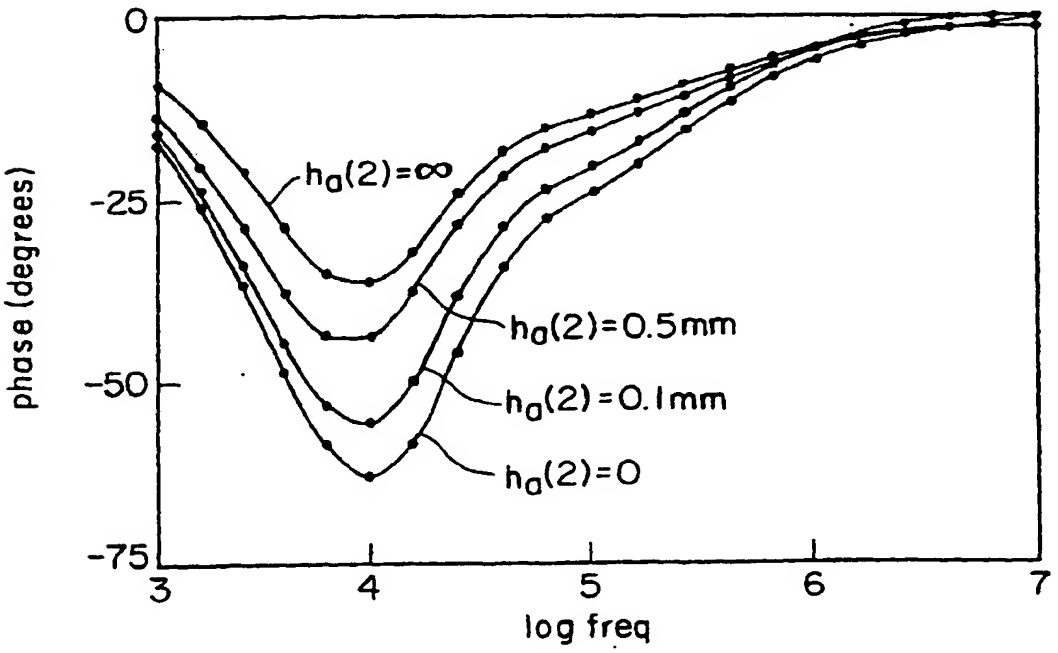

FIG. 46b

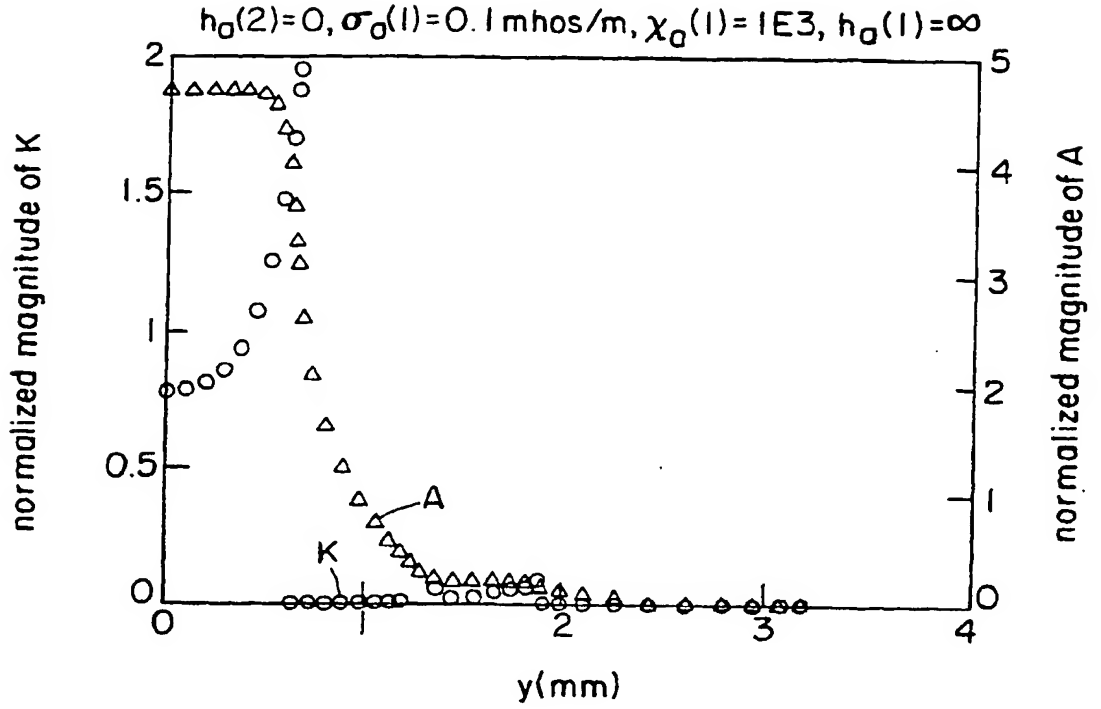

FIG. 47a

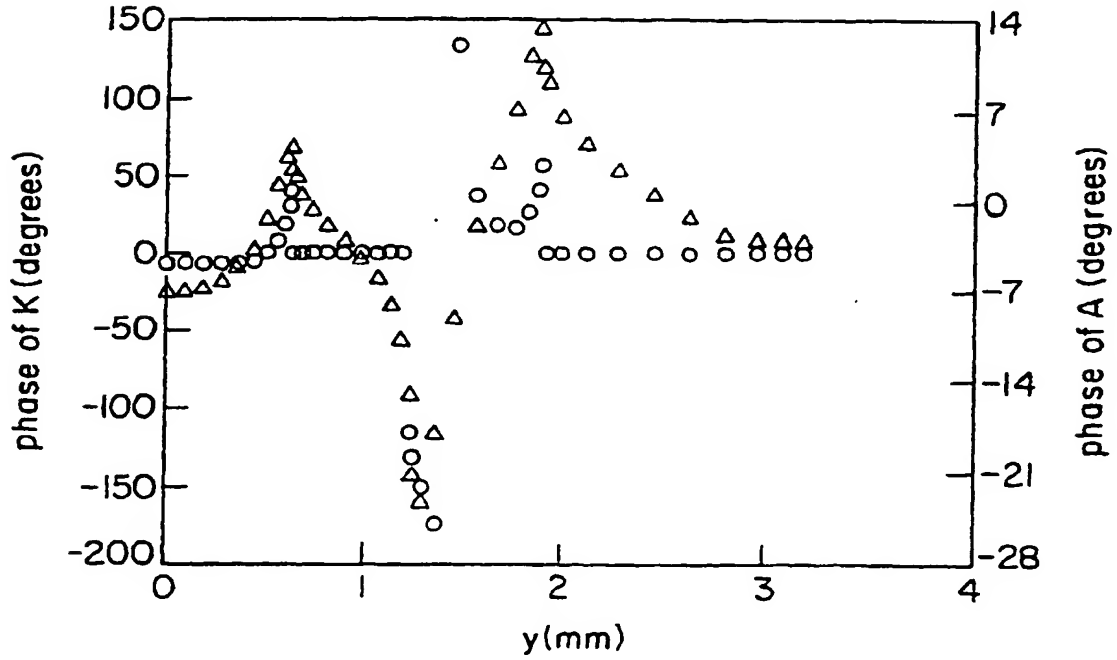

FIG. 47b

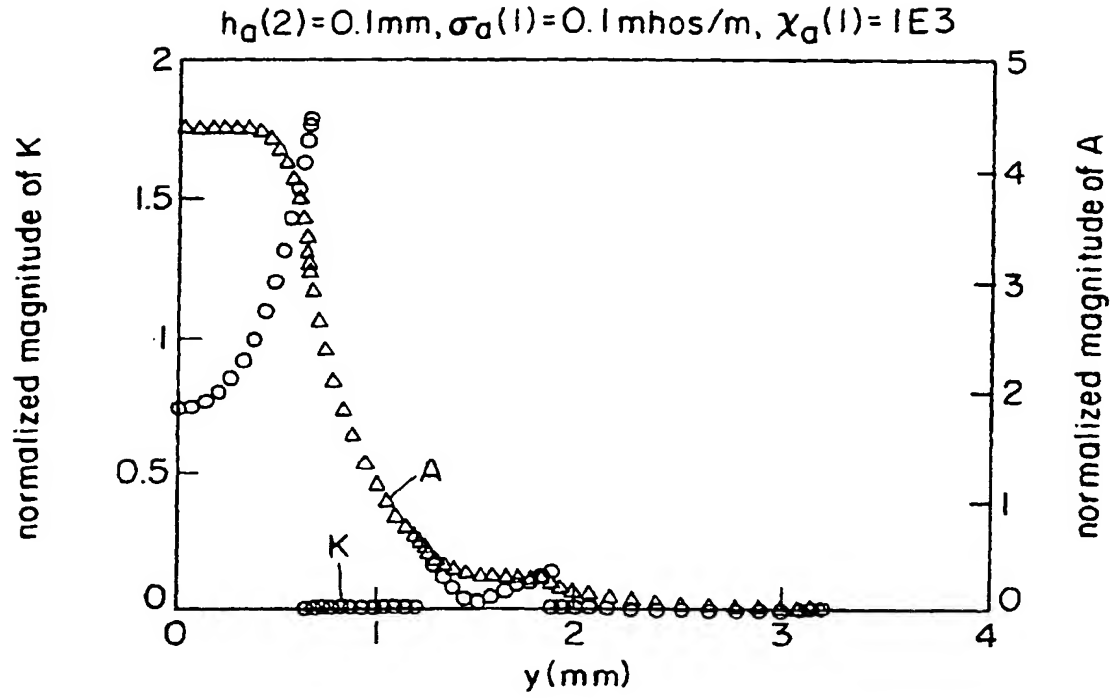

FIG. 48a

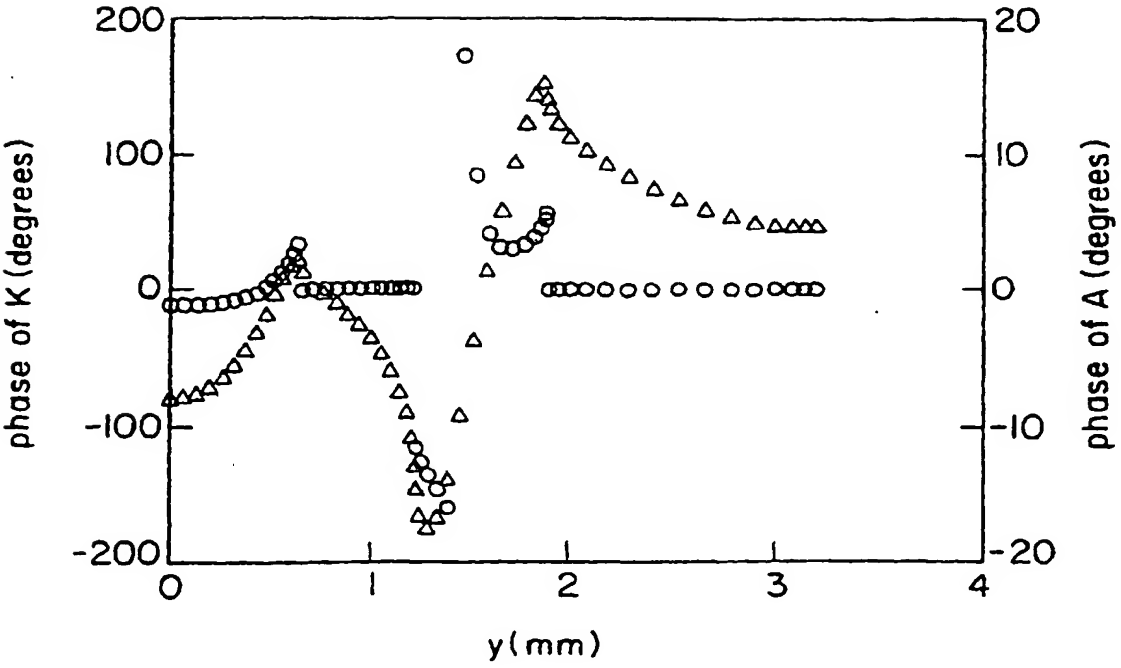

FIG. 48b

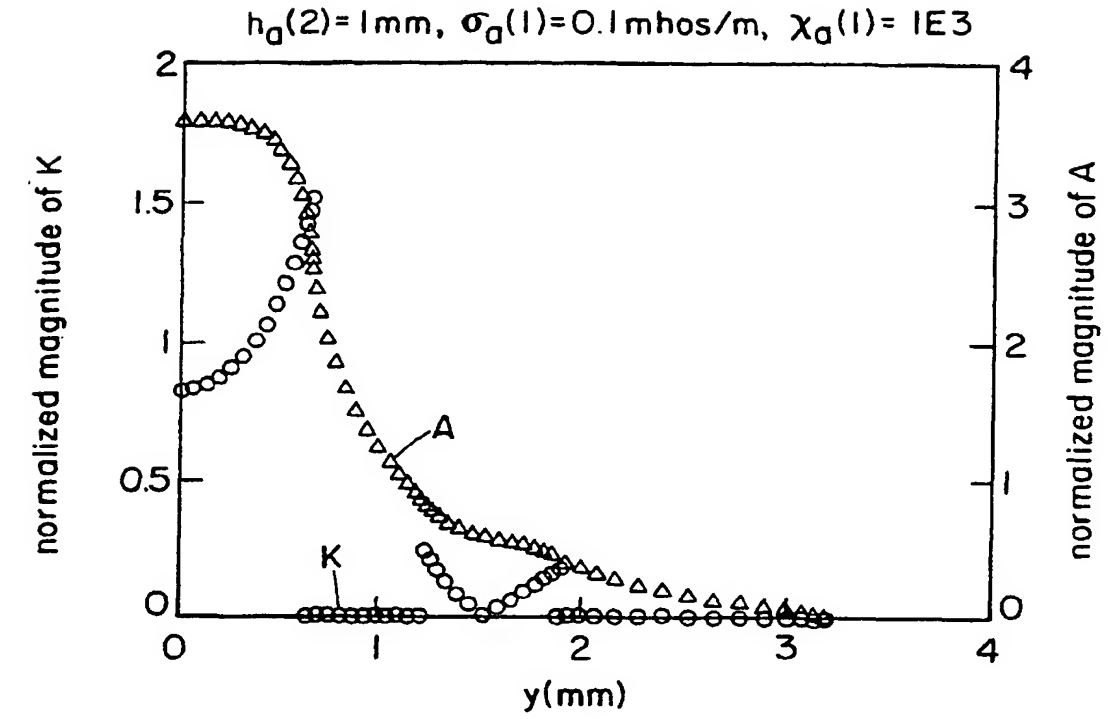

FIG. 49a

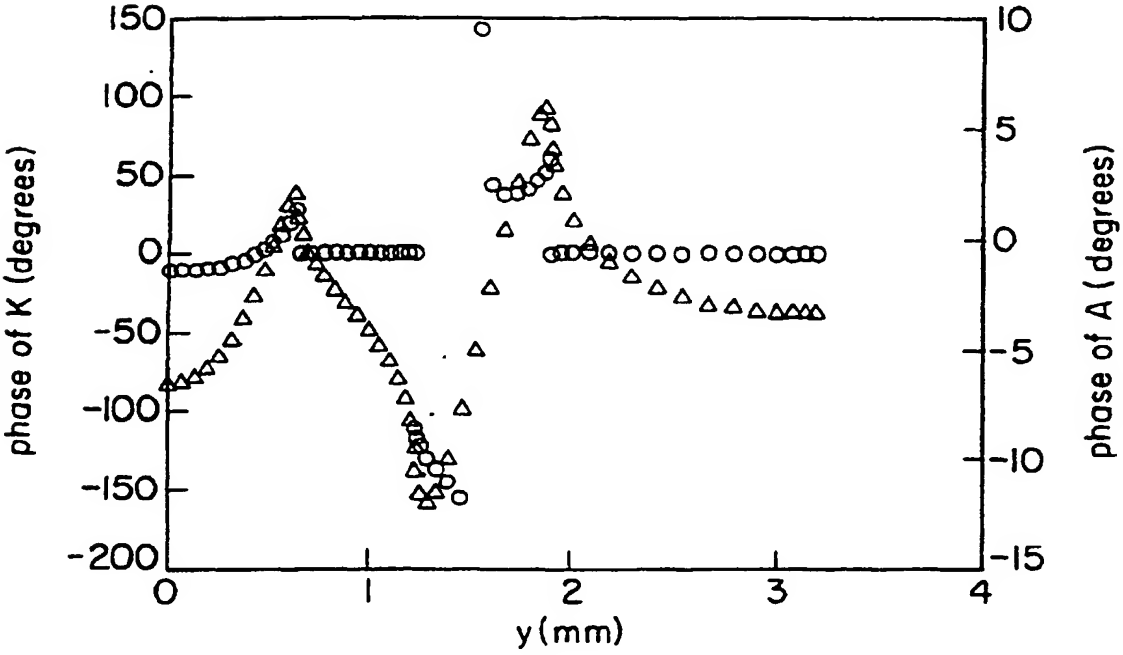

FIG. 49b

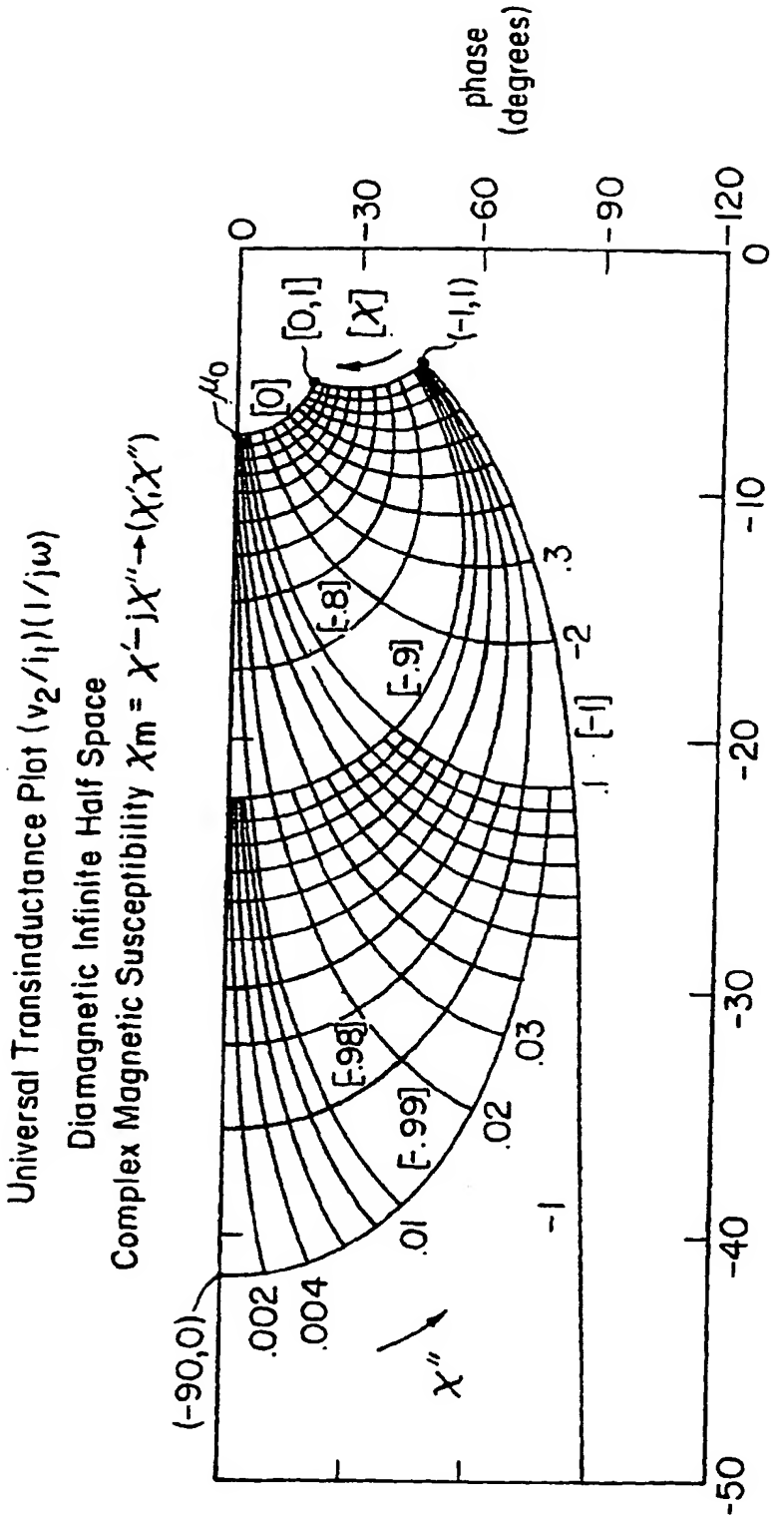

FIG. 50

log (freq.)	Transinductance $v_2 / j\omega i_1$			
	magnitude ($\mu\Omega$sec/rad)		phase (degrees)	
	$h_a(3) = 0$	$h_a(3) = 0.8$mm	$h_a(3) = 0$	$h_a(3) = 0.8$mm
4.4	0.374	0.393	-9.9	-5.4
4.6	0.348	0.376	-11.8	-6.5
4.8	0.321	0.359	-12.8	-6.9
5.0	0.296	0.342	-12.6	-6.8
5.2	0.276	0.329	-12.1	-6.3
5.4	0.259	0.318	-11.1	-5.7
5.6	0.244	0.310	-10.1	-5.0
5.8	0.232	0.302	-8.9	-4.3
6.0	0.223	0.297	-7.8	-3.59
6.2	0.216	0.293	-6.71	-2.95
6.4	0.211	0.292	-5.68	-2.4
6.6	0.209	0.294	-4.80	-1.95

FIG. 51a

log (freq.)	Complex Magnetic Susceptibility	
	χ^*_m First Guess	χ^*_m Estimate
4.4	-.10-j.20	-.2176-j.2542
4.6	-.20-j.20	-.3242-j.2493
4.8	-.25-j.18	-.4120-j.2232
5.0	-.30-j.15	-.4709-j.1883
5.2	-.40-j.10	-.5245-j.1549
5.4	-.55-j.09	-.5701-j.1227
5.6	-.60-j.08	-.5932-j.1028
5.8	-.62-j.06	-.6164-j.0829
6.0	-.64-j.05	-.6338-j.0673
6.2	-.66-j.04	-.6459-j.0545
6.4	-.68-j.03	-.6543-j.0438
6.6	-.70-j.02	-.6570-j.0356

FIG. 51b

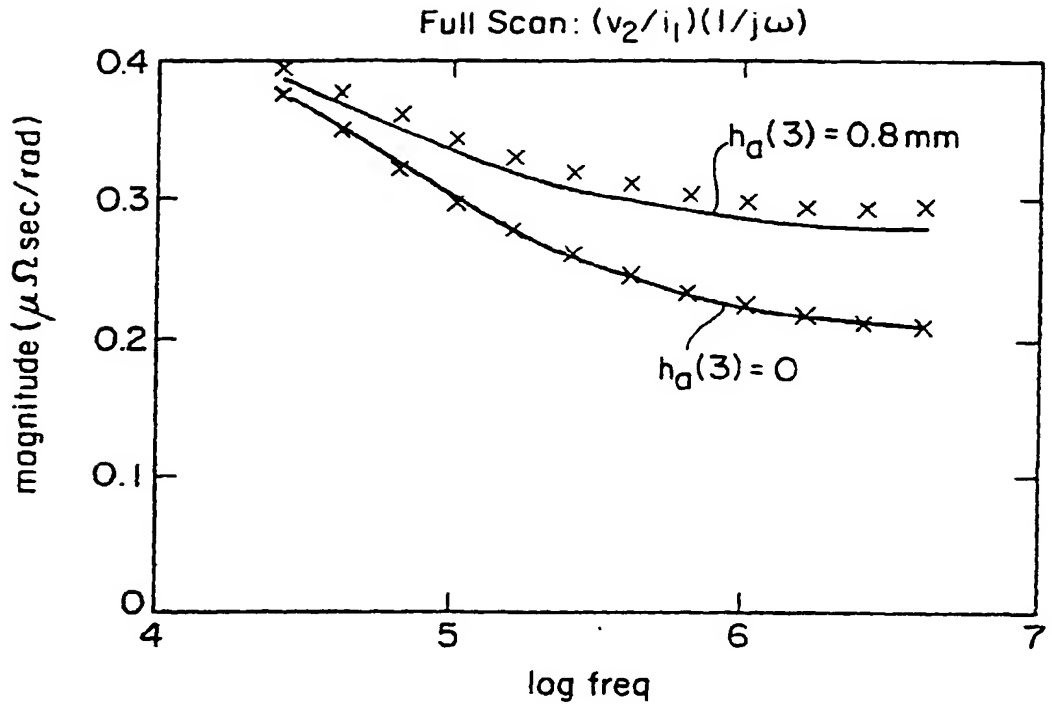

FIG. 52a

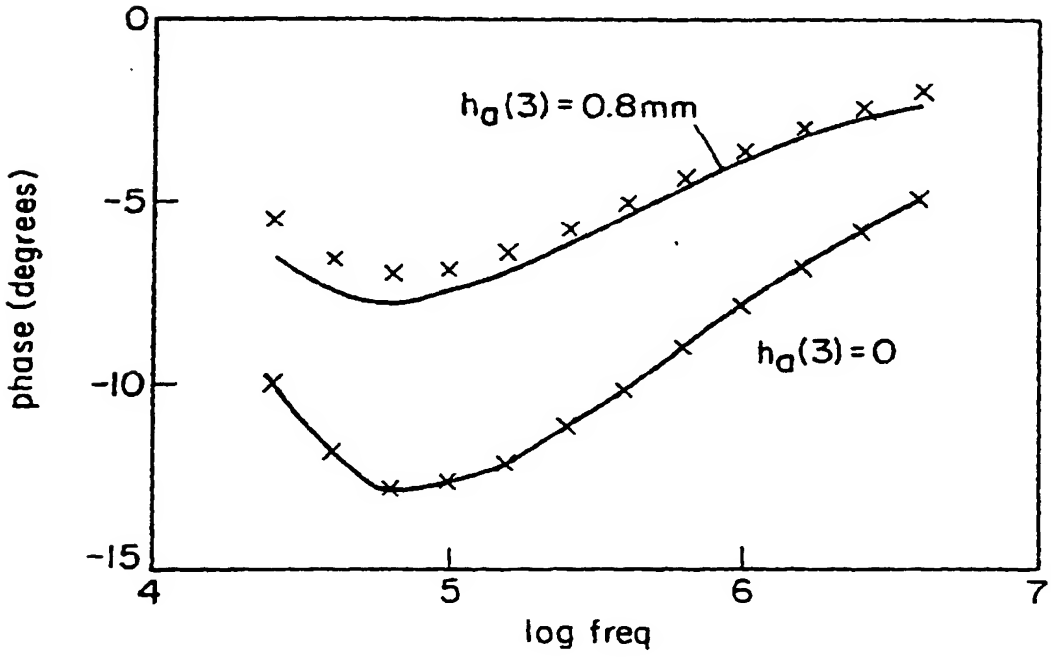

FIG. 52b

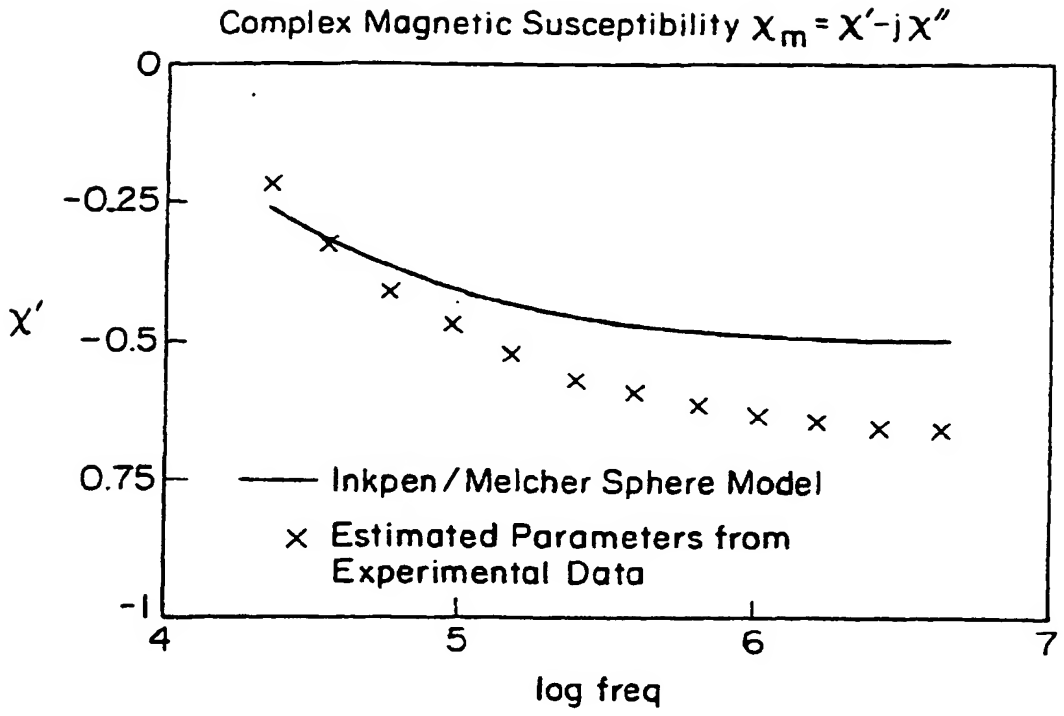

FIG. 53a

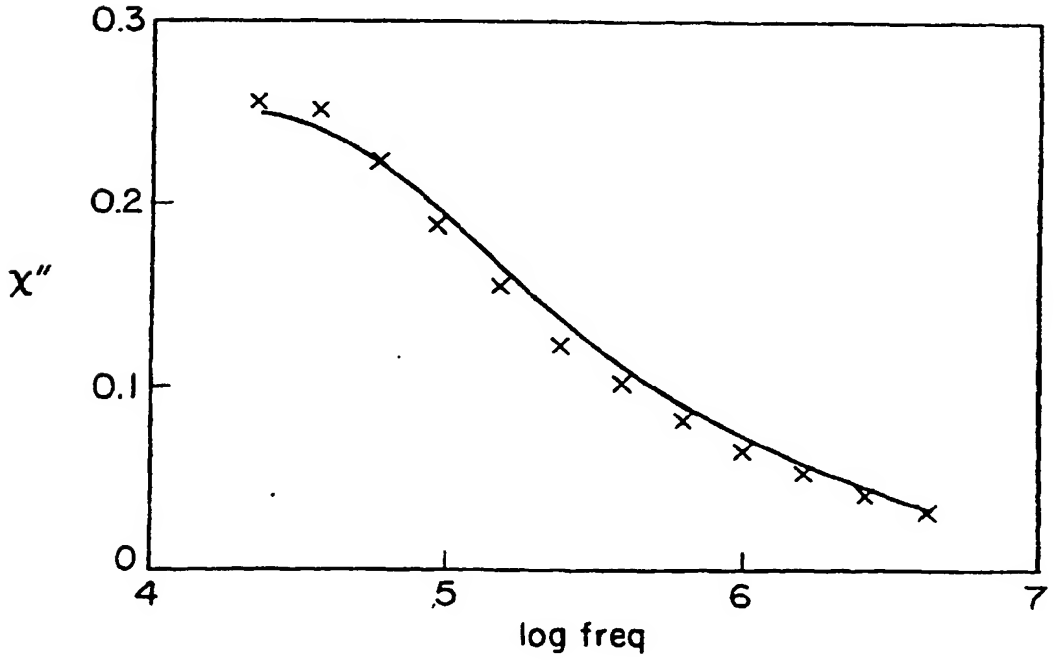

FIG. 53b

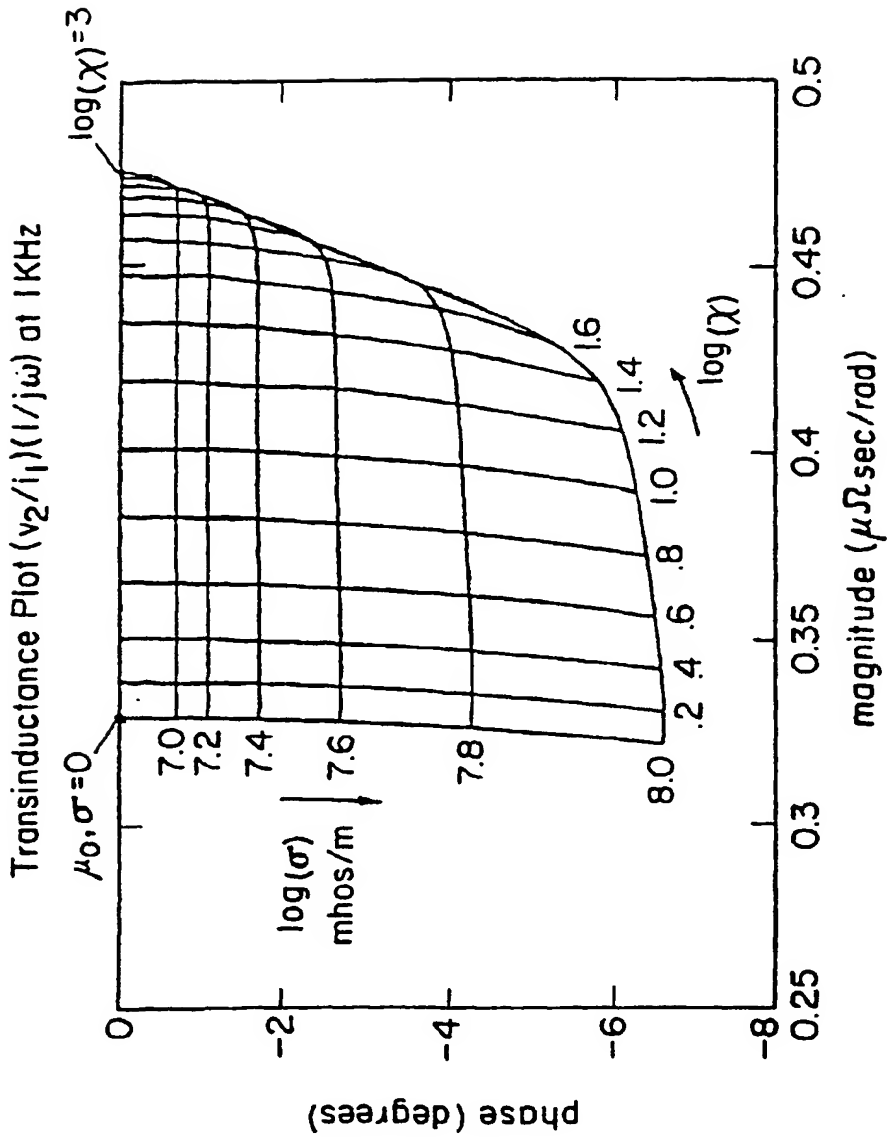

FIG. 54

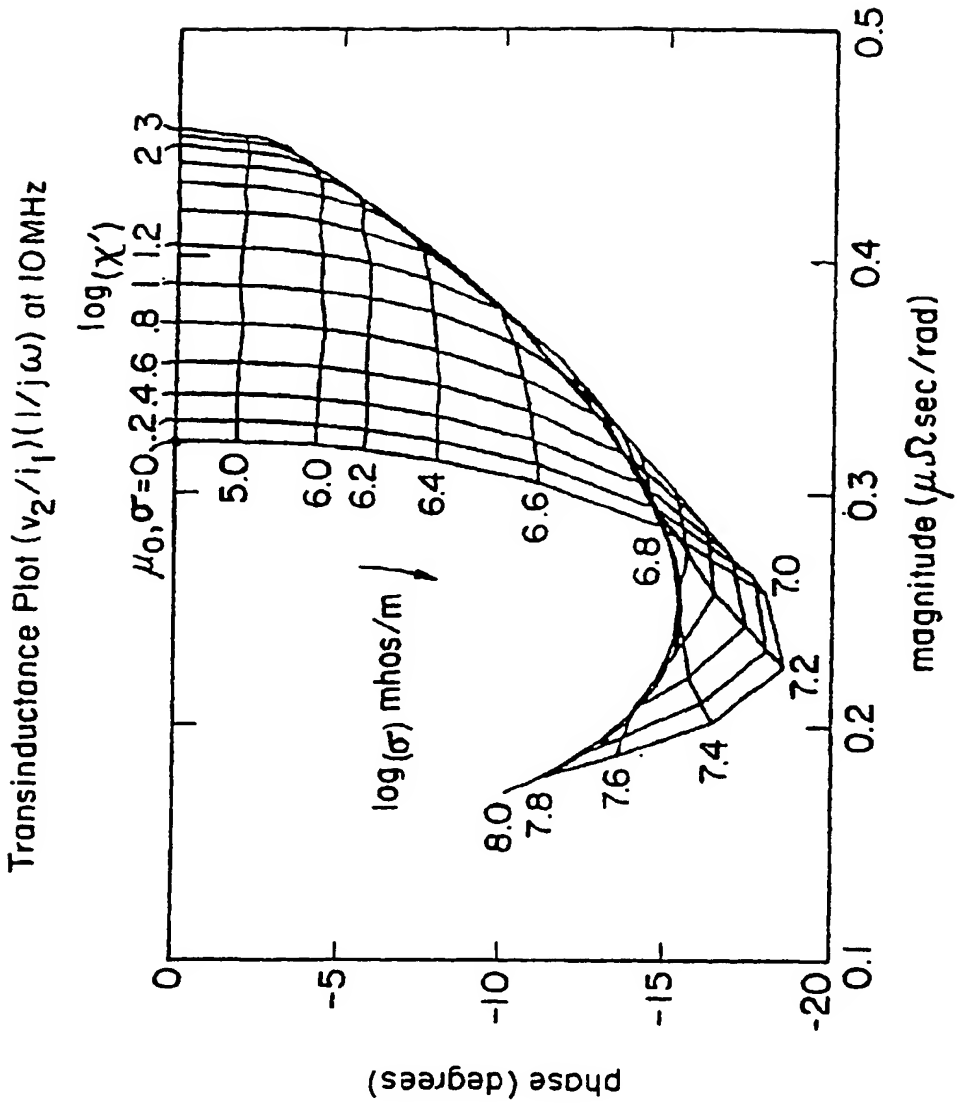

FIG. 55

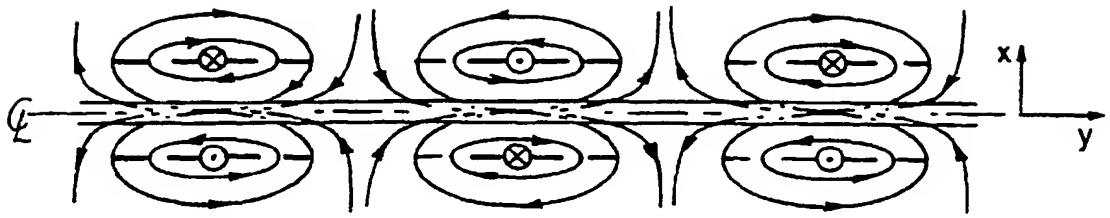

ODD

FIG. 56a

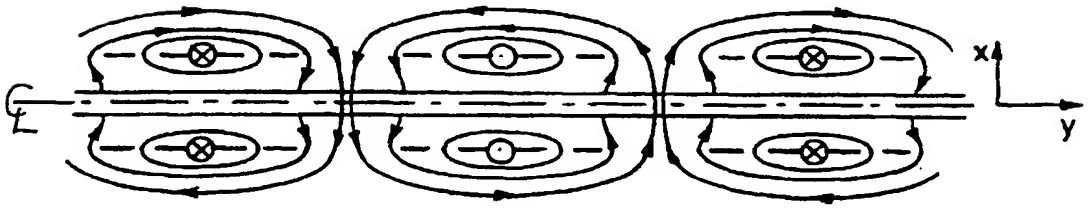

EVEN

FIG. 56b

(19) Europäisches Patentamt
European Patent Office
Office européen des brevets

(11) EP 1 037 043 A3

(12) EUROPEAN PATENT APPLICATION

(88) Date of publication A3:
27.09.2000 Bulletin 2000/39

(43) Date of publication A2:
20.09.2000 Bulletin 2000/38

(21) Application number: **00112223.3**

(22) Date of filing: **30.11.1992**

(51) Int. Cl.[7]: **G01N 27/72**, G01R 33/12

(84) Designated Contracting States:
DE FR GB IT LU NL SE

(30) Priority: **06.12.1991 US 803504**

(62) Document number(s) of the earlier application(s) in accordance with Art. 76 EPC:
93900764.7 / 0 615 619

(71) Applicant:
MASSACHUSETTS INSTITUTE OF TECHNOLOGY
Cambridge, MA 02139 (US)

(72) Inventors:
- **Goldfine, Neil J.**
  Burlington, MA 01803 (US)
- **Melcher, James R.**
  DECEASED (US)

(74) Representative:
Style, Kelda Camilla Karen et al
Page White & Farrer,
54 Doughty Street
London WC1N 2LS (GB)

(54) Magnetometer of increased sensitivity, selectivity and dynamic range

(57) A magnetometer for measuring a geometric property and the conductivity of a material comprising:

an electromagnetic winding structure capable of imposing a magnetic filed in the material when driven by an electric signal and sensing an electromagnetic response;
an analyzer for applying the electric signal to the winding structure to define a spatial wavelength associated with the imposed magnetic field in the material, the electric signal having a preselected temporal excitation frequency; and
a property estimator coupled to the winding structure for receiving sensed responses, the property estimator accessing a property estimation grid for translating sensed responses into substantially independent geometric property and conductivity estimates at the single preselected temporal excitation frequency.

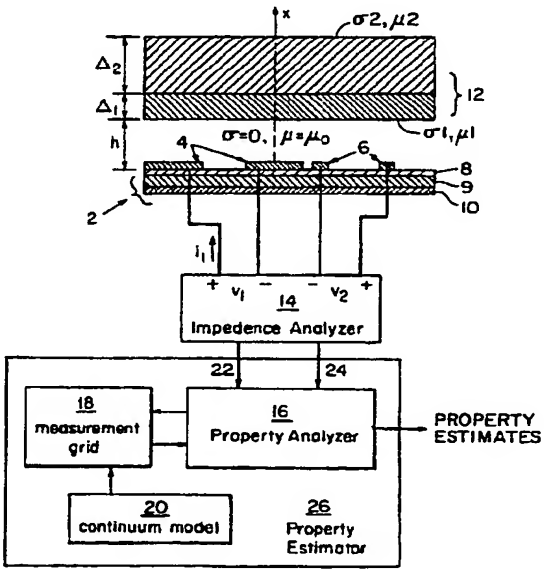

FIG. 1

EP 1 037 043 A3

European Patent Office

EUROPEAN SEARCH REPORT

Application Number
EP 00 11 2223

DOCUMENTS CONSIDERED TO BE RELEVANT

Category	Citation of document with indication, where appropriate, of relevant passages	Relevant to claim	CLASSIFICATION OF THE APPLICATION (Int.Cl.7)
A	US 5 015 951 A (MELCHER) 14 May 1991 (1991-05-14) * the whole document *	1-22	G01N27/72 G01R33/12
A	US 3 249 854 A (NEVIUS) 3 May 1966 (1966-05-03) * the whole document *	1-22	
A	US 4 757 259 A (CHARPENTIER) 12 July 1988 (1988-07-12) * the whole document *	1-22	
A	US 4 922 201 A (VERNON ET AL) 1 May 1990 (1990-05-01) * the whole document *	1-22	
A	US 5 086 274 A (GOBIN ET AL.) 4 February 1992 (1992-02-04) * the whole document *	1-22	
A	US 5 059 902 A (LINDER) 22 October 1991 (1991-10-22) * the whole document *	1-22	TECHNICAL FIELDS SEARCHED (Int.Cl.7) G01N

The present search report has been drawn up for all claims

Place of search	Date of completion of the search	Examiner
THE HAGUE	7 August 2000	Kempf, G

CATEGORY OF CITED DOCUMENTS

X : particularly relevant if taken alone
Y : particularly relevant if combined with another document of the same category
A : technological background
O : non-written disclosure
P : intermediate document

T : theory or principle underlying the invention
E : earlier patent document, but published on, or after the filing date
D : document cited in the application
L : document cited for other reasons

& : member of the same patent family, corresponding document

EPO FORM 1503 03.82 (P04C01)

ANNEX TO THE EUROPEAN SEARCH REPORT ON EUROPEAN PATENT APPLICATION NO. EP 00 11 2223

This annex lists the patent family members relating to the patent documents cited in the above-mentioned European search report. The members are as contained in the European Patent Office EDP file on
The European Patent Office is in no way liable for these particulars which are merely given for the purpose of information.

07-08-2000

Patent document cited in search report	Publication date	Patent family member(s)	Publication date
US 5015951 A	14-05-1991	US 4814690 A	21-03-1989
		AT 100593 T	15-02-1994
		CA 1288477 A	03-09-1991
		DE 3887343 D	03-03-1994
		EP 0393068 A	24-10-1990
		JP 3502728 T	20-06-1991
		WO 8903047 A	06-04-1989
US 3249854 A	03-05-1966	NONE	
US 4757259 A	12-07-1988	FR 2589566 A	07-05-1987
		DE 3637794 A	07-05-1987
		GB 2187844 A	16-09-1987
		JP 62156501 A	11-07-1987
US 4922201 A	01-05-1990	NONE	
US 5086274 A	04-02-1992	FR 2648236 A	14-12-1990
		BR 9002779 A	20-08-1991
		CA 2018689 A,C	12-12-1990
		DE 69013236 D	17-11-1994
		DE 69013236 T	11-05-1995
		EP 0403344 A	19-12-1990
US 5059902 A	22-10-1991	SE 451886 B	02-11-1987
		AT 98367 T	15-12-1993
		AU 608784 B	18-04-1991
		AU 8100987 A	06-05-1988
		DE 3788429 D	20-01-1994
		DE 3788429 T	21-04-1994
		EP 0349528 A	10-01-1990
		FI 891597 A	03-04-1989
		JP 7078489 B	23-08-1995
		JP 2500215 T	25-01-1990
		WO 8802842 A	21-04-1988

EPO FORM P0459

For more details about this annex : see Official Journal of the European Patent Office, No. 12/82